

Fluctuation spectroscopy: From Rayleigh-Jeans waves to Abrikosov vortex clusters

A. A. Varlamov


*CNR-SPIN (Istituto Superconduttori, Materiali Innovativi e Dispositivi),
Viale del Politecnico 1, I-00133, Rome, Italy*

A. Galda

*James Franck Institute, University of Chicago, Chicago, Illinois 60637, USA
and Materials Science Division, Argonne National Laboratory,
9700 South Cass Avenue, Argonne, Illinois 60439, USA*

A. Glatz

*Materials Science Division, Argonne National Laboratory,
9700 South Cass Avenue, Argonne, Illinois 60439, USA
and Department of Physics, Northern Illinois University, DeKalb, Illinois 60115, USA*

 (published 27 March 2018)

Superconducting (SC) fluctuations, discovered in the late 1960s, have constituted an important research area in superconductivity as they are manifest in a variety of phenomena. Indeed, the underlying physics of SC fluctuations makes it possible to elucidate the fundamental properties of the superconducting state. The interest in SC fluctuation phenomena was further enhanced with the discovery of cuprate high-temperature superconductors (HTSs). In these materials, superconducting fluctuations appear over a wide range of temperatures due to the superconductors extremely short coherence lengths and low effective dimensionality of the electron systems. These strong fluctuations lead to anomalous properties of the normal state in some HTS materials. Within the framework of the phenomenological Ginzburg-Landau theory, and more extensively in the diagrammatic microscopic approach based on BCS theory, SC fluctuations as well as other quantum contributions (weak localization, etc.) enabled a new way to investigate and characterize disordered electron systems, granular metals, Josephson structures, artificial superlattices, and others. The characteristic feature of SC fluctuations is its strong dependence on temperature and magnetic field in the vicinity of the superconducting phase transition. This dependence allows the separation of fluctuation effects from other contributions and provides information about the microscopic parameters of a material, in particular, the critical temperature and the zero-temperature critical magnetic field. As such, SC fluctuations are very sensitive to the relaxation processes that break phase coherence and can be used as a versatile characterization instrument for SCs: Fluctuation spectroscopy has emerged as a powerful tool for studying the properties of superconducting systems on a quantitative level. Here the physics of SC fluctuations is reviewed, commencing from a qualitative description of thermodynamic fluctuations close to the critical temperature and quantum fluctuations at zero temperature in the vicinity of the second critical field. The analysis of the latter allows us to present fluctuation formation as a fragmentation of the Abrikosov lattice. This review highlights a series of experimental findings followed by microscopic description and numerical analysis of the effects of fluctuations on numerous properties of superconductors in the entire phase diagram and beyond the superconducting phase.

DOI: [10.1103/RevModPhys.90.015009](https://doi.org/10.1103/RevModPhys.90.015009)

CONTENTS

I. Introduction	2	2. Manifestation of QF above $H_{c2}(0)$	10
II. Qualitative Picture	5	III. Basic Elements of Microscopic Description of SF in Magnetic Field	11
A. Thermodynamic fluctuations in superconductors close to T_{c0}	5	IV. Fluctuation Diamagnetism	14
1. Rayleigh-Jeans waves rather than Boltzmann particles	5	A. General expression for magnetic susceptibility	14
2. Manifestations of SF close to T_{c0}	6	B. Asymptotic analysis	14
B. Quantum fluctuations in superconductors above $H_{c2}(0)$	9	1. Region close to the line $H_{c2}(T)$ (domains IV–VII)	14
1. Dynamic clustering of fluctuation Cooper pairs	9	2. Limit of weak fields (domains I–III and VIII)	15
		a. Vicinity of T_{c0} (domains I–III)	15
		b. High temperatures (domain VIII)	15

3. Limit of very strong fields (domain IX)	16	B. Fluctuations in two-band superconductors	44
C. Fluctuation spectroscopy: Analysis of the isothermal magnetization curves	16	C. Fluctuations in clean superconductors in strong fields	45
V. Fluctuation Conductivity	17	D. Fluctuation spectroscopy of artificial nanosolids	46
A. General expression for fluctuation conductivity	17	E. Fluctuation spectroscopy of inhomogeneous films: Pseudogap and confinement	47
B. Asymptotic analysis	19	XI. Numerical Fluctuation Spectroscopy	48
C. Fluctuation spectroscopy: Analysis of the conductivity	20	List of Symbols and Abbreviations	49
1. Manifestation of different contributions to conductivity	20	Acknowledgments	51
2. Observation of fluctuation conductivity in experiments	21	References	51
a. Indium oxide films	21		
b. Fluctuations in ultrathin TiN films	22		
c. Transverse magnetoresistance above $H_{c2}(0)$	23		
VI. Fluctuation Hall Conductivity	24		
A. Fluctuation Hall effect and the special role of particle-hole asymmetry	24		
B. Microscopic theory of fluctuation Hall effect	25		
C. Asymptotic analysis and comparison to experiments	25		
1. Region close to the line $H_{c2}(T)$	25		
2. Limit of weak fields	26		
3. Limit of strong fields	26		
VII. Fluctuation Nernst-Ettingshausen Effect	27		
A. General expression for the fluctuation Nernst-Ettingshausen coefficient	27		
1. Definition of the NE coefficient	28		
2. Onsager relations and magnetization currents	28		
3. Microscopic expression for fluctuation NE coefficient	29		
B. Asymptotic analysis	30		
C. Fluctuation spectroscopy: Analysis of Nernst signal measurements	31		
1. Giant Nernst signal in NbSi	31		
2. Analysis of the ghost critical field	32		
VIII. Fluctuation Pseudogap and Low-bias Anomaly	33		
A. Fluctuation depletion of the electron DOS	33		
B. Fluctuation pseudogap in tunneling conductivity: Phenomenological approach	34		
C. General expression for the fluctuation tunneling conductivity	34		
D. Fluctuation pseudogap: Asymptotic analysis	35		
1. Tunnel conductivity in weak magnetic field	35		
2. Vicinity of the line $H_{c2}(T)$	36		
E. Weak pair breaking: Low-bias anomaly	38		
F. Epilogue of the theoretical analysis	38		
G. Fluctuation spectroscopy: Analysis of experiments	38		
1. Observation of the fluctuation pseudogap	39		
2. Observation of the low-bias anomaly	40		
IX. Effect of Fluctuations on the NMR Relaxation Rate	40		
A. General expression for the fluctuation NMR relaxation rate	40		
1. Asymptotic analysis	41		
a. Vicinity of T_{c0} (domains I–III)	41		
2. Region close to the line $H_{c2}(T)$ (domains IV–VII)	42		
3. Suppression of the fluctuation contribution to the NMR rate beyond the GL region	43		
B. Fluctuation spectroscopy: Analysis of the NMR relaxation rate	43		
X. Further Developments of Fluctuation Spectroscopy	43		
A. Extension of fluctuation spectroscopy on quasi-two-dimensional superconductors	44		

I. INTRODUCTION

“Happy families are all alike; every unhappy family is unhappy in its own way” is the famous beginning line of Leo Tolstoy’s novel, *Anna Karenina*. About 100 years later, Vladimir Nabokov turned this line on its head and opened his novel *Ada or Ardor: A Family Chronicle* with “All happy families are more or less dissimilar; all unhappy ones are more or less alike” in reference to Tolstoy.

We do not want to say whose assertion is more astute, but can confidently assume that scientists, studying the ramifications of superconducting fluctuations for nearly half a century, are content with their discoveries. Neither can we say whether electrons or Cooper pairs [“coupled” electrons in superconductors (SC)] are happy or not, but we know that while *stable* Cooper pairs in the superconducting state form a sort of condensate below the critical temperature T_{c0} , all conducting in the same way, the behavior of *fluctuating* Cooper pairs (FCPs)¹ beyond the superconducting region is more complex and results in a multitude of interesting physical phenomena.

These FCPs affect thermodynamic and transport properties of a metal, both directly and through changes which they cause in the quasiparticle subsystem. The investigation of superconductivity through superconducting fluctuations (SFs) provides valuable information about the microscopic properties of the normal and superconducting state and details about the formation of the latter (Larkin and Varlamov, 2009). For example, direct measurements of the second critical field $H_{c2}(0)$ of some high-temperature superconductors is a challenging problem due to its extremely large predicted values, restricting their measurements to only a few available pulsed high-field facilities. Yet this important material property can be extracted from the study of the fluctuation-induced Nernst signal above the critical temperature (Tafti *et al.*, 2014) at considerably lower field ranges.

The phenomenon of superconducting fluctuations came into the focus of the superconductivity community nearly half a century after the discovery of superconductivity. There were several reasons for this suspended interest. For example, the early samples were inhomogeneous, resulting in substantial extrinsic broadening of the superconducting transition, which

¹One has to distinguish the notion of a FCP from that of a “preformed Cooper pair” appearing in some BEC-BCS scenarios of high-temperature superconductivity. While preformed Cooper pairs are supposed to be equilibrium bosons composed of two electrons due to their effective attraction in real space, a FCP is a useful “image” of superconducting-type correlations occurring in a Fermi liquid of electrons in the normal phase of a superconductor.

obfuscated the manifestation of thermal fluctuations. Later, when homogeneous bulk materials became available, the very sharp superconducting transition of these clean materials also concealed the fluctuation phenomena. The temperature region over which the superconducting transition is smeared due to fluctuations is determined by the so-called Ginzburg-Levanyuk number Gi (Levanyuk, 1959; Ginzburg, 1960). For a three-dimensional superconductor, it has a typical value range of $(10^{-14}-10^{-6})T_{c0}$ (depending on the concentration of impurities).

The search for superconductors with high critical parameters led scientists to the investigation of disordered superconducting films and quasi-one-dimensional systems, where the transition from the resistive to the superconducting state is smeared over a much wider temperature interval $\sim(10^{-2}-10^{-3})T_{c0}$ (Glover, 1967). A careful analysis of the transition region in low-dimensional systems resulted in the concurrent formulation of the phenomenological theory of fluctuations based on the Ginzburg-Landau (GL) theory (Schmidt, 1966, 1968) and the development of a diagrammatic microscopic approach (Aslamasov and Larkin, 1968; Maki, 1968; Thompson, 1970). These advances explained the experimental observations and opened a new field of interdisciplinary research involving superconductivity and the theory of phase transitions. Furthermore, close to the critical temperature and in relatively weak magnetic field regions of the phase diagram, both approaches essentially led to the same conclusions regarding the effect of FCPs on various superconducting properties.²

The fluctuation “boom” started with the investigation of corrections to the heat capacity (Suzuki and Tsuboi, 1977; Tsuboi and Suzuki, 1977), the conductivity (Glover, 1967), the density of states (Cohen, Abeles, and Fuselier, 1969; Abeles, Cohen, and Fuselier, 1971), and the emergence of collective modes in the superconducting phase (Carlson and Goldman, 1973) close to T_{c0} . All of them were found to be small everywhere beyond the immediate vicinity of the transition. This relatively negligible effect of fluctuations on the SC transition was found to be in striking contrast to the properties of liquid ^4He at the transition to the superfluid state, where fluctuations smear the heat capacity jump so strongly that the corresponding temperature was called the λ point. This discrepancy was explained by the large value of the Cooper pairs coherence length with respect to interatomic distances: namely, the inverse ratio of these quantities constitutes a small parameter to the theory of SF, the Ginzburg-Levanyuk number, and determines the weakness of SF in conventional superconductors.

In the vicinity of the superconducting transition temperature, the thermodynamics of SF can be described within the framework of the GL functional. Such description for small, effectively zero-dimensional, SC granules was successfully considered by Schmidt (1966). Here the shape of the superconducting transition, smeared by fluctuations, is essentially

²The microscopic approach yields additional contributions related to the quantum interference and indirect effects of fluctuation pairing on the properties of the quasiparticle subsystem. The latter are generally less singular in the vicinity of the critical temperature.

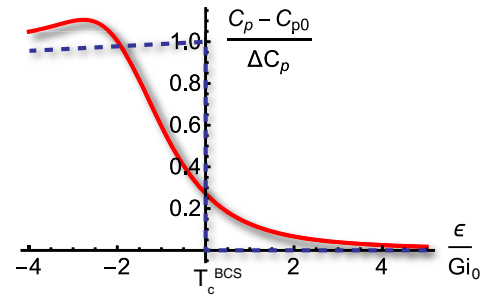


FIG. 1. Smearing of the superconducting transition by fluctuations ($\epsilon \approx T/T_{c0} - 1$). The temperature dependences of the heat capacity of a superconducting grain in the vicinity of the transition temperature in accordance with the BCS theory (dashed line) and the one accounting for fluctuations obtained by Schmidt (1966) (solid line). The typical temperature scale for the change of the heat capacity is given by $Gi_{(0)}T_{c0}$.

determined by the fourth order term in the GL functional (see Fig. 1). Unfortunately, a functional integration over all modes of the fluctuating order parameter in the partition function using the complete GL functional is an infeasible task for higher dimensional ($d = 1, 2, 3$) superconductors. Yet beyond the immediate vicinity of the critical temperature, the leading fluctuation contribution to the heat capacity arises from low-energy (long-wavelength) modes of the fluctuating order parameter. Their scale is characterized by the so-called Ginzburg-Landau coherence length $\xi_{GL}(T)$, which is much larger than the size of the “true” Cooper pairs emerging in BCS theory. This fact enables the GL functional to describe fluctuation effects with the quadratic approximation, which allows for solving a wide range of problems. However, the description of fluctuations in the immediate vicinity of the transition ($\epsilon \lesssim Gi_{(d)}$) remains beyond the validity of this approximation and requires renormalization group approaches.

The situation is similar to the effect of fluctuations on transport coefficients: they are mainly determined by low-energy modes of the order parameter (Aslamasov and Larkin, 1968; Maki, 1968; Abrahams, Redi, and Woo, 1970; Scalapino, 1970).

In the early 1970s, the only experimentally observed characteristic exhibiting a long tail in its temperature dependence was the magnetization, which extended Meissners diamagnetism far into the normal phase of superconductors. It considerably exceeded the values for the electron diamagnetism predicted by Langevin’s and Landau’s theories over a wide range of temperatures. Moreover, even at temperatures close to the transition difficulties appeared in explaining the field dependence of the fluctuation magnetization in high magnetic fields. For example, it was quite clear that strong magnetic fields should suppress fluctuations (and this was indeed observed experimentally); the GL approach, even in its nonlinear version, failed to explain this behavior (Patton, Ambegaoker, and Wilkins, 1969; Prange, 1970; Skocpol and Tinkham, 1975). Furthermore, in the zero- and one-dimensional cases, the precursor of the Meissner signal as a function of the magnetic field first increases (in absolute terms) linearly with the field until it reaches a

maximum and finally decreases slowly to zero. In the two-dimensional case it saturates, and in the 3D case it increases indefinitely, in contrast to the experimental results and common sense. The discrepancy between the then available theory and experimental findings demonstrated the important role of short-wavelength and dynamical fluctuation modes, which involve energies much larger than those accessible with the Ginzburg-Landau approach (Kurkijärvi, Ambegaokar, and Eilenberger, 1972). The sharp contradiction between theory and experiment in this case may be compared to the paradox of the Rayleigh-Jeans catastrophe that led to Planck's theory.

Early results obtained first in the vicinity of the transition temperature T_{c0} were generalized in the 1970s to 1980s to temperature ranges far from the transition (Maki, 1973; Bulaevskii, 1974; Aslamazov and Larkin, 1975; Aslamazov and Varlamov, 1980; Larkin, 1980; Altshuler, Reizer, and Varlamov, 1983) and to relatively high fields (Lopes dos Santos and Abrahams, 1985). More recently, quantum fluctuations (QFs), appearing in SC at low temperatures and fields close to the second critical field $H_{c2}(0)$, have also been considered (Beloborodov and Efetov, 1999; Beloborodov, Efetov, and Larkin, 2000; Galitski and Larkin, 2001a). Focusing on the vicinity of the quantum phase transition one obtains a qualitative picture of superconducting fluctuations quite different from that in the GL region close to T_{c0} . FCPs close to $H_{c2}(0)$ should be seen as rotating fluctuating vortices with cyclotron frequency $\Omega_H \sim \Delta_{BCS}/\hbar$ and Larmor radius $r_L \sim \xi_{BCS}$ rather than being considered as long-wavelength modes. Since the characteristic coherence length of QFs and their lifetime considerably exceed the corresponding size and period of rotation of a BCS Cooper pair in a single vortex ($\xi_{QF} \gg r_L$, $\tau_{QF} \gg \hbar/\Delta_{BCS}$) in this region, one can assume that they form a peculiar dynamic state (Glatz, Varlamov, and Vinokur, 2011b), which consists of clusters of coherently rotating FCPs. These form some kind of quantum liquid (see Fig. 2, top left).

Finally, renewed interest in superconducting fluctuations was triggered by the observation of a giant Nernst-Ettingshausen (NE) signal over a wide range of temperatures and magnetic fields in underdoped phases of high-temperature

superconductors (Xu *et al.*, 2000) and later also in conventional superconductors above the critical temperature (Pourret, Aubin *et al.*, 2006)—now in their most general manifestation, including the quantum regime. The origin of the giant signal generated a lively discussion and was finally explained by Ussishkin, Sondhi, and Huse (2002), Michaeli and Finkel'stein (2009a), Serbyn *et al.* (2009), Levchenko, Norman, and Varlamov (2011), and Boyack *et al.* (2018). These papers outlined the profound relationship between the fluctuation Nernst-Ettingshausen signal, magnetization currents, and the dominant role of these effects with respect to the other fluctuation entities.

In this review, we emphasize the general approach to describe the fluctuation phenomena in the entire phase diagram of a superconductor above the upper critical field line $H_{c2}(T)$ and its importance for *fluctuation spectroscopy*. We concentrate mainly on the most interesting case of a two-dimensional *s*-wave superconductor, restricting the consideration to the representative limit of a dirty superconductor ($k_B T_{c0} \tau \ll \hbar$). Moving along the $H_{c2}(T)$ line one can see how long-wavelength fluctuations of the order parameter, due to the effect of increasing magnetic field, gradually transform into fluctuation vortices. The crossover between these two, very different, pictures takes place where the FCP's Larmor radius becomes of the order of its coherence length. At higher fields and at lower temperatures the quantum nature of fluctuations becomes more pronounced and the picture starts to resemble an Abrikosov vortex lattice rather than a set of Ginzburg-Landau long waves. Variations in the character of the SFs determine their contributions to the thermodynamic and transport behaviors of the superconductor.

In recent years, a microscopic approach emerged, which accounts for short-wavelength and dynamical SFs, elucidating the challenging experimental findings of the last decade over the entire phase diagram. Those include the giant Nernst signal, the nonmonotonic temperature behavior of conductivity above the phase transition in disordered SC films, the pseudogap opening above the transition line, the peculiarities of the nuclear magnetic resonance relaxation above the Abrikosov vortex state, and many more.

At this point a word of caution is in order. The theoretical starting point for the microscopic considerations presented in this review is the BCS theory (Bardeen, Cooper, and Schrieffer, 1957a, 1957b). In its original version it describes the Cooper pair formation as a result of electron-phonon interaction, which was broadly successful in explaining the properties of conventional superconductors. Yet, prescinding from its physical nature, one can perceive the BCS theory as a mean-field theory, and the underlying origin of the interaction responsible for the Cooper pair formation is not that important for its applicability. One can replace the phonons mediating the electron-electron interaction in the BCS Hamiltonian by other collective bosonic excitations of the solid. For example, this approach successfully describes the physics of superfluid ^3He , where the role of intermediate bosons is played by ferromagnetic paramagnons. Superconductivity mediated by magnetic excitations has been proposed for various organic and heavy fermion superconductors. The collective bosonic degrees of freedom can mediate electron-electron interaction

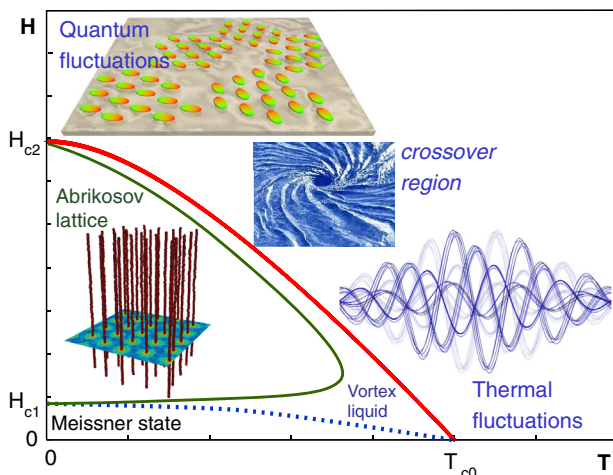


FIG. 2. Schematic phase diagram of type-II superconductors, showing the domains of qualitatively different physical behavior.

either in spin or in charge channels. The resulting interaction does not even need to be attractive. Also the type of pairing symmetry is not important, as the BCS theory can be extended to p -, d -, and higher angular momenta pairing mechanisms (Tsuei and Kirtley, 2000; Chubukov, Pines, and Schmalian, 2008; Scalapino, 2012; Loktev and Pogorelov, 2015). In this language we can say that fluctuations in the framework of the generic BCS scheme describe thermodynamic and transport properties of superconductors beyond the mean-field approximation.

With the discovery of high-temperature superconductors (HTSs) a new field of research was generated, yet a generally accepted mechanism of this phenomenon is still not available. Underdoped cuprates show clear features of electron state localization (Mott physics), such that the BCS theory does not apply to them. HTS oxide superconductors with low superconducting carrier density are characterized by a relatively small phase stiffness and poor screening, both of which imply a significantly larger role for phase fluctuations (Emery and Kivelson, 1995). However, SC properties of optimally doped and overdoped cuprates can be described, at least to a first approximation, using models with moderately strong electron-electron interaction. The fundamental properties of such systems are not qualitatively different from BCS superconductors. For this reason, we will also apply the fluctuation-spectroscopy approach to analyze the measurements on optimally and overdoped HTSs in addition to experimental results obtained for conventional superconductors.

This review is organized as follows: In Sec. II we present the qualitative picture of fluctuation phenomena in superconductors by demonstrating how the main results can be obtained from the point of view of the uncertainty principle and basic formulas of condensed matter physics. In Sec. III we report on the main ideas and necessary mathematical elements of the microscopic description of SFs at arbitrary temperatures and magnetic fields. The following sections are organized in a common systematic way: we focus on one physical property of the superconductor at a time, briefly review how it is calculated in the Matsubara diagrammatic technique, present the general analytical expression for the corresponding fluctuation contribution including its asymptotic analysis, when possible present 3D visualization obtained as a result of numerical calculation for the entire phase diagram, and, finally, its comparison with the available experimental data. We start this sequence of properties with the discussion of the fluctuation diamagnetism (Sec. IV), followed by the fluctuation conductivity (Sec. V), Hall conductivity (Sec. VI), Nernst-Ettingshausen effect (Sec. VII), pseudogap and low-bias anomaly (Sec. VIII), and nuclear magnetic resonance (NMR) relaxation rate (Sec. IX). In Sec. X we discuss some aspects of fluctuation corrections in quasi-2D, two-band, clean, and nanocrystalline superconductors. Finally, we summarize the more technical aspects required for the numerical evaluation of the complete expressions for fluctuation corrections and *numerical fluctuation spectroscopy* in Sec. XI. The numerical codes needed to fit experimental data and, as a result, to extract the fundamental microscopic parameters of the superconducting systems (fluctuation spectroscopy) are supplied

as Supplemental Material [242]. These codes were also used to produce the 3D surface plots of fluctuation corrections presented in this review.

II. QUALITATIVE PICTURE

A. Thermodynamic fluctuations in superconductors close to T_{c0}

1. Rayleigh-Jeans waves rather than Boltzmann particles

The BCS theory (Bardeen, Cooper, and Schrieffer, 1957a, 1957b), being a mean-field approximation, deals only with thermally equilibrated Cooper pairs, which form a Bose-Einstein condensate. Any deviations from this mean-field model can be considered fluctuations. For example, four-particle interactions with the formation of one or two non-equilibrium Cooper pairs, or vice versa, interactions resulting in the decay of a Cooper pair belonging to the condensate into two quasiparticles are taken into account in the fluctuation theory (Dinter, 1977; Kulik, Entin-Wohlman, and Orbach, 1981; Varlamov and Dorin, 1986). Using the language of the Ginzburg-Landau approach, one can say that the BCS approximation corresponds to the saddle point solution of the GL functional. The latter describes the equilibrium distribution of the order parameter in a superconductor and allows for the study of its properties in the mean-field approximation. Yet, any other imaginable $\Delta(\mathbf{r})$ also contributes to the partition function of a superconductor, being weighted by means of the corresponding canonical distribution.

Above the critical temperature of the superconducting transition T_{c0} , the conditions for the formation of persistent Cooper pairs are not yet fulfilled. Nevertheless, these kind of objects appear even in the normal phase of superconductors as fluctuations before the system undergoes the phase transition into the superconducting state (see Fig. 3). These FCPs appear and decay, without forming a condensate. The corresponding lifetime τ_{GL} , the so-called Ginzburg-Landau time, can be estimated by utilizing the uncertainty principle. At the transition temperature, an equilibrium superconducting condensate with infinite lifetime emerges. Hence, for continuity reasons τ_{GL} must diverge to infinity when $T \rightarrow T_{c0}$. Let us estimate the binding energy of FCPs Δ_E using dimensionality arguments: While the Fermi energy, the Debye temperature, and the critical temperature can be expressed in units of energy, the only quantity that vanishes at the critical temperature is $k_B(T - T_{c0})$. Assuming that the binding energy of a FCP is proportional to this quantity, we immediately see that $\tau_{GL} \sim \hbar/\Delta_E$ becomes infinite at the phase transition point. The microscopic theory confirms this hypothesis and gives the exact coefficient

$$\tau_{GL} = \frac{\pi\hbar}{8k_B(T - T_{c0})}. \quad (1)$$

One can also estimate the characteristic “size” of a FCP ξ_{GL} , which is determined by the distance in which two electrons fly away from each other in a time τ_{GL} . In the case of a dirty superconductor, the electron motion is diffusive, with the diffusion coefficient $\mathcal{D} \sim v_F^2\tau$ (τ is the electron scattering time)

and $\xi_D(T) = \sqrt{D\tau_{GL}} \sim v_F\sqrt{\tau\tau_{GL}}$.³ In the case of a clean superconductor, where $k_B T \tau \gg \hbar$, impurity scattering no longer affects the electron-electron correlations. In this case, the characteristic time of the ballistic electron motion turns out to be less than the electron-impurity scattering time τ and is determined by the uncertainty principle, being $\sim \hbar/k_B T$. It is this latter time that has to be used to estimate the effective FCP size $\xi_{cl}(T) \sim v_F\sqrt{\hbar\tau_{GL}/k_B T}$. In both cases, the coherence length grows as $\epsilon^{-1/2}$ when approaching the critical temperature, where

$$\epsilon \equiv \ln \frac{T}{T_{c0}} \approx \frac{T - T_{c0}}{T_{c0}} \ll 1 \quad (2)$$

is the reduced temperature. In the GL region (close to, but beyond the immediate vicinity of T_{c0} , i.e., $\text{Gi} \lesssim \epsilon \ll 1$) we define the coherence length as

$$\xi_{GL}(\epsilon) = \xi/\sqrt{\epsilon}. \quad (3)$$

Here $\xi = \xi_{cl,D}$,

$$\xi^2 = -\frac{\tau^2 v_F^2}{d_e} \left[\psi\left(\frac{1}{2} + \frac{1}{4\pi T \tau}\right) - \psi\left(\frac{1}{2}\right) - \frac{1}{4\pi T \tau} \psi'\left(\frac{1}{2}\right) \right], \quad (4)$$

where $d_e = 1, 2, 3$ is the effective dimension of the electron motion.⁴ Equation (4) was obtained for the first time by Gor'kov (1960) as a result of a microscopic calculation. It is important to note that it differs only by a numerical coefficient from the BCS expression for the coherence length at zero temperature ξ_{BCS} . We see that the fluctuating order parameter $\Delta^{(f)}(\mathbf{r}, t)$ varies close to T_{c0} on the relatively large scale $\xi_{GL}(\epsilon) \gg \xi_{BCS}$; see Eq. (3).

It is important to note that FCPs, strictly speaking, cannot be considered as Landau quasiparticles. Indeed, while the energy of a well-defined quasiparticle has to be much larger than its inverse lifetime, the binding energy ΔE_s for a FCP turns out to be of the same order \hbar/τ_{GL} . Yet, close to T_{c0} , they still can be treated as classical objects, but in the sense of Rayleigh-Jeans waves rather than Boltzmann particles. This means that in the general Bose-Einstein distribution function only small energies $\epsilon(\mathbf{q}) \ll k_B T$ (\mathbf{q} is the momentum of the center of mass of FCP) are involved, and the exponential function in the Bose-Einstein distribution can be expanded:

³Strictly speaking, in the majority of expressions below τ has the meaning of the electron transport scattering time τ_{tr} . Nevertheless, as is well known, in the case of isotropic scattering these values coincide; so for simplicity we use hereafter the symbol τ .

⁴With the introduction of d_e we stress the difference between the effective dimensionality for FCPs d and electron motion. When we discuss a 2D superconductor, we mean a superconducting film of thickness $s \ll \xi$, or a strongly layered material with the interlayer distance larger than the perpendicular coherence length. This condition is less restrictive in the GL region, where the requirement $s \ll \xi_{GL}(\epsilon)$ is sufficient for two-dimensional FCP motion. Regarding the effective dimensionality of the electron motion d_e , it is determined by the specifics of its spectrum or confined electron diffusion due to sample geometry.

$$n(\mathbf{q}) = \frac{1}{\exp[\epsilon(\mathbf{q})/k_B T] - 1} \rightarrow \frac{k_B T}{\epsilon(\mathbf{q})}. \quad (5)$$

For this reason, the more appropriate tool to study fluctuation phenomena is the GL equation written for classical fields rather than the Boltzmann transport equation.

Nevertheless, the treatment of FCPs as particles often turns out to be useful. In this approach, their energy consists of the ‘‘binding energy’’ and the kinetic energy of the center of mass motion:

$$\epsilon(\mathbf{q}) = k_B(T - T_{c0}) + \frac{\mathbf{q}^2}{2m^*}, \quad (6)$$

where m^* is the effective mass of FCP.

The concentration of FCPs can be estimated by integration of the distribution function (5) over the momenta in the range $|\mathbf{q}| \leq \hbar\xi^{-1}$ [corresponding to the conditions $\epsilon(\mathbf{q}) \ll k_B T$]:

$$N_{(d)} = \int_{|\mathbf{q}| \lesssim \hbar/\xi} n(\mathbf{q}) \frac{d^d \mathbf{q}}{(2\pi\hbar)^d} = \frac{m^* k_B T_{c0}}{2\pi\hbar^2} \begin{cases} 2\pi\xi_{GL}(\epsilon) & d = 1, \\ \ln(1/\epsilon) & d = 2, \\ \text{const} - \xi_{GL}^{-1}(\epsilon) & d = 3. \end{cases} \quad (7)$$

The physical three-dimensional concentration for wires and films can be related to Eq. (7) by $\tilde{N}_{(3)} = N_{(d)} s^{d-3}$.⁵ It turns out to be divergent when approaching the transition in the 1D and 2D cases. Recall that these results were obtained in the long-wavelength approximation (i.e., not too far from the transition) and do not account for the interaction of fluctuations (i.e., not too close to T_{c0}), which means $\text{Gi} \lesssim \epsilon \ll 1$.

2. Manifestations of SF close to T_{c0}

Using the estimates for the lifetime, Eq. (1), coherence length, Eqs. (3) and (4), and concentration of FCPs, Eq. (7), we can evaluate their contribution to different physical characteristics of a metal close to (but above) the transition to the superconducting state. For example, we can quantify the smearing of the jump of the heat capacity at the transition. We start with the evaluation of the energy density of FCPs in the Rayleigh-Jeans approximation (5):

$$\frac{E^{(\text{FCP})}}{V} = \int \epsilon(\mathbf{q}) n(\mathbf{q}) \frac{d^d \mathbf{q}}{(2\pi\hbar)^d} \approx k_B T_{c0} \int_{|\mathbf{q}| \lesssim \hbar/\xi} \frac{d^d \mathbf{q}}{(2\pi\hbar)^d} \sim \frac{k_B T_{c0}}{\xi^d}.$$

⁵We define the FCP concentration in d -dimensional space. This means that it determines the number of pairs per volume in the 3D case, the number of pairs per unit square in the 2D case, and the number of pairs per unit length in 1D. Since both wires and films are actual objects in three-dimensional space, we can approximate the 3D concentration of FCPs $\tilde{N}_{(3)}$ by $\tilde{N}_{(3)} = N_{(1)}/s^2$ for wires, where s^2 is the wire cross section and $\tilde{N}_{(3)} = N_{(2)}/s$ for films, where s is the thickness of the film, respectively.

One can see that in this approximation this contribution does not depend on ϵ and, hence, does not contribute to the heat capacity. At this point we note that the formation of FCPs is accompanied by a depletion of the quasiparticle subsystem, i.e., the concentration of the latter is reduced by $2N_{(d)}$; see Eq. (7). Therefore, the total energy density of the system changes by $E^{(n)} \sim -2k_B T N_{(d)}$ with related correction to heat capacity

$$C_V^{(n)} = \left(\frac{dE^{(n)}}{dT} \right)_V \sim -2k_B \frac{dN_{(d)}(\epsilon)}{d\epsilon} \sim \frac{k_B}{\xi^d} \epsilon^{d/2-2}.$$

Similarly, a qualitative understanding of the increase in the diamagnetic susceptibility above the critical temperature can be obtained from the well-known Langevin expression for the atomic susceptibility (Kittel, 2012). Identifying the concentration of FCPs with Eq. (7), their mass with m^* , their charge with $2e$, and the average square rotation radius by $\xi_{GL}^2(\epsilon)$, one finds

$$\Delta\chi^{(n)} = -\frac{2e^2 \tilde{N}_{(3)}}{3c^2 m^*} \xi_{GL}^2(\epsilon) \rightarrow -\frac{e^2}{c^2} \frac{k_B T_{c0}}{\pi \hbar^2 s^{3-d}} \xi_{GL}^{4-d}(\epsilon). \quad (8)$$

Equation (8) is valid for $d = 2, 3$ (with logarithmic accuracy in $d = 2$).

Analogously, one can evaluate the direct contribution of FCPs to the conductivity (Aslamazov-Larkin paraconductivity). It may be done by using the Drude formula. It is important to remember that impurities do not present obstacles for the FCP motion in an applied electric field. Indeed, the diffusive character of electron motion was already taken into account when we estimated the size of FCPs. Its square ξ^2 determines the inverse effective mass m^* , i.e., its inertia. The motion of FCPs in an electric field has ballistic character and applying the Drude formula, one should use for the lifetime τ_{GL} rather than the elastic scattering time τ , $2e$ for the carrier charge, m^* for its mass, and $N_{(d)}(\epsilon)$ for the concentration of FCPs. Using Eqs. (1) and (7) one finds

$$\sigma_{xx}^{(AL)} = \frac{4\tilde{N}_{(3)}(\epsilon)e^2\tau_{GL}(\epsilon)}{m^*} \sim \frac{e^2}{\hbar s^{3-d}} \xi^{2-d} \epsilon^{d/2-2}. \quad (9)$$

This contribution to conductivity of the normal phase of a superconductor corresponds to the opening of a new channel of charge transfer above T_{c0} due to the formation of FCPs.

Besides the direct FCP effect on the properties of a superconductor in its normal phase, indirect manifestation of SFs can be found due to their influence on the quasiparticle subsystem. These have a purely quantum nature and, in contrast to paraconductivity, require microscopic consideration.

The first of them is the Maki-Thompson (MT) contribution (Maki, 1968; Thompson, 1970), which is relevant for transport coefficients of dirty SCs near T_{c0} , where its singular temperature dependence is similar to that of paraconductivity. The physical origin of the MT contribution is a result of the fact that, in a system with impurities, an electron can move along a self-intersecting trajectory during the process of diffusion and return to its origin after some time. The

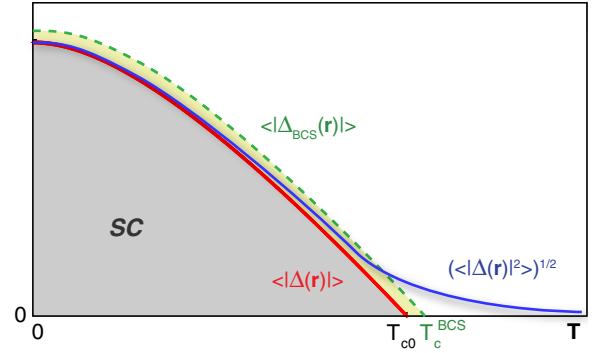


FIG. 3. The temperature dependence of the averaged mean square value of the superconducting order parameter (solid blue line). The dashed green line corresponds to the mean-field BCS picture ($\langle |\Delta_{BCS}(\mathbf{r})| \rangle$) and becomes zero at the point T_c^{BCS} . The thick red line describes the same $\langle |\Delta(\mathbf{r})| \rangle$ dependence, but with the fluctuation renormalized transition temperature T_{c0} , which is lower than the mean-field value T_c^{BCS} (Larkin and Varlamov, 2009). A finite concentration of fluctuating Cooper pairs, without long-range spatial coherence, exists in the normal phase of a superconductor for any temperature above T_{c0} . Their lifetime increases approaching the transition line from the normal state.

interference of the wave functions of two electrons, moving along such trajectories in the opposite directions, leads to the decrease of the Drude conductivity [this is the phenomenon of weak localization (Abrikosov, 1988)]. This quantum effect is nothing more than the precursor of the metal-insulator transition.

One can imagine that along such a trajectory, two electrons with opposite spins move simultaneously with opposite momenta, interacting with each other (see Fig. 4). They can form some specific FCPs. Here one should note that the amplitude of the BCS interaction of electrons drastically increases when $T \rightarrow T_c^{BCS}$ (Bardeen, Cooper, and Schrieffer, 1957a, 1957b):

$$g_{\text{eff}} = \frac{g}{1 - \rho_e g \ln(\omega_D/2\pi T)} = \frac{1}{\ln(T/T_c^{BCS})} \rightarrow \frac{1}{\epsilon},$$

where ω_D is the Debye frequency, g is the electron-electron interaction constant, and ρ_e is the one-electron density of

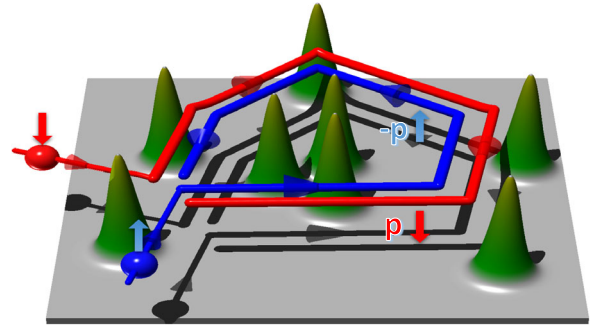


FIG. 4. Anomalous MT Cooper pairing. One electron moves clockwise with momentum \mathbf{p} , scattering at impurity potentials (green Gaussian peaks), while interacting with another electron with momentum $-\mathbf{p}$ on almost the same path (counterclockwise).

states. What is the reason for this increase? One possible mechanism is electron-electron scattering accompanied by the formation of virtual Cooper pairs. The probability of such induced pair irradiation (remember that Cooper pairs are Bose particles) is proportional to their number in the final state, i.e., $n(\mathbf{p})$ [see Eq. (5)]. For small momenta $n(\mathbf{p}) \sim 1/\epsilon$.

During the diffusive motion of an electron, the volume it explores grows as $(\mathcal{D}t)^{d/2}$. During a time dt the electron covers the elementary volume $\lambda_F^{d-1} v_F dt$. Hence the probability to return to the initial point is (Abrikosov, 1988)

$$w \sim \int_{t_{\min}}^{t_{\max}} \frac{\lambda_F^{d-1}}{(\mathcal{D}t)^{d/2}} v_F dt.$$

Since we are interested in fluctuation Cooper pairing of electrons, the corresponding minimal time on such trajectories is τ_{GL} . The upper limit of the integral is governed by the phase-breaking time τ_φ since for larger time intervals the phase coherence, which is necessary for the pair formation, is broken. As a result, the relative correction to conductivity due to such processes is equal to the product of the self-intersecting trajectory probability and the effective interaction constant $\sigma_{xx}^{(MT)}/\sigma = wg_{\text{eff}}$. In the 2D case,

$$\sigma_{(2)}^{(MT,an)} \sim \frac{e^2}{8\epsilon\hbar} \ln \frac{\tau_\varphi}{\tau_{GL}}.$$

One can see that the MT contribution is extremely sensitive to the electron phase-breaking processes and to the type of symmetry of orbital pairing; this is why it can often be suppressed.

However, the Aslamazov-Larkin (AL) and MT contributions, which are positive and singular in ϵ close to T_{c0} , do not capture the full picture of fluctuation effects on conductivity. The involvement of quasiparticles in the fluctuation pairing results in the depletion of their density of states at the Fermi level, i.e., in the opening of a pseudogap in the one-electron spectrum and the consequent decrease of the one-particle Drude-like conductivity. This indirect effect of FCP formation is usually referred to as the density of states (DOS) contribution and can be estimated using the Drude formula with doubled concentration of FCPs compared to the concentration of electrons missing at the Fermi level:

$$\sigma_{xx(2)}^{(DOS)} \sim -\frac{2N_{(2)}e^2\tau}{m_e} \sim -\frac{e^2}{\hbar} \ln \frac{1}{\epsilon}. \quad (10)$$

It is seen that the DOS contribution has an opposite sign compared to the AL and MT contributions. In the close vicinity of T_{c0} it does not compete with them, since it has a weaker dependence on temperature (Larkin and Varlamov, 2009). Let us point out the different roles FCPs play in the cases of heat capacity and conductivity: In the former their formation is ‘‘cheap’’ in terms of energy, and the main change in heat capacity of the system is related to the removal of quasiparticles. In the case of conductivity, the opening of a new channel for the charge transfer due to the formation of FCPs dominates over the changes in the one-particle conductivity.

Finally, a renormalization of the one-electron diffusion coefficient (DCR) in the presence of fluctuation pairing happens. Close to T_{c0} , this contribution is not singular in ϵ :

$$\sigma_{xx}^{(DCR)} \sim \frac{e^2}{\hbar} \ln \ln \frac{1}{T_{c0}\tau} + O(\epsilon).$$

For this reason it was ignored until recently. A few years ago Serbyn *et al.* (2009) and Glatz, Varlamov, and Vinokur (2011a) showed that the renormalization of the one-electron diffusion coefficient becomes of primary importance relatively far from T_{c0} and at very low temperatures. Because of the term $\sigma_{xx}^{(DCR)}$, the sign of the overall contribution of fluctuations to the conductivity $\sigma_{xx(2)}^{(fl)}$ is changed in a wide region of the phase diagram, especially close to $T = 0$, in the region of quantum fluctuations (Glatz, Varlamov, and Vinokur, 2011a); see Fig. 5, where regions with dominating fluctuation contributions to magnetoconductivity are shown.

Special attention has been paid to the giant Nernst-Ettingshausen effect observed in the pseudogap state of underdoped phases of HTSs (Xu *et al.*, 2000). After the observation in HTSs, a giant Nernst-Ettingshausen signal (3 orders of magnitude larger than the value of the corresponding coefficient in typical metals) was detected in a wide range of temperatures in the conventional, disordered superconductor $\text{Nb}_x\text{Si}_{1-x}$ (Pouret, Behnia *et al.*, 2006). These groundbreaking experiments have led to experimental and theoretical activities in the last decade (Ussishkin, Sondhi, and Huse, 2002; Michaeli and Finkel’stein, 2009a; Serbyn *et al.*, 2009; Levchenko, Norman, and Varlamov, 2011; Chang *et al.*, 2012; Kavokin and Varlamov, 2015; Behnia and Aubin, 2016).

The origin of the giant contribution of fluctuations to the thermomagnetic signal is closely related to giant fluctuations in the diamagnetic susceptibility occurring in the normal phase of superconductors. It was noticed half a century ago (Obraztsov, 1964) that noncompensated magnetization currents, which appear in nonhomogeneously heated samples, can play a crucial role for the correct calculation of the

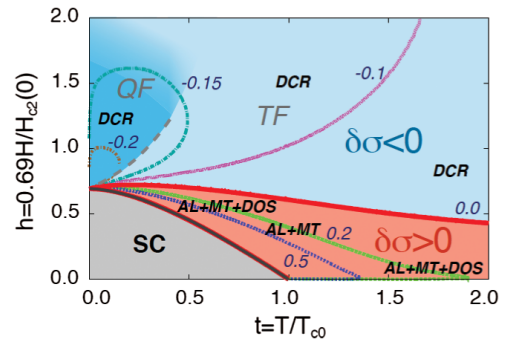


FIG. 5. Contours of constant fluctuation conductivity $[\sigma_{xx}^{(fl)}(t, h)]$ is shown in units of e^2/\hbar . The dominant fluctuation contributions are indicated by the bold italic labels (AL for Aslamazov-Larkin, MT for Maki-Thompson, DOS for density of states, and DCR for diffusion coefficient renormalization). The dashed line separates the domain of quantum fluctuations (QF) (the dark area of $\sigma_{xx}^{(fl)} > 0$) and thermal fluctuations (TF). From Glatz, Varlamov, and Vinokur, 2011a.

Nernst coefficient, in particular, validating the third law of thermodynamics.

In the case of measurements of the Nernst-Ettingshausen coefficient with a high resistive voltmeter, its thermodynamic part (without the contribution of magnetization currents) can be related to the temperature derivative of the chemical potential (Serbyn *et al.*, 2009; Varlamov and Kavokin, 2009)

$$\nu_{(d)}^{(\text{th})} = \frac{\sigma_{(d)}}{N_{(d)} c e^2} \left(\frac{d\mu_{(d)}}{dT} \right). \quad (11)$$

For the electron gas in a normal metal $\mu(T) \approx \mu(0) - \pi k_B^2 T^2 / [12\mu(0)]$ and Eq. (11) leads to the known Sondheimer result (Sondheimer, 1948) for the case of electron scattering on elastic impurities:

$$\nu_e = -\frac{\pi\tau}{6m_e c} \left(\frac{k_B T}{\mu(0)} \right),$$

proportional to the small electron-hole asymmetry factor.

Alternatively, one could also try to use Eq. (11) with the values $\sigma_{xx(d)}^{(\text{AL})}(\epsilon)$ and $N_{(d)}(\epsilon)$ presented earlier. However, one needs to clarify what the chemical potential of fluctuating Cooper pairs $\mu^{(\text{fl})}$ is since it is known that in thermal equilibrium the chemical potential of a system with variable number of particles is zero, such as the textbook examples of photon or phonon gases. A naive application of this ‘‘theorem’’ to the FCP ‘‘gas’’ leads to the wrong conclusion that $\mu^{(\text{fl})} = 0$. However, one needs to be careful when dealing with Cooper pairs, since they do not form an isolated system, but are rather only one subsystem with the other being formed by fermionic quasiparticles, which always have to be taken into account as well. In a multicomponent system, the chemical potential of the i th component μ_i is defined as the derivative of the free energy with respect to the number of particles of the i th kind:

$$\mu_i = (\partial F^{(\text{fl})} / \partial N_i)_{V,T,N_j}, \quad (12)$$

provided the numbers of particles of all other species are fixed $N_{j \neq i} = \text{const}$. In deriving the condition for thermodynamic equilibrium, one should now take into account the fact that the creation of a Cooper pair must be accompanied by removing two quasiparticles from the fermionic subsystem. This leads to $\mu^{(\text{fl})} - 2\mu^{(\text{qp})} = 0$, where $\mu^{(\text{qp})}$ is the chemical potential of quasiparticles. Therefore, the equilibrium condition does not fix $\mu^{(\text{fl})}$, $\mu^{(\text{qp})}$ to zero, even though the numbers of Cooper pairs and quasiparticles are not conserved. The simplest way to estimate $\mu^{(\text{fl})}$ is to identify it with the binding energy of FCPs ΔE_s taken with the opposite sign $\mu^{(\text{fl})} = T_{c0} - T$.

A more consistent consideration performed in the framework of the Ginzburg-Landau fluctuation theory confirms this estimate. The fluctuation part of free energy close to T_{c0} takes the form (Larkin and Varlamov, 2009)

$$F_{(2)}^{(\text{fl})}(\epsilon) = -\frac{T_{c0}}{4\pi\xi^2} \epsilon \ln \frac{1}{\epsilon}. \quad (13)$$

Similarly, the coefficient in Eq. (7) can be expressed in terms of the correlation length, Eq. (4), due to the relation between

the coefficients of the Ginzburg-Landau functional (Larkin and Varlamov, 2009):

$$N_{(2)}^{(\text{fl})}(\epsilon) = \frac{1}{4\pi\xi^2} \ln \frac{1}{\epsilon}. \quad (14)$$

Substituting these expressions into Eq. (12) one finds

$$\mu_{(2)}^{(\text{fl})} = \left(\frac{\partial F_{(2)}^{(\text{fl})}}{\partial N_{(2)}^{(\text{fl})}} \right)_{V,T} = \frac{\partial F_{(2)}^{(\text{fl})} / \partial \xi}{\partial N_{(2)}^{(\text{fl})} / \partial \xi} = -T_{c0} \epsilon. \quad (15)$$

Applying Eq. (15) to the subsystem of FCPs close to T_{c0} and identifying its conductivity with Eq. (9), one finds the Nernst-Ettingshausen coefficient generated by FCPs in weak fields close to T_{c0} :

$$\nu_{(2)}^{(\text{th}),(\text{fl})} = -\frac{\sigma_{xx(2)}^{(\text{AL})}}{(2e)^2 N_{(2)}^{(\text{fl})} c} = -\frac{\tau_{\text{GL}}(\epsilon)}{m^* c} \sim -\frac{k_B \xi^2}{c \hbar} \frac{1}{\epsilon}, \quad (16)$$

which dramatically exceeds Sondheimer’s value. These strong fluctuation effects are a consequence of the extremely strong dependence of the chemical potential of FCPs on temperature and the relatively small concentration of FCPs.

B. Quantum fluctuations in superconductors above $H_{c2}(0)$

1. Dynamic clustering of fluctuation Cooper pairs

The qualitative picture for SF in the quantum region, at very low temperatures and close to $H_{c2}(0)$, drastically differs from the Ginzburg-Landau one, valid close to T_{c0} . As we saw, the latter can be described in terms of a set of long-wavelength fluctuation modes [with $\lambda \sim \xi_{\text{GL}}(T) \gg \xi_{\text{BCS}}$] of the order parameter, with characteristic lifetime $\tau_{\text{GL}} = \pi \hbar / 8 k_B (T - T_{c0})$. In the former, the order parameter oscillates on much smaller scales, such that fluctuation modes with wavelengths up to ξ_{BCS} and frequencies up to $\Delta_{\text{BCS}} / \hbar$ are excited.

Indeed, one can visualize the situation in this region as rotating FCPs, analogously to Cooper pairs within Abrikosov vortices, just below $H_{c2}(0)$. The period of Cooper pairs rotating in an Abrikosov vortex in that region is $\tau_{\text{cp}} \sim \Omega_{H_{c2}(0)}^{-1} \sim \Delta_{\text{BCS}}$ ($\Omega_H = 4DeH/c$ is the cyclotron frequency of Cooper pairs) and the corresponding Larmor radius is $r_L \sim \xi_{\text{BCS}}$.

The microscopic theory (Galitski and Larkin, 2001a; Glatz, Varlamov, and Vinokur, 2011a) shows that close to $H_{c2}(0)$ at zero temperature SFs are characterized by the lifetime

$$\tau_{\text{QF}} \sim \frac{\Delta_{\text{BCS}}^{-1}}{\hbar} \gg \tau_{\text{cp}}, \quad \tilde{h} = [H - H_{c2}(0)] / H_{c2}(0), \quad (17)$$

and by the spatial scale

$$\xi_{\text{QF}}(\tilde{h}) \sim \frac{\xi_{\text{BCS}}}{\sqrt{\tilde{h}}} \gg \xi_{\text{BCS}}. \quad (18)$$

One sees that the dependence of both these values on the parameter governing the transition is completely symmetric to

that of $\tau_{\text{GL}}(\epsilon)$ and $\xi_{\text{GL}}(\epsilon)$: it is sufficient to note that $\Delta_{\text{BCS}} \sim k_{\text{B}}T_{\text{c}0}$ and to replace the reduced temperature ϵ by the reduced field \tilde{h} .

The strong inequalities obtained allow us to assume that at zero temperature, slightly above $H_{\text{c}2}(0)$, in the normal phase of a type-II superconductor, the regions of superconducting coherence are extended to distances much larger than the size of an Abrikosov vortex and such ‘‘superconducting puddles’’ remain coherent for times much longer than τ_{cp} .

Equation (17) can also be obtained from the uncertainty principle. Indeed, the energy characterizing the proximity to the quantum phase transition is $\Delta E = \hbar\Omega_{\text{H}} - \hbar\Omega_{H_{\text{c}2}(0)} \sim \Delta_{\text{BCS}}\tilde{h}$ and it is this value that should be used in the Heisenberg relation instead of $k_{\text{B}}(T - T_{\text{c}0})$, as was done in the vicinity of $T_{\text{c}0}$. The spatial coherence scale $\xi_{\text{QF}}(\tilde{h})$ can be estimated from the value of τ_{QF} analogously to the case close to $T_{\text{c}0}$. Indeed, two electrons with given phase shift starting from the same point get separated by the distance

$$\xi_{\text{QF}}(\tilde{h}) \sim (D\tau_{\text{QF}})^{1/2} \sim \xi_{\text{BCS}}/\sqrt{\tilde{h}},$$

after time τ_{QF} .

In order to clarify the physical meaning of τ_{QF} and ξ_{QF} , we note that near the quantum phase transition (QPT) at zero temperature, where $H \rightarrow H_{\text{c}2}(0)$, the fluctuations of the order parameter $\Delta^{(\text{n})}(\mathbf{r}, t)$ become highly inhomogeneous, contrary to the situation near $T_{\text{c}0}$. Indeed, slightly below $H_{\text{c}2}(0)$ (but in the region where the notion of vortices is still adequate), the spatial distribution of the order parameter reflects the existence of an Abrikosov vortex lattice with average spacing

$$a(H) = \xi_{\text{BCS}}/\sqrt{H/H_{\text{c}2}(0)} \rightarrow \xi_{\text{BCS}}.$$

Therefore, one expects that close to and above $H_{\text{c}2}(0)$ the fluctuation order parameter $\Delta^{(\text{n})}(\mathbf{r}, t)$ also has a ‘‘vortexlike’’ spatial structure varying on the scale of ξ_{BCS} . This structure is preserved for the lifetime of the superconducting puddle, which is of the order of τ_{QF} .

In the language of FCPs one can describe this situation in the following way: A FCP at zero temperature and in a magnetic field close to $H_{\text{c}2}(0)$ rotates with the Larmor radius $r_{\text{L}} \sim \xi_{\text{BCS}}$, which represents its effective size. During time τ_{QF} two initially selected electrons participate in multiple fluctuating Cooper pairings, maintaining their coherence. The coherence length $\xi_{\text{QF}}(\tilde{h}) \gg \xi_{\text{BCS}}$ is thus a characteristic size of a cluster of such coherently rotating FCPs (which we called a superconducting puddle), and τ_{QF} estimates the lifetime of such a flickering cluster. One can view the whole system as an ensemble of flickering domains of coherently rotating FCPs, precursors of vortices (see Fig. 6).

Let us return to the scenario of ‘‘defragmentation’’ of the Abrikosov lattice by fluctuations in view of the described qualitative picture of SF in the regime of the QPT. Approaching $H_{\text{c}2}(0)$ from below, puddles of fluctuating vortices, which are nothing other than FCPs rotating in the magnetic field, are formed. Their characteristic size is $\xi_{\text{QF}}(|\tilde{h}|)$, and they flicker

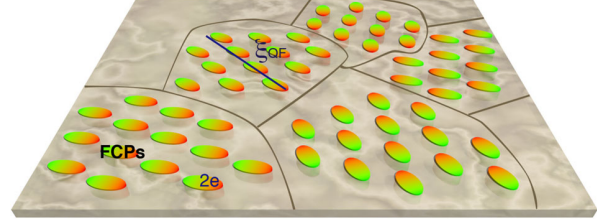


FIG. 6. Sketch of the cluster structure of fluctuation Cooper pairs above the upper critical field. From Glatz, Varlamov, and Vinokur, 2011b.

with characteristic time $\tau_{\text{QF}}(|\tilde{h}|)$. At this stage supercurrents still can flow through the sample until these puddles do not break the last percolating superconducting channel. The magnetic field for this to happen determines the value of the second critical field renormalized by QFs: $H_{\text{c}2}^*(0) = H_{\text{c}2}(0)[1 - 2\text{Gi}_{(2)} \ln(1/\text{Gi}_{(2)})]$ (Larkin and Varlamov, 2009). Above this field, no supercurrent can flow through the sample anymore—i.e., one reaches the normal state of a type-II superconductor.

Nevertheless, as demonstrated by our previous estimates, the properties of the normal phase are also affected by quantum fluctuations. The fragments of the Abrikosov lattice can still be observed in the normal phase as can be demonstrated by the following *gedanken experiment*: Clusters of rotating FCPs (*exvortices*) of size ξ_{QF} with some kind of the superconducting order should be found in the background of the normal metal when one takes a picture with exposure time shorter than τ_{QF} . When the exposure time is chosen longer than τ_{QF} the picture is smeared out and no traces of the Abrikosov vortex state can be found. However, what kind of the order can be detected there is still unclear. It would be interesting to identify these clusters as remains of the Abrikosov lattice, but more probably this is some kind of FCP quantum liquid. Indeed, the presence of structural disorder can result in the formation of a hexatic phase close to $H_{\text{c}2}^*(0)$, where the translational invariance no longer exists although it still conserves the orientational order in the vortex positioning (Nelson and Kosterlitz, 1977; Halperin and Nelson, 1978; Nelson and Halperin, 1979).

2. Manifestation of QF above $H_{\text{c}2}(0)$

At zero temperature and fields above $H_{\text{c}2}(0)$, the systematics of fluctuation contributions to conductivity change considerably compared to that close to $T_{\text{c}0}$. The collision-free rotation of FCPs (let us recall that they do not ‘‘feel’’ the presence of elastic impurities, and all information related to electron scattering is already included in the effective mass of the Cooper pairs) results in the absence of a direct contribution to the transverse electric transport along the applied electric field [analogously to the suppression of the one-electron conductivity in strong magnetic fields ($\omega_c\tau \gg 1$): $\sigma_{\text{xx}}^{(\text{e})} \sim (\omega_c\tau)^{-2}$ (Abrikosov, 1988)] and the AL contribution to $\delta\sigma_{(2)}^{(\text{n})}$ vanishes. The anomalous MT and DOS contributions become zero as well but due to different reasons. Namely, the former vanishes since magnetic fields as large as $H_{\text{c}2}(0)$

completely destroy the phase coherence, whereas the latter disappears since the magnetic field suppresses the fluctuation gap in the one-electron spectrum. Therefore the effect of fluctuations on the conductivity at zero temperature is reduced to the renormalization of the one-electron diffusion coefficient. In this region FCPs occupy the lowest Landau level, but all dynamic fluctuations in the frequency interval from 0 to Δ_{BCS} should be taken into account:

$$\sigma_{xx}^{(\text{DCR})} \sim -\frac{e^2}{\Delta_{\text{BCS}}} \int_0^{\Delta_{\text{BCS}}} \frac{d\omega}{\tilde{h} + \hbar\omega/\Delta_{\text{BCS}}} \sim -\frac{e^2}{\tilde{h}} \ln \frac{1}{\tilde{h}}. \quad (19)$$

In terms of the characteristics τ_{QF} and ξ_{QF} for QFs, one can understand the meaning of the QF contributions to different physical values in the vicinity of $H_{c2}(0)$ and derive others, which are essential in this region. For example, one could estimate the direct contribution of the FCPs to conductivity by replacing $\tau_{\text{GL}} \rightarrow \tau_{\text{QF}}$ in the classic AL formula, which would give $\sigma_*^{(\text{AL})} \sim (e^2/\hbar)\tau_{\text{QF}}$. Nevertheless, as already noted, FCPs at zero temperature cannot drift along the electric field but rotate only around fixed centers. As temperature deviates from zero, the FCPs can change their state due to the interaction with the thermal bath, i.e., hopping to an adjacent rotation trajectory along the applied electric field becomes possible. This means that FCPs can participate in longitudinal charge transport as well. This process can be mapped to the paraconductivity of granular superconductors (Lerner, Varlamov, and Vinokur, 2008) at temperatures above T_{c0} , where the tunneling of FCPs between grains occurs in two steps: first one electron jumps, then the second follows. The probability of each hopping event is proportional to the intergrain electron tunneling rate Γ . To conserve the superconducting coherence between both events, the latter should occur in the FCP lifetime τ_{GL} . The probability of FCP tunneling between two grains is determined by the conditional probability of two one-electron hopping events and is given by $W_\Gamma = \Gamma^2\tau_{\text{GL}}$. Returning to the situation of FCPs above $H_{c2}(0)$, one can identify the tunneling rate by the temperature T , while τ_{GL} corresponds to τ_{QF} . In order to get a final expression, $\sigma_*^{(\text{AL})}$ should be therefore multiplied by the probability factor $W_{\text{QF}} = T^2\tau_{\text{QF}}$ of the FCP hopping to a neighboring trajectory:

$$\sigma_{xx}^{(\text{AL})} \sim \frac{e^2}{\tilde{h}} \left(\frac{T}{T_{c0}}\right)^2 \frac{1}{\tilde{h}^2}.$$

In order to estimate the contribution of QFs to the fluctuation magnetic susceptibility of the SC in the vicinity of $H_{c2}(0)$, one can apply Langevin's formula to a coherent cluster of FCPs and identify its average size with the rotator radius; one finds

$$\chi_{(2)}^{(\text{AL})} = \frac{e^2 N_{(2)}^{\text{QF}}}{c^2 m^*} \langle \xi_{\text{QF}}^2(\tilde{h}) \rangle \sim \frac{e^2 \Delta_{\text{BCS}} \xi_{\text{BCS}}^2}{c^2 \tilde{h}}, \quad (20)$$

in complete agreement with Galitski and Larkin (2001a). Here it was assumed that the ratio of the FCP concentration over its mass in the region of quantum fluctuations is

$N_{(2)}^{\text{QF}}/m^* \sim \Delta_{\text{BCS}}$ —with logarithmic accuracy and in analogy to Eq. (7).

Finally, one can reproduce the contribution of QFs to the Nernst coefficient. Close to $H_{c2}(0)$, the chemical potential of FCPs can be written as $\mu^{(\text{QF})} = -\Delta_{\text{BCS}}\tilde{h}$ (in analogy to that one close to T_{c0}). Its temperature derivative differs from zero due to the temperature dependence of $H_{c2}(T)$:

$$d\mu^{(\text{QF})}/dT \sim dH_{c2}(T)/dT \sim -T/\Delta_{\text{BCS}}. \quad (21)$$

Using the relation between the latter and the Nernst coefficient, it is possible to reproduce one of the results of Serbyn *et al.* (2009) (with accuracy up to the numerical factor):

$$\nu^{(\text{QF})} \sim \frac{\tau_{\text{QF}}}{m^*c} \left(\frac{d\mu^{(\text{QF})}}{dT}\right) \sim -\frac{k_{\text{B}}\xi_{\text{BCS}}^2}{c\hbar} \left(\frac{k_{\text{B}}T}{\Delta_{\text{BCS}}}\right) \frac{1}{\tilde{h}}. \quad (22)$$

III. BASIC ELEMENTS OF MICROSCOPIC DESCRIPTION OF SF IN MAGNETIC FIELD

Let us begin by recalling the basic ideas of the microscopic description of fluctuations in the normal phase of a superconductor. For this purpose one can employ the formalism of the Matsubara diagrammatic technique. In the BCS theory, the electron-electron attraction leads to the reconstruction of the ground state of the electron system of a normal metal upon approaching the critical temperature from above ($T \rightarrow T_c^{\text{BCS}} + 0$). Formally, this fact is manifested by the appearance of a pole in the two-particle Green's function

$$L(p, p', q) = \langle T_\tau [\tilde{\psi}_{p+q, \sigma} \tilde{\psi}_{-p, -\sigma}^+ \tilde{\psi}_{p'+q, \sigma}^+ \tilde{\psi}_{-p', -\sigma}^-] \rangle, \quad (23)$$

where $\tilde{\psi}_{p+q, \sigma}$ are electron field operators, T_τ is the time ordering operator, and 4D vector notations for electron momentum (or other quantum numbers) are used. The two-particle Green's function can be expressed in terms of the vertex part (Abrikosov *et al.*, 1965). It is this vertex part of the electron-electron interaction in the Cooper channel $L(\mathbf{q}, \Omega_k)$ that is called the *fluctuation propagator*.

The Dyson equation for $L(\mathbf{q}, \Omega_k)$, accounting for the electron-electron attraction in the ladder approximation, is represented graphically in Fig. 7. The solid lines denote the single-particle Green's functions, and the wavy lines correspond to the fluctuation propagators. The equation can be written analytically as

$$L^{-1}(\mathbf{q}, \Omega_k) = -g^{-1} + \langle\langle \Pi(\mathbf{q}, \Omega_k) \rangle\rangle_{\text{imp}}, \quad (24)$$

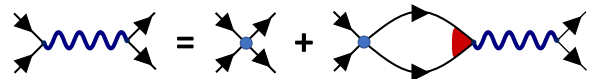


FIG. 7. The Dyson equation for the fluctuation propagator (wavy lines) in the ladder approximation. Solid lines represent one-electron Green's functions, the circles represent the electron-electron interactions, and the triangles correspond to the Cooperons (see Fig. 8).

where the polarization operator $\Pi(\mathbf{q}, \Omega_k)$ is defined as a loop of two single-particle Green's functions in the particle-particle channel⁶:

$$\Pi(\mathbf{q}, \Omega_k) = T \sum_{\varepsilon_n} \int \frac{d^3 \mathbf{p}}{(2\pi)^3} G(\mathbf{p} + \mathbf{q}, \varepsilon_{n+k}) G(-\mathbf{p}, \varepsilon_n). \quad (25)$$

Here $\Omega_k = 2\pi T$ and $\varepsilon_n = (2n + 1)\pi T$ are bosonic and fermionic Matsubara frequencies, the symbol $\langle\langle \dots \rangle\rangle_{\text{imp}}$ denotes averaging over the position of impurities.

Let us emphasize that the two quantities $\mathcal{L}(p, p', q)$ and $L(\mathbf{q}, \Omega_k)$ are closely connected to each other (Larkin and Varlamov, 2009). Upon integration over the momenta p and p' , the former becomes an average of the product of two Fourier components of the superconducting order parameter (Abrikosov *et al.*, 1965):

$$\int dp dp' \mathcal{L}(p, p', q) = \frac{1}{g^2} \langle \Delta_q \Delta_q^* \rangle. \quad (26)$$

From the Dyson equation in the ladder approximation for the two-particle Green's function (23), similar to the one shown in Fig. 7, it follows that the expression in Eq. (26) can be written in terms of the polarization operator Π and the quantity L :

$$\int dp dp' \mathcal{L}(p, p', q) = -\frac{\Pi}{1 - g\Pi} = \frac{\Pi}{g} L. \quad (27)$$

After analytic continuation to real frequencies, the fluctuation propagator $L(\mathbf{q}, i\Omega)$ coincides (up to a constant) with the quantity defined by Eq. (26).

Next we consider a disordered 2D superconductor characterized by the diffusion coefficient $\mathcal{D} = v_F^2 \tau / d_e$, placed in a perpendicular magnetic field H at temperatures $T > T_c(H)$. In order to be in the regime of Gaussian superconducting fluctuations, i.e., to avoid the region of critical fluctuations, the temperature must be above a certain value, which for transport properties is determined by the condition $T/T_c(H) - 1 \gg \sqrt{\text{Gi}_{(2)}(H)}$. The Ginzburg-Levanyuk number close to T_{c0} has the form

$$\text{Gi}_{(2)} = \frac{7\zeta(3)}{32\pi^3} \frac{1}{\rho_e T_{c0} \xi_{(2)}^2}, \quad (28)$$

with a slight dependence on the applied magnetic field away from T_{c0} (Larkin and Varlamov, 2009). Here ρ_e is the one-electron density of states. The Ginzburg-Levanyuk parameter is of the order of $(\rho_e^2 l_s)^{-1}$ on both ends of the line $H_{c2}(T)$ and can reach values of up to 10^{-2} . The constant $\xi_{(2)}$, already introduced in Eq. (4), coincides with the BCS coherence length of Cooper pairs at zero temperature, up to a numerical factor. In the case of a superconductor with impurities, it is related to the electron diffusion coefficient $\xi^2 = \pi \mathcal{D} / 8 T_{c0}$.

⁶In the following we mainly use units with $\hbar = k_B = c = 1$.

We assume for the temperature $T \ll \min\{\tau^{-1}, \omega_D\}$ in order to stay both in the diffusive regime of electron scattering and in the framework of the BCS model (τ is the electron elastic scattering time at impurities). The magnitude of the magnetic field is limited by two conditions: it must (i) remain below the regime of Shubnikov-de Haas oscillations $\Omega_H \tau \lesssim 1 \Leftrightarrow H \lesssim (T_{c0} \tau)^{-1} H_{c2}(0)$, and (ii) stay below the Clogston limit $H \lesssim (\varepsilon_F \tau) H_{c2}(0)$, i.e., $H/H_{c2}(0) \ll \min\{(T_{c0} \tau)^{-1}, \varepsilon_F \tau\}$.

The single-electron state in the magnetic field in the presence of impurity scattering can be described by the Green's function written in the form of a series over Landau state eigenfunctions $\varphi_k(x - \ell_H^2 p_y)$:

$$G(x, x', p_y, p_z, \varepsilon_l) = \sum_k \frac{\varphi_k(x - \ell_H^2 p_y) \varphi_k^*(x' - \ell_H^2 p_y)}{i\tilde{\varepsilon}_l - \xi(k, p_z)}, \quad (29)$$

where $\tilde{\varepsilon}_l = \varepsilon_l + (1/2\tau) \text{sgn} \varepsilon_l$, $\xi(k, p_z) = \omega_c(k + 1/2) + \xi_z(p_z)$ is the quasiparticle energy at the corresponding Landau level (ω_c is its cyclotron frequency), $\ell_H = \sqrt{c\hbar/(eH)}$ is the electron magnetic length, and $\xi_z(p_z)$ is its part related to the motion along the direction of the magnetic field. The latter will be omitted in the discussion of the properties of 2D superconductors. For the energy-independent width of the Landau levels, a closed expression for the Green's function can be obtained by a straightforward summation over quantum numbers or by using Schwinger's proper time method [see, for example, Gusynin, Loktev, and Shvokvyyi (1995)].

In addition to the appearance of the imaginary part of the self-energy in the one-particle Green's function [see Eq. (29)], the effect of coherent electron scattering on impurities results in the renormalization of the vertex part in the particle-particle channel. It is determined by the Dyson equation in the ladder approximation (see Fig. 8).

The details of the derivations can be found in Larkin and Varlamov (2009); here we present only the results necessary for further discussion. The Cooperon shown in Fig. 8 has the following form in the Landau representation:

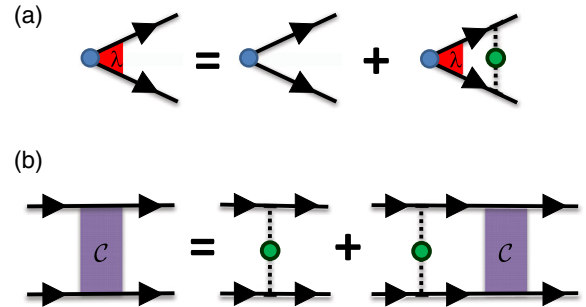


FIG. 8. (a) The Dyson equation for the Cooperon, i.e., the vertex that accounts for the result of averaging over elastic impurity scattering of electrons in the ladder approximation. Solid lines correspond to bare one-electron Green's functions. The dashed line is associated with an impurity correlator $\langle U^2 \rangle = 1/(2\pi\rho_e\tau)$. (b) The analogous Dyson equation for the four-leg Cooperon in the ladder approximation.

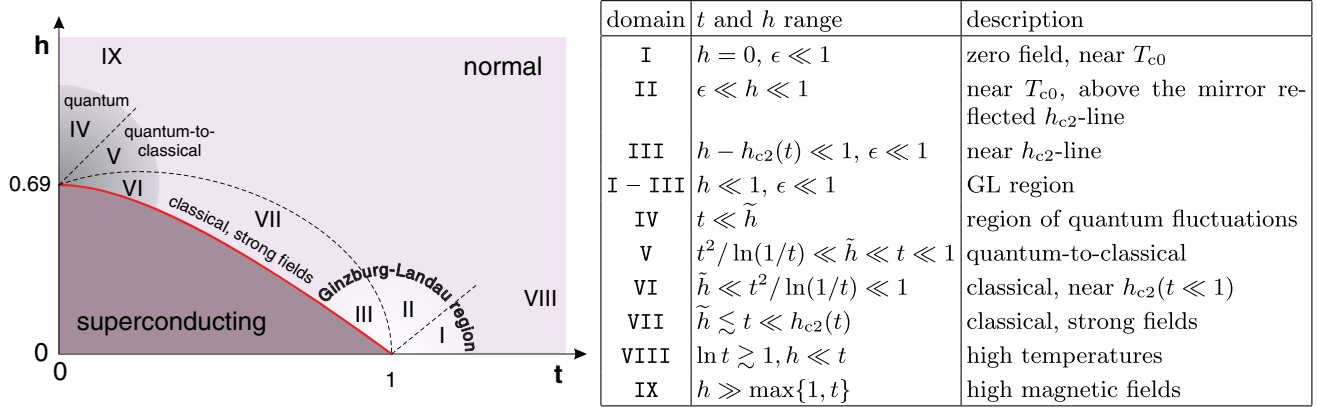


FIG. 9. Left: Schematic representation of the regions of different behavior of superconducting fluctuations in the h - t diagram. From Glatz, Varlamov, and Vinokur, 2011a. Right: Classification of domains in terms of different limits for t and h . Here $\epsilon \equiv \ln t$, $\tilde{h} = [H - H_{c2}(T)]/H_{c2}(T)$; $H > H_{c2}(T)$.

$$\lambda_n(\varepsilon_1, \varepsilon_2) = \frac{\tau^{-1}\theta(-\varepsilon_1\varepsilon_2)}{|\varepsilon_1 - \varepsilon_2| + \Omega_H(n + 1/2) + \tau_\phi^{-1}}, \quad (30)$$

where n is the quantum number of the Landau state of Cooper pairs, $\theta(x)$ is the Heaviside step function, ε_1 and ε_2 are the fermionic frequencies, and τ_ϕ is the phase-breaking time of electron scattering. In the process of impurity averaging, one also encounters the corresponding four-leg vertex, which differs from Eq. (30) only by the factor $\langle U^2 \rangle$:

$$C_n(\varepsilon_1, \varepsilon_2) = \frac{1}{2\pi\rho_e\tau} \frac{\tau^{-1}\theta(-\varepsilon_1\varepsilon_2)}{|\varepsilon_1 - \varepsilon_2| + \Omega_H(n + 1/2) + \tau_\phi^{-1}}. \quad (31)$$

Finally, the expression for the fluctuation propagator in this representation takes the form

$$L_n^{-1}(\Omega_k) = -\rho_e \left[\ln \frac{T}{T_{c0}} + \psi \left(\frac{1}{2} + \frac{|\Omega_k| + \Omega_H(n + 1/2)}{4\pi T} \right) - \psi \left(\frac{1}{2} \right) \right]. \quad (32)$$

An important characteristic property of Eqs. (30)–(32) is that they are valid in a large region of the phase diagram of a superconductor above the line $H_{c2}(T)$ for magnetic fields $H/H_{c2}(0) \ll \min\{(T_{c0}\tau)^{-1}, \varepsilon_F\tau\}$, temperatures $T \ll \min\{\tau^{-1}, \omega_D\}$, frequencies $|\Omega_k| \ll \tau^{-1}$, and Landau levels with $n \ll (T_{c0}\tau)^{-1}$.

In the following, it is convenient to use the dimensionless temperature and magnetic field

$$t = \frac{T}{T_{c0}}, \quad h = \frac{H}{\tilde{H}_{c2}(0)},$$

with the latter normalized by the value of the second critical field obtained by linear extrapolation of its temperature dependence near T_{c0} :

$$\tilde{H}_{c2}(0) = \frac{\Phi_0}{2\pi\xi^2},$$

where $\Phi_0 = \pi/e$ is the magnetic flux quantum. The magnetic field $\tilde{H}_{c2}(0)$ is $8\gamma_E/\pi^2 = 1.45$ times larger than the true second critical field $H_{c2}(0)$:

$$h = \frac{H}{\tilde{H}_{c2}(0)} = \frac{\pi^2}{8\gamma_E} \frac{H}{H_{c2}(0)} = 0.69 \frac{H}{H_{c2}(0)}.$$

In these dimensionless units, the fluctuation propagator (32) acquires the form

$$L_n^{-1}(\Omega_k) = -\rho_e \mathcal{E}_n(t, h, |k|).$$

The function

$$\mathcal{E}_n(t, h, x) \equiv \ln t + \psi \left[\frac{x+1}{2} + \frac{4h}{\pi^2 t} \left(n + \frac{1}{2} \right) \right] - \psi \left(\frac{1}{2} \right) \quad (33)$$

and its derivatives with respect to the argument x ,

$$\begin{aligned} \mathcal{E}_n^{(n)}(t, h, x) &\equiv \frac{\partial^n}{\partial x^n} \mathcal{E}_n(t, h, x) \\ &= 2^{-n} \psi^{(n)} \left[\frac{1+x}{2} + \frac{4h}{\pi^2 t} \left(n + \frac{1}{2} \right) \right], \end{aligned} \quad (34)$$

play an important role for the fluctuation contributions discussed in the following sections, as well as its derivatives with respect to the magnetic field:

$$\begin{aligned} \left(\frac{\partial \mathcal{E}_n}{\partial h} \right) &= \frac{8}{\pi^2 t} \left(n + \frac{1}{2} \right) \mathcal{E}'_n, \\ \left(\frac{\partial^2 \mathcal{E}_n}{\partial h^2} \right) &= \left[\frac{8}{\pi^2 t} \left(n + \frac{1}{2} \right) \right]^2 \mathcal{E}''_n. \end{aligned} \quad (35)$$

Throughout this review we present asymptotic expressions of fluctuation contributions in nine different domains of the phase diagram, shown and described in Fig. 9. Domains I–III encompass the region of temperatures close to T_{c0} and fields $h \ll 1$, corresponding to the regime of classical thermal fluctuations accessible in the GL approach (with some restrictions for fluctuation diamagnetism). The vicinity of the

quantum phase transition at $H = H_{c2}(0)$ is covered by the domains IV–VI: quantum fluctuations in the domain IV gradually acquire thermal nature in domain VI, despite the low temperature ($t \ll 1$). The crossover between the regimes of quantum and classical fluctuations occurs in region V, where $h \sim t$. This part of the phase diagram can be described microscopically in the approximation of the lowest Landau level for the FCP motion. This approach can be extended along the line $H_{c2}(T)$ (domain VII). The high-temperature region VIII, $T_{c0} \ll T$, having also relatively weak fields, $H \ll H_{c2}(0)$, accounts for short-wavelength and dynamic fluctuations. The same is true in the strong magnetic field domain IX.

IV. FLUCTUATION DIAMAGNETISM

A. General expression for magnetic susceptibility

The qualitative estimate of the fluctuation diamagnetic susceptibility in Sec. II demonstrates that for 2D systems, even at high temperatures $T \gg T_{c0}$, it noticeably exceeds the one-electron diamagnetic contribution (Maki, 1973; Bulaevskii, 1974; Aslamazov and Larkin, 1975).

In order to recognize the role of fluctuation diamagnetism in the entire phase diagram of a superconductor beyond the line $H_{c2}(T)$, let us start from the first-order fluctuation correction to the free energy per unit square, graphically represented by Fig. 10. After integration over electronic momenta and summation over corresponding fermionic frequencies, it can be written in the form (Galitski and Larkin, 2001a; Larkin and Varlamov, 2009)

$$F^{(\text{fl})}(H, T) = -T \sum_{\Omega_k} \frac{H}{s\Phi_0} \sum_{m=0} \ln[gL_m^{-1}(\Omega_k)], \quad (36)$$

where s is the film thickness. Equation (36) can be rewritten in dimensionless variables with accuracy up to an irrelevant constant:

$$F^{(\text{fl})}(h, t) = -\frac{T_{c0}}{2\pi s \xi^2} t \sum_{\Omega_k} h \sum_{m=0} \ln \mathcal{E}_m(t, h, |k|). \quad (37)$$

The fluctuation part of the bulk magnetic susceptibility is determined by the negative second derivative of the free energy with respect to magnetic field:

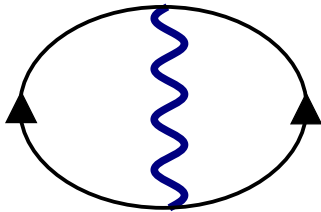


FIG. 10. The first-order fluctuation correction to the free energy. The wavy line represents the fluctuation propagator, and the solid lines with arrows are impurity-averaged normal-state Green's functions.

$$\chi^{(\text{fl})}(h, t) = -\frac{32e^2 \xi^2 T_{c0}}{\pi^3 s} \sum_{\Omega_k} \sum_{m=0}^{M_t} \left(m + \frac{1}{2}\right) \left[\frac{\mathcal{E}'_m}{\mathcal{E}_m(t, h, |k|)} + \frac{4h}{\pi^2 t} \left(m + \frac{1}{2}\right) \frac{\mathcal{E}''_m \mathcal{E}_m - (\mathcal{E}'_m)^2}{\mathcal{E}_m^2(t, h, |k|)} \right], \quad (38)$$

with the cutoff $M_t = 1/tT_{c0}\tau$.

B. Asymptotic analysis

We begin the analysis of the general Eq. (38) with the limit of low temperatures, moving along the line $H_{c2}(T)$ from the point of the quantum phase transition ($T = 0$) to higher temperatures, followed by the limits of high temperatures and high fields away from the $H_{c2}(T)$ line.

1. Region close to the line $H_{c2}(T)$ (domains IV–VII)

In the case of low temperatures $t \ll h_{c2}(t) = H_{c2}(T)/\tilde{H}_{c2}(0)$ one can use the lowest Landau level (LLL) approximation, i.e., restrict the summation over Landau levels in Eq. (38) by the lowest one with $m = 0$. Along the line $h_{c2}(t)$, i.e., when $\tilde{h}(t) \ll 1$, the function \mathcal{E}_0 , Eq. (33), acquires the simple form

$$\mathcal{E}_0(t, h, |k|) = \tilde{h}(t) + \frac{\pi^2 t |k|}{4h_{c2}(t)}. \quad (39)$$

The limit of low temperatures also allows one to replace the sum over Matsubara frequencies by an integral, which was calculated by Galitski and Larkin (2001b):

$$\chi^{(\text{fl})}(t, h) = \frac{12\chi_L l}{s} \left(\frac{8\gamma_E}{\pi^2}\right)^2 h_{c2}^2(t) \left[\frac{1}{2\gamma_E t} \psi' \left(\frac{\tilde{h}}{2\gamma_E t}\right) - \frac{\gamma_E t}{\tilde{h}^2} \right], \quad (40)$$

where $l = v_F \tau$ is the electron mean free path, and $\chi_L = e^2 v_F / 12\pi^2$ is the absolute value of Landau diamagnetic susceptibility ($\gamma_E = e^{\gamma_e}$, where γ_e is the Euler-Mascheroni constant).

Using the asymptotic expression for the ψ function, one obtains the result for the fluctuation magnetic susceptibility close to $H_{c2}(0)$, in the regimes of both quantum and thermal fluctuations (domains IV and VI, respectively):

$$\chi^{(\text{fl})}(t, h) = 12\chi_L \left(\frac{l}{s}\right) \begin{cases} \frac{1}{\tilde{h}} & t \ll \tilde{h}, \\ \frac{\gamma_E t}{\tilde{h}^2} & \tilde{h} \ll t. \end{cases} \quad (41)$$

In the region of quantum fluctuations, $\chi^{(\text{fl})}(t \ll h)$ is temperature independent and describes the diamagnetism generated by clusters of rotating FCPs. Its positive sign and strong dependence of \tilde{h} indicate a rapid decrease of this fluctuation effect as the distance from the critical field increases. Let us stress that the microscopically obtained Eq. (40) is in complete agreement with the evaluation of the contribution of quantum fluctuations to the magnetic susceptibility Eq. (20).

Taking the factor $h_{c2}(t)$ in Eq. (40) into account allows one to obtain the diamagnetic susceptibility in domain VII:

$$\chi^{(n)}(\tilde{h} \ll t \lesssim h_{c2}(t)) = \frac{3 \times 2^9 \chi_L \lambda_E^3}{\pi^4} h_{c2}^2(t) \left(\frac{l}{s}\right) \frac{t}{h^2}. \quad (42)$$

One can see that the fluctuating contribution to magnetic susceptibility remains positive along the line $H_{c2}(T)$ and exceeds the conventional Landau diamagnetism in a very large region of the phase diagram.

2. Limit of weak fields (domains I–III and VIII)

Moving along the line $H_{c2}(T)$ to the region of weak fields, one finds that the summation over Landau levels in the general formula for fluctuation diamagnetic susceptibility, Eq. (38), leads to a divergent result. The problem can be resolved in the case of weak fields by separating the magnetic field-dependent part of the free energy from the temperature background (the meaning of “weak fields” depends on the domain of the phase diagram under consideration). In order to do this, one can apply the Euler-Maclaurin formula

$$\begin{aligned} & \lambda \sum_{m=0}^{\infty} f\left[\lambda\left(m + \frac{1}{2}\right)\right] \\ &= \lambda \int_{-\frac{1}{2}}^{\infty} f\left[\lambda\left(m + \frac{1}{2}\right)\right] dm - \frac{\lambda^2}{24} [f'(\infty) - f'(0)] \end{aligned}$$

to Eq. (37), which gives

$$\frac{4h}{\pi^2 t} \sum_{m=0}^{\infty} \ln \mathcal{E}_m = \int_0^{\infty} \ln \mathcal{E}_{\xi} d\xi - \frac{1}{12} \left(\frac{4h}{\pi^2 t}\right)^2 \frac{\mathcal{E}'_0(t, 0, |k|)}{\mathcal{E}_0(t, 0, |k|)}.$$

The first term does not depend on the magnetic field, and one finds for the diamagnetic susceptibility in the approximation of weak fields

$$\chi^{(n)}(h, t) = -\chi_L \left(\frac{l}{s}\right) \sum_{\Omega_k} \frac{\mathcal{E}'_0(t, 0, |k|)}{\mathcal{E}_0(t, 0, |k|)}. \quad (43)$$

a. Vicinity of T_{c0} (domains I–III)

In the case of temperatures close to T_{c0} and small magnetic fields $h \ll \epsilon \ll 1$ (domain I of the phase diagram), the zero Matsubara frequency in Eq. (43) gives the most singular contribution, leading to the following asymptotic behavior:

$$\chi^{(n)}(h \ll \epsilon) = -\frac{\pi^2}{4} \chi_L \left(\frac{l}{s}\right) \frac{1}{\epsilon}. \quad (44)$$

At higher magnetic fields, when h exceeds the reduced temperature ϵ , Eq. (43) becomes no longer applicable. Yet, the GL approach (Larkin and Varlamov, 2009), valid in the vicinity of T_{c0} , allows one to obtain an expression for the fluctuation susceptibility applicable in the vicinity of the critical temperature (domains I–III):

$$\chi^{(n)}(\epsilon, h \ll 1) = -\frac{3\pi^2}{4} \chi_L \left(\frac{l}{s}\right) \frac{\epsilon}{h^2} \left[1 - \frac{\epsilon}{2h} \psi' \left(\frac{1}{2} + \frac{\epsilon}{2h}\right)\right]. \quad (45)$$

Its asymptotic expression in the weak-field domain I reproduces Eq. (44). At higher fields, in domain II the expansion of Eq. (45) gives

$$\chi^{(n)}(\epsilon \ll h \ll 1) = -\frac{3\pi^2}{4} \chi_L \left(\frac{l}{s}\right) \frac{\epsilon}{h^2}. \quad (46)$$

Finally, in domain III one obtains

$$\chi^{(n)}(\epsilon + h \ll 1) = \frac{3\pi^2}{2} \chi_L \left(\frac{l}{s}\right) \frac{h}{(\epsilon + h)^2}. \quad (47)$$

One can see that the magnetic susceptibility changes its sign between domains II and III as the line $H_{c2}(T)$ is approached.

Equation (47) can be rewritten as the function of the reduced field \tilde{h} , which characterizes the distance from the line $h_{c2}(t)$. Indeed, the value $\epsilon + h$ is nothing else, but the reduced temperature $\epsilon(H) = [T - T_c(H)]/T_c(H)$, with respect to $T_c(H)$. The latter can be expressed in terms of the reduced field $\epsilon(H) = \tilde{h}/h_{c2}(t)$. It is therefore evident that Eq. (47) at $t \sim h_{c2}(t)$ (middle of the domain VII) is in full agreement with Eq. (42), up to a numerical factor. The latter was obtained in the LLL approximation, i.e., using a set of approximations very different from the GL approach.

b. High temperatures (domain VIII)

In the domain of high temperatures $T_{c0} \ll T \ll \tau^{-1}$, one can replace the summation over Matsubara frequencies by an integration. In the 2D case, the integration in Eq. (43) can be performed exactly

$$\chi^{(n)}_{(2)}(T, H) = -2\chi_L \left(\frac{l}{s}\right) \left(\ln \ln \frac{1}{T_{c0}\tau} - \ln \ln \frac{T}{T_{c0}}\right). \quad (48)$$

Here the weak double logarithmic ultraviolet divergence of Eq. (43) was cut off by the applicability limit of the dirty

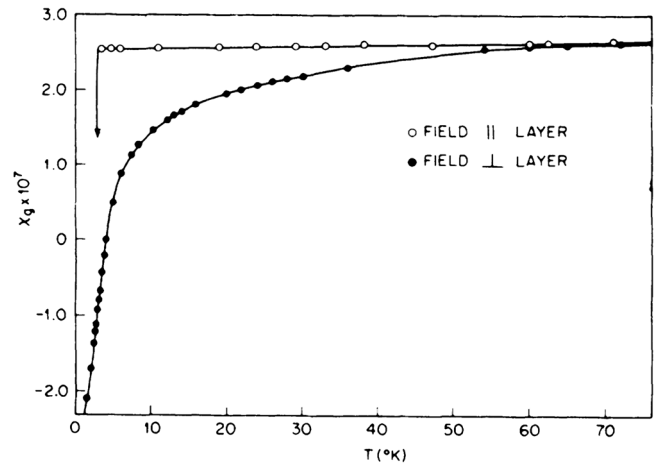


FIG. 11. Magnetic susceptibility per gram of $\text{TaS}_2(\text{pyridine})_{1/2}$ as a function of temperature. $\chi_{\perp}(\chi_{\parallel})$ was measured with the applied field perpendicular (parallel) to the layers. The points above 5 K were taken from several samples and field values between 1 and 8 kOe. No magnetic field dependence within experimental errors (size of the dots) was observed. From Geballe *et al.*, 1971.

superconductor approximation $\Omega_k \sim \tau^{-1}$. This expression was first obtained by [Maki \(1973\)](#) and [Bulaevskii \(1974\)](#). The extremely slow decrease of the fluctuation diamagnetism explains the long tails in the diamagnetic susceptibility observed in intercalated dichalcogenides TaS₂ and NbSe₂ in the early 1970s ([Geballe *et al.*, 1971](#); [Morris and Coleman, 1973](#)); see Fig. 11. The weak magnetic field limit is not restrictive here: $H \ll H_{c2}(0) \ln(T/T_{c0})$. In the 3D case, the ultraviolet divergence is even stronger, yet it can be eliminated by subtracting the corresponding quantity taken at $T \sim T_{c0}$. This yields

$$\chi_{(3)}^{(fl)}(T) = -2\chi_L \frac{\sqrt{T\tau}}{\ln(T/T_{c0})}. \quad (49)$$

$$M(h, T=0) = -\frac{8\gamma_E e^2 \mathcal{D} H_{c2}(0)}{\pi^4 s} h \left[\ln \frac{\ln(1/T_{c0}\tau)}{\ln[(8\gamma_E/\pi^2)h]} - \frac{2}{\pi} \int_0^\infty dx \frac{\ln(1 - e^{-\pi x}) \{ \ln[(8\gamma_E/\pi^2)h] + (1/2) \ln(1 + x^2) \}}{\{ \ln[(8\gamma_E/\pi^2)h] + (1/2) \ln(1 + x^2) \}^2 + \arctan^2 x} \right]. \quad (50)$$

One can see that when the magnetic field approaches $H_{c2}(0)$, the corresponding magnetic susceptibility is determined by the first term in Eq. (50), it is positive, and reproduces the first line of Eq. (41), obtained in the LLL approximation. Domain IX corresponds to the fields $H_{c2}(0) \ll H \ll (e\mathcal{D}\tau)^{-1}$, where $\ln h \gg 1$. Here the magnetic susceptibility changes its sign⁷:

$$\chi^{(fl)}(h, 0) = -\frac{e^2 \mathcal{D}}{\pi^2 s} \left[\ln \ln \frac{1}{T_{c0}\tau} - \ln \ln h \right]. \quad (51)$$

The asymptotic expressions in all domains are summarized in Table I.

A comparison of the susceptibilities obtained from Bulaevskii's approximation (50) and the full expression (38) at very low temperatures is shown in Fig. 12.

It is necessary to note that [Maki and Takayama \(1971\)](#) and [Maki \(1973\)](#) already obtained the large, weakly temperature-dependent, divergent contribution to the fluctuation magnetization in weak fields and they identified it with zero-point oscillations of the FCPs. Bulaevskii demonstrated its occurrence at zero temperature above the second critical field. The question of whether such oscillations exist generated lively discussions in the 1970s; today their existence is commonly accepted, and they are quantum fluctuations that appear when the system approaches the quantum phase transition.

Quantum fluctuations give a noticeable contribution to the diamagnetism of two-dimensional impure superconductors placed in perpendicular fields in a wide range of magnetic fields and temperatures.

C. Fluctuation spectroscopy: Analysis of the isothermal magnetization curves

As an example of the successful application of fluctuation spectroscopy in characterization of specific

⁷With logarithmic accuracy we omitted the factor $8\gamma_E/\pi^2 = 1.45$ under the logarithm in the high-field asymptotic expressions.

3. Limit of very strong fields (domain IX)

The remaining region of very strong fields is the domain of dynamic and short-wavelength fluctuations. It is beyond the limits of applicability of all three approximations used: neither the GL approach nor the LLL approximation, nor the Euler-Maclaurin weak-field expansion is valid there. Following [Maki and Takayama \(1971\)](#), [Bulaevskii \(1974\)](#) transformed the sum over Matsubara frequencies into the contour integral and then applied the generalized Euler-Maclaurin transformation for the summation over Landau levels valid for arbitrary fields. As a result, he obtained the expression for fluctuation magnetization in strong fields $H > H_{c2}(0)$ at zero temperature:

superconducting systems, see [Bernardi *et al.* \(2006\)](#), in which they addressed a particular case of the fluctuation contribution to the diamagnetic response of an assembly of lead nanoparticles of size d , smaller than the coherence length, placed in an insulating matrix above the superconducting critical temperature.

For the fluctuation magnetization of an effectively 0D granule in the GL region $Gi_{(0)} \lesssim \epsilon$, one can write the expression valid for a wide range of magnetic fields $H \ll H_{c2}(0)$ ([Larkin and Varlamov, 2009](#))

$$M_{(0)}(\epsilon, H) = -\frac{6\pi T \xi^2}{5\Phi_0^2 d} \frac{H}{\epsilon + (\pi^2 \xi^2 / 10 \Phi_0^2) H^2 d^2}. \quad (52)$$

In accordance with Eq. (52), the fluctuation magnetization turns out to be negative and linear in the magnetic field up to some crossover-temperature-dependent upper critical field of the granule

$$H_{c2(0)}(\epsilon) \sim \frac{\Phi_0}{d \xi(\epsilon)} \sim \frac{\xi}{d} H_{c2}(0) \sqrt{\epsilon}$$

where it reaches a minimum. At higher fields, $H_{c2(0)}(\epsilon) \lesssim H \ll H_{c2}(0)$, the fluctuation magnetization of

TABLE I. Asymptotic expressions in the different domains shown in Fig. 9.

Domain	$\chi_{(2)}^{(fl)}/(\chi_L \frac{L}{s})$
I–III	$-\frac{3\pi^2}{4} \frac{\epsilon}{h^2} [1 - \frac{\epsilon}{2h} \psi'(\frac{1}{2} + \frac{\epsilon}{2h})] = \frac{\pi^2}{4} \begin{cases} -\frac{1}{\epsilon}, & \text{I} \\ -\frac{3\epsilon}{h^2}, & \text{II} \\ \frac{6h}{(\epsilon+h)^2}, & \text{III} \end{cases}$
IV–VII	$12 (\frac{8\gamma_E}{\pi^2})^2 h_{c2}^2(t) [\frac{1}{2\gamma_E t} \psi'(\frac{\tilde{h}}{2\gamma_E t}) - \frac{\gamma_E t}{h^2}] = 12 \begin{cases} \frac{1}{h}, & \text{IV} \\ \frac{\gamma_E t}{h^2}, & \text{VI} \\ 0.252 h_{c2}^2(t) \frac{t}{h^2}, & \text{VII} \end{cases}$
VIII	$-2(\ln \ln \frac{1}{T_{c0}\tau} - \ln \ln t)$
IX	$-2(\ln \ln \frac{1}{T_{c0}\tau} - \ln \ln h)$

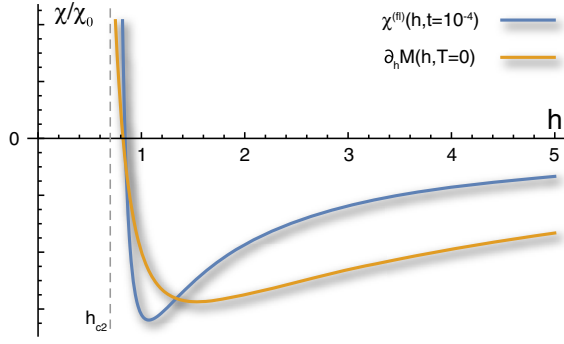


FIG. 12. Fluctuation contribution to the susceptibility of a 2D impure superconductor at low temperatures as a function of the magnetic field above h_{c2} . The solid blue (darker) line shows the behavior of Eq. (38) at $t = 10^{-4}$, while the solid orange (lighter) line shows the approximate expression at zero temperature obtained from Eq. (50) as $\partial_h M(h, T=0)$. Both curves show similar asymptotic behavior in domains IV and IX. The units of χ are arbitrary.

the OD granule is inversely proportional to the magnetic field.

In Fig. 13, we present isothermal magnetization curves from Lascialfari and Rigamonti (2017). The average size of the

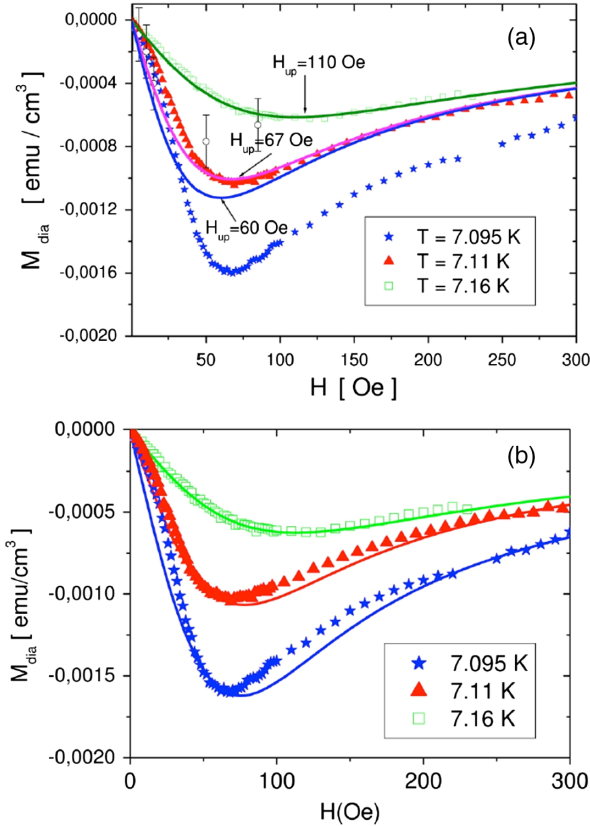


FIG. 13. Magnetization curves above $T_{c0} = 7.09 \pm 0.005$ K for the Pb sample with average particle diameters $d = 75$ nm. (a) The experimental data are compared to the theoretical curves obtained in the GL quadratic approximation [see Eq. (52)]. (b) The same experimental data are compared with the predictions done using the complete GL functional. From Lascialfari and Rigamonti, 2017.

particles, calculated based on the analysis of the up-turn field, was found to be in excellent agreement with direct experimental measurements. In the immediate vicinity of the transition, the authors observed a deviation of the experimental curves from the predictions of the quadratic GL approximation. Yet these data (even the curve corresponding to $T = 7.095$ K) turned out to be in good agreement with the curves of fluctuation magnetization obtained using the complete GL functional including the fourth order term (Larkin and Varlamov, 2009).

V. FLUCTUATION CONDUCTIVITY

A. General expression for fluctuation conductivity

In the standard Kubo formalism, the electric current is related to the vector potential by means of the electromagnetic response operator

$$j_\alpha = - \int Q_{\alpha\gamma}(\mathbf{r}, \mathbf{r}', t, t') \mathbf{A}_\gamma(\mathbf{r}', t') d\mathbf{r}' dt'. \quad (53)$$

In the framework of the diagrammatic technique at finite temperatures, the latter is graphically represented by a loop diagram comprised of two-electron Green's functions connected through electromagnetic vertices.

Taking fluctuation pairing into account leads to a renormalization of the Green's functions and the vertices by interactions in the Cooper channel (see Fig. 7), with additional averaging over impurity positions. This results in ten leading-order corrections to the electromagnetic response operator shown in Fig. 14, each containing a small parameter of the fluctuation theory [Ginzburg-Levanyuk number, Eq. (28)] as a prefactor.

The fluctuation correction to conductivity is determined by the imaginary part of the sum of all these diagrams:

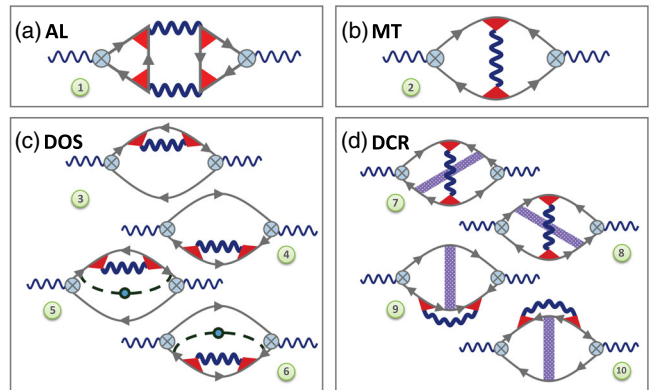


FIG. 14. Feynman diagrams for the leading-order contributions to the electromagnetic response operator. Wavy lines correspond to fluctuation propagators [Eq. (32)], solid lines with arrows represent impurity-averaged normal-state electron Green's functions, crossed circles are electric field vertices, dashed lines with a circle represent additional impurity renormalizations, and triangles and dotted rectangles are impurity ladders accounting for the electron scattering at impurities [Cooperons, see Eqs. (30) and (31)]. From Glatz, Varlamov, and Vinokur, 2011a.

$$\sigma^{(n)}(T, H) = -\lim_{\omega \rightarrow 0} \frac{\text{Im}Q^{(n)}(\omega, T, H)}{\omega}. \quad (54)$$

As mentioned, the effect of SF on conductivity close to the superconducting critical temperature T_{c0} is typically discussed in terms of three major contributions: the Aslamazov-Larkin process, corresponding to the opening of a new channel for the charge transfer (Aslamazov and Larkin, 1968), the anomalous Maki-Thompson process, which describes single-particle quantum interference at impurities in the presence of SFs (Maki, 1968; Thompson, 1970), and the change of the single-particle DOS due to their involvement in the pairing of FCPs (Dorin *et al.*, 1993; Ioffe *et al.*, 1993). The AL and MT processes result in the appearance of positive singular contributions to conductivity (diagrams 1 and 2 in Fig. 14). In contrast, the DOS process depletes single-particle excitations at the Fermi level and leads to a decrease of the Drude conductivity (diagrams 3–6 in Fig. 14). The latter contribution is less singular in temperature than the first two and can compete with them only if the AL and MT processes are suppressed (for example, in the case of c -axis transport in layered superconductors). Diagrams 7–10 represent the renormalization of the diffusion coefficient (DCR diagrams) due to the presence of fluctuations, which are nonsingular close to T_{c0} in two and three dimensions.

These results were first obtained for the vicinity of T_{c0} and later generalized to temperatures far from the transition (Aslamazov and Varlamov, 1980; Larkin, 1980; Altshuler, Reizer, and Varlamov, 1983) and to high magnetic fields (Lopes dos Santos and Abrahams, 1985). In 2D superconductors the slowly (double-logarithmically) decreasing contributions described by diagrams 3–10 start to dominate far from the critical temperature ($T \gg T_{c0}$). Later, the effect of quantum fluctuations on conductivity was studied. Beloborodov and Efetov (1999) and Beloborodov, Efetov, and Larkin (2000)

found that in granular superconductors at very low temperatures and close to $H_{c2}(0)$, the singular AL contribution decays as T^2 , while the fluctuation suppression of the quasiparticle DOS at zero temperature results in a negative contribution to conductivity, which grows logarithmically in magnitude for $H \rightarrow H_{c2}(0)$. In Sec. X.D, we come back to the case of granular superconductors.

The effects of quantum fluctuations on the magnetoconductivity of 2D superconductors, close to zero temperatures, were studied by Galitski and Larkin (2001a). In this work, all ten diagrams shown in Fig. 14 were analyzed in the LLL approximation, which is valid close to the critical line $H_{c2}(T)$. A nontrivial nonmonotonic temperature dependence of the fluctuation conductivity at fields close to $H_{c2}(0)$ was found and, analogously to the situation in granular SCs close to zero temperature, the fluctuation contribution is shown to be negative, i.e., QFs increase *resistivity* and not conductivity—in contrast to the behavior close to T_{c0} .

The problem of calculating the fluctuation conductivity of a disordered 2D superconductor placed in a perpendicular magnetic field was revisited ten years later in the frameworks of two different approaches by Glatz, Varlamov, and Vinokur (2011b) (the Matsubara diagrammatic technique) and Tikhonov, Schwiete, and Finkel'stein (2012) (the quantum transport equation). In these papers exact calculations (without the use of the LLL approximation) were performed in the first order of perturbation theory, valid in the entire H - T phase diagram beyond the superconducting region, i.e., for fields and temperature obeying $H \geq H_{c2}(T)$ or, equivalently, $T \geq T_{c0}(H)$.⁸

The complete expression for the fluctuation correction to in-plane conductivity $\sigma_{xx}^{(n)}(T, H)$ of a disordered 2D SC in a perpendicular magnetic field that holds in the T - H phase diagram beyond the line $H_{c2}(T)$ has the form (Glatz, Varlamov, and Vinokur, 2011a, 2011b)

$$\begin{aligned} \sigma_{xx}^{(n)}(t, h) = & \underbrace{\frac{e^2}{\pi} \sum_{m=0}^{M_l} (m+1) \int_{-\infty}^{\infty} \frac{dx}{\sinh^2 \pi x} \left\{ \frac{[\text{Re}^2(\mathcal{E}_m - \mathcal{E}_{m+1}) - \text{Im}^2(\mathcal{E}_m - \mathcal{E}_{m+1})] \text{Im}\mathcal{E}_m \text{Im}\mathcal{E}_{m+1}}{|\mathcal{E}_m|^2 |\mathcal{E}_{m+1}|^2} \right\}}_{\sigma_{xx}^{(AL)+}} \\ & - \underbrace{\frac{\text{Re}(\mathcal{E}_m - \mathcal{E}_{m+1}) \text{Im}(\mathcal{E}_m - \mathcal{E}_{m+1}) (\text{Im}\mathcal{E}_m \text{Re}\mathcal{E}_{m+1} + \text{Im}\mathcal{E}_{m+1} \text{Re}\mathcal{E}_m)}{|\mathcal{E}_m|^2 |\mathcal{E}_{m+1}|^2}}_{+\sigma_{xx}^{(AL)}} \\ & + \underbrace{\frac{e^2}{\pi} \left(\frac{h}{t}\right) \sum_{m=0}^{M_l} \frac{1}{\gamma_\phi + (2h/t)(m+1/2)} \int_{-\infty}^{\infty} \frac{dx}{\sinh^2 \pi x} \frac{\text{Im}^2 \mathcal{E}_m}{|\mathcal{E}_m|^2}}_{\sigma_{xx}^{(MT,an)} + \sigma_{xx}^{(MT,reg2)}} + \underbrace{\frac{e^2}{\pi^4} \left(\frac{h}{t}\right) \sum_{m=0}^{M_l} \sum_{k=-\infty}^{\infty} \frac{4\mathcal{E}_m''(t, h, |k|)}{\mathcal{E}_m(t, h, |k|)}}_{\sigma_{xx}^{(MT,reg1)}} \\ & + \underbrace{\frac{4e^2}{\pi^3} \left(\frac{h}{t}\right) \sum_{m=0}^{M_l} \int_{-\infty}^{\infty} \frac{dx}{\sinh^2 \pi x} \frac{\text{Im}\mathcal{E}_m \text{Im}\mathcal{E}_m'}{|\mathcal{E}_m|^2}}_{\sigma_{xx}^{(DOS)}} + \underbrace{\frac{4e^2}{3\pi^6} \left(\frac{h}{t}\right)^2 \sum_{m=0}^{M_l} \left(m + \frac{1}{2}\right) \sum_{k=-\infty}^{\infty} \frac{8\mathcal{E}_m'''(t, h, |k|)}{\mathcal{E}_m(t, h, |k|)}}_{\sigma_{xx}^{(7-10)}}, \quad (55) \end{aligned}$$

where $\gamma_\phi = \pi/(8T_{c0}\tau_\phi)$.

This complete expression allows for a straightforward numerical evaluation and to derive asymptotic expressions in all of its qualitatively different domains. A typical example

⁸The calculations were done within the model constraints specified in Sec. III and beyond the critical region.

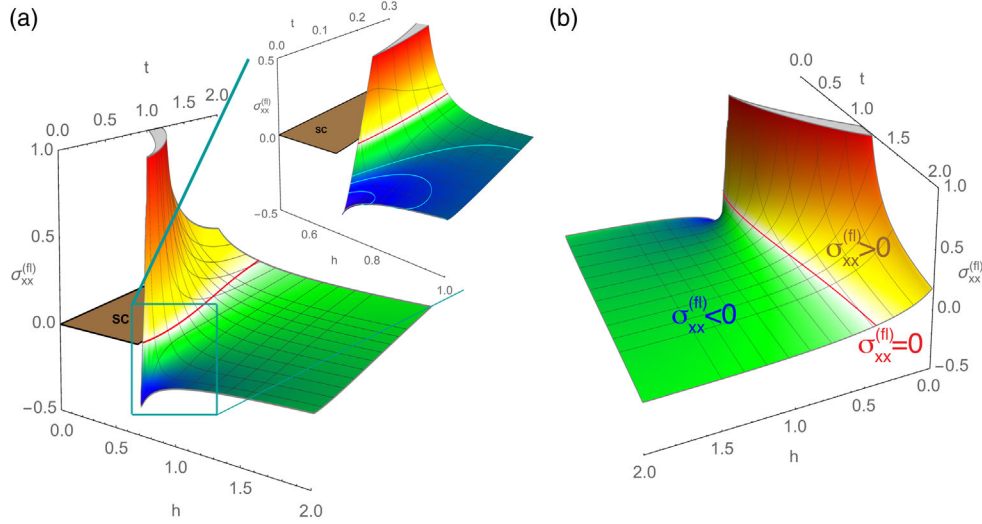


FIG. 15. Fluctuation correction to conductivity (FC) $\sigma_{xx}^{(f)}(t, h)$ as a function of the reduced temperature $t = T/T_{c0}$ and magnetic field $h = 0.69H/H_{c2}(0)$ plotted as the surface. The FC changes its sign along the thick red (black) line [$\sigma_{xx}^{(f)}(t, h) = 0$]. The superconducting region is marked by “SC.” Here $\sigma_{xx}^{(f)}$ is plotted for constant $\tau T_{c0} = 10^{-2}$ and $\tau_{\phi} T_{c0} = 10$. (a) A view at the quantum region at low temperatures, and the inset shows a closeup of the trough with a few negative contour lines [cyan (light gray)]. (b) A view at the high-temperature region.

of the surface $\sigma_{xx}^{(f)}(T, H)$ is plotted in Fig. 15. It demonstrates the important fact that the fluctuation conductivity is positive only in the domain bound by the lines $H_{c2}(T)$ and $\sigma_{xx}^{(f)}(T, H) = 0$ and negative throughout the rest of the phase diagram [see Fig. 5, showing the domains of different overall signs of $\sigma_{xx}^{(f)}(T, H)$ and contours of constant $\sigma_{xx}^{(f)}$ in the whole phase diagram]. Contrary to a common perception, the fluctuation correction to conductivity is only positive in weak fields. The region in which $\sigma_{xx}^{(f)}$ is positive depends on the (positive) anomalous MT contribution (i.e., on the value of the phase-breaking time τ_{ϕ}). With increasing magnetic field, the temperature interval where $\sigma_{xx}^{(f)}(T, H) > 0$ shrinks and vanishes close to $H_{c2}(0)$. As a result, the fluctuation conductivity exhibits a highly nontrivial behavior at low temperatures. Near the QPT, the surface $\sigma_{xx}^{(f)}(T, H)$ has a trough-shaped structure with a “sink” at the point ($H = H_{c2}(0), T = 0$) and the dependence $\sigma_{xx}^{(f)}(T, H = \text{const})$ is nonmonotonic. This feature is also observed in experiments, which we review later.

Figure 5 gives an overview of the entire phase diagram where the leading fluctuation contributions to magnetoconductivity are indicated. In particular, near T_{c0} the singular contributions (paraconductivity, anomalous MT, and DOS) determine the overall behavior, while in the QF region they become zero as $\sim T^2$ [cf. Beloborodov and Efetov (1999), Beloborodov, Efetov, and Larkin (2000), and Mineev and Sigrist (2001)] and the leading contribution comes from the sum of diagrams 7–10 and the regular part

of the MT diagram (Glatz, Varlamov, and Vinokur, 2011a), which are usually ignored.⁹

B. Asymptotic analysis

Asymptotic expressions of Eq. (55) for fluctuation conductivity throughout the entire h - t phase diagram are summarized in Table II.

We begin their discussion with domains I–III, corresponding to the Ginzburg-Landau region of fluctuations close to T_{c0} and in zero magnetic field (domain I). The contribution of diagrams 7–10 was analyzed by Glatz, Varlamov, and Vinokur (2011a) and is also discussed here. It was usually ignored in the literature, since it does not diverge close to T_{c0} . Nevertheless, its constant contribution $\sim \ln \ln (T_{c0}\tau)^{-1}$ is necessary for matching the GL results with the neighboring domains VIII and IX. Domains II and III are still described by the GL theory in weak magnetic fields and Eq. (55) reproduces all asymptotic expressions found in the literature.

⁹Here we note that there is some controversy regarding the origin of the logarithmic singularity in $\sigma_{xx}^{(f)}(t \ll \tilde{h})$ (Galitski and Larkin, 2001a; Glatz, Varlamov, and Vinokur, 2011a; Tikhonov, Schwieta, and Finkel’stein, 2012). The asymptotic expression for the fluctuation conductivity in the QF region is the same in all three works. However, in Galitski and Larkin (2001a) and Tikhonov, Schwieta, and Finkel’stein (2012) all ten diagrams of Fig. 14 contribute to the logarithm, while Glatz, Varlamov, and Vinokur (2011a) states that the quantum phase transition in conductivity is governed only by the sum of diagrams 7–10 and the regular part of the MT diagram and all other contributions in this domain cancel out.

TABLE II. Asymptotic expressions for the fluctuation corrections to conductivity in different domains of the phase diagram.

Domain	$\sigma_{xx}^{(n)}$
I–III	$\underbrace{\frac{e^2}{2\epsilon} \left(\frac{\epsilon}{2h}\right)^2 [\psi(\frac{1}{2} + \frac{\epsilon}{2h}) - \psi(\frac{\epsilon}{2h}) - \frac{h}{\epsilon}]}_{\sigma_{xx}^{(AL)}} + \underbrace{\frac{e^2}{8} \frac{1}{\epsilon - \gamma_\phi} [\psi(\frac{1}{2} + \frac{\epsilon}{2h}) - \psi(\frac{1}{2} + \frac{\gamma_\phi}{2h})]}_{\sigma_{xx}^{(MT,an)}} - \underbrace{\frac{28\zeta(3)e^2}{\pi^4} [\psi(\frac{1}{2h}) - \psi(\frac{1}{2} + \frac{\epsilon}{2h})]}_{\sigma_{xx}^{(MT,reg)} + \sigma_{xx}^{(DOS)}} + \underbrace{\frac{e^2}{3\pi^2} \ln \ln \frac{1}{T_{c0}\tau}}_{\sigma_{xx}^{(DCR)}}$ $= \begin{cases} \frac{e^2}{16\epsilon} + \frac{e^2}{8(\epsilon - \gamma_\phi)} \ln \frac{\epsilon}{\gamma_\phi} - O[\ln(\frac{1}{\epsilon})] + \frac{e^2}{3\pi^2} \ln \ln \frac{1}{T_{c0}\tau}, & \text{I} \\ (1 + \frac{\pi^2}{4}) \frac{e^2}{8h} - O[\ln(\frac{1}{h})] + \frac{e^2}{3\pi^2} \ln \ln \frac{1}{T_{c0}\tau}, & \text{II} \\ \frac{e^2}{2h(\epsilon+h)} + \frac{e^2}{3\pi^2} \ln \ln \frac{1}{T_{c0}\tau}, & \text{III} \end{cases}$
IV–VII	$\begin{cases} -\frac{2e^2}{3\pi^2} \ln \frac{1}{h} - \frac{2\gamma_E e^2}{3\pi^2} \frac{t}{h} + O[(\frac{t}{h})^2], & \text{IV} \\ \frac{4\gamma_E e^2}{3\pi^2} \frac{t}{h}, & \text{V} \\ \frac{e^2}{6} \frac{t}{h(t)}, & \text{VI, VII} \end{cases}$
VIII	$-\frac{2e^2}{3\pi^2} (\ln \ln \frac{1}{T_{c0}\tau} - \ln \ln t) + \frac{0.05e^2}{\ln^2 t} \ln(1.82\gamma_\phi) + \frac{0.12e^2}{\ln^3 t}$
IX	$-\frac{2e^2}{3\pi^2} (\ln \ln \frac{1}{T_{c0}\tau} - \ln \ln h) - \frac{0.11e^2}{\ln^2(2h/\pi^2)} (\frac{t}{h})^2 + \frac{0.03e^2}{\ln^3(2h/\pi^2)} (\frac{t}{h})^2$

In the domain of quantum fluctuations (IV) (see Fig. 5), the AL paraconductivity term (which is the leading, singular contribution close to T_{c0}) decays with decreasing temperature as T^2 . The same happens with the anomalous MT contribution, which in that domain is equal to the AL contribution. Moreover, it is exactly canceled by the negative contribution of the four DOS-like diagrams 3–6:

$$\sigma_{xx}^{(AL)} = \sigma_{xx}^{(MT,an)} = -\sigma_{xx}^{(DOS)} = \frac{4e^2\gamma_E^2 t^2}{3\pi^2 h^2}. \quad (56)$$

The total fluctuation contribution to conductivity $\sigma_{xx}^{(n)}$ in this important region ($t \ll \tilde{h}$) turns out to be negative and at zero temperature diverges logarithmically when the magnetic field approaches $H_{c2}(0)$. The nontrivial fact following from Eq. (55) is that an increase of temperature at a fixed magnetic field mainly results in a further decrease of conductivity in this domain

$$\sigma_{xx}^{(n)} = -\frac{2e^2}{3\pi^2} \ln \frac{1}{\tilde{h}} - \frac{2\gamma_E e^2}{3\pi^2} \frac{t}{\tilde{h}} + O\left[\left(\frac{t}{\tilde{h}}\right)^2\right]. \quad (57)$$

Only at the boundary with domain V, when $t \sim \tilde{h}$, the fluctuation conductivity $\sigma_{xx}^{(n)}$ passes through a minimum and starts to increase. Such nonmonotonic behavior of the conductivity close to $H_{c2}(0)$ was observed multiple times in experiments (Gantmakher *et al.*, 2003; Leridon *et al.*, 2007; Jin *et al.*, 2008; Caprara *et al.*, 2009).

Domain V describes the transition regime between quantum and classical fluctuations, while in domains VI–VII [along the line $H_{c2}(T)$] superconducting fluctuations already have a classical character and can be considered in a generalized time-dependent Ginzburg-Landau (TDGL) scheme (Mineev and Sigrist, 2001).

Finally, in the peripheral domain VIII, the direct positive contribution of fluctuation Cooper pairs (AL) to conductivity decays faster than all the others: $\sim \ln^{-3}(T/T_{c0})$. We stress that

this result differs from the evaluation of the AL paraconductivity far from the transition of Aslamasov and Varlamov (1980), but is in complete agreement with the high-temperature asymptotic expression for the paraconductivity of a clean 2D superconductor (Reggiani, Vaglio, and Varlamov, 1991). This agreement seems natural: FCP transport is insensitive to impurity scattering. The anomalous MT contribution decays as $\sim \ln \gamma_\phi^{-1} / \ln^{-2}(T/T_{c0})$, in complete agreement with Aslamasov and Varlamov (1980) and Larkin (1980). The contribution of diagrams 3–6 also decays as $\ln^{-2}(T/T_{c0})$, but without the large factor $\ln \gamma_\phi^{-1}$. Finally, the regular MT contribution together with the ones from diagrams 7–10 decays extremely slowly, in fact double logarithmically:

$$\sigma_{xx}^{(DCR)} = -\frac{2e^2}{3\pi^2} \left(\ln \ln \frac{1}{T_{c0}\tau} - \ln \ln \frac{T}{T_{c0}} \right). \quad (58)$$

Up to the numerical prefactor this expression coincides with the results of Aslamasov and Varlamov (1980) and Altshuler, Reizer, and Varlamov (1983).

C. Fluctuation spectroscopy: Analysis of the conductivity

1. Manifestation of different contributions to conductivity

Equation (55) provides a basis for a fluctuation spectroscopy of superconductors. This means the extraction of microscopic parameters of a measured sample based on the analysis of fluctuation corrections. In the case of $\sigma_{xx}^{(n)}$ one can extract four parameters: T_{c0} , $H_{c2}(0)$, the elastic scattering time τ , and the (temperature-dependent) phase-breaking time $\tau_\phi(T)$. In particular, the critical temperature T_{c0} and critical field $H_{c2}(0)$ can be precisely determined as opposed to the often used rule “half width of transition” for T_{c0} , while the elastic scattering time can also be obtained from the normal-state properties of the superconductor. In case of phase-breaking time $\tau_\phi(T)$, an analysis of the fluctuation correction

is an invaluable tool for the study of its temperature dependence.

In general, the total conductivity of the disordered system is the sum of the bare Drude conductivity σ_0 , corrections due to quantum interference of the electron waves [weak localization (WL)] which impede the electrons' propagation, corrections from the interaction between particles with close momenta [diffusion channel (ID)], and superconducting fluctuations:

$$\sigma = \sigma_0 + \sigma^{(WL)} + \sigma^{(ID)} + \sigma_{xx}^{(fl)}, \quad (59)$$

where the fluctuation part itself consists of the contributions from Fig. 14. Drude conductivity, ID, and WL corrections are subtracted from the measured conductivity, such that Eq. (55) can then be used to fit the fluctuation corrections.

The exemplary surface of $\sigma_{xx}^{(fl)}(T, H)$ presented in Fig. 15 for $T_{c0}\tau = 10^{-2}$ and $T_{c0}\tau_\phi = 10$ shows that the value of τ_ϕ determines the behavior of fluctuation corrections only in the region of low fields. It is convenient to analyze Fig. 15 side by side with Fig. 5 where contour lines $\sigma_{xx}^{(fl)}(T, H) = \text{const}$ throughout the phase diagram are shown. It is interesting to note that the numerical analysis of Eq. (55) shows that the logarithmic asymptotic Eq. (57) is valid only within an extremely narrow field range $\tilde{h} \lesssim 10^{-6}$.

Figure 16 shows detailed plots of two particular curves of $\sigma_{xx}^{(fl)}(T, H)$, which illustrate the different contributions from Figs. 14(a)–14(d). These are curves for $T_{c0}\tau_\phi = 5$ at lowest

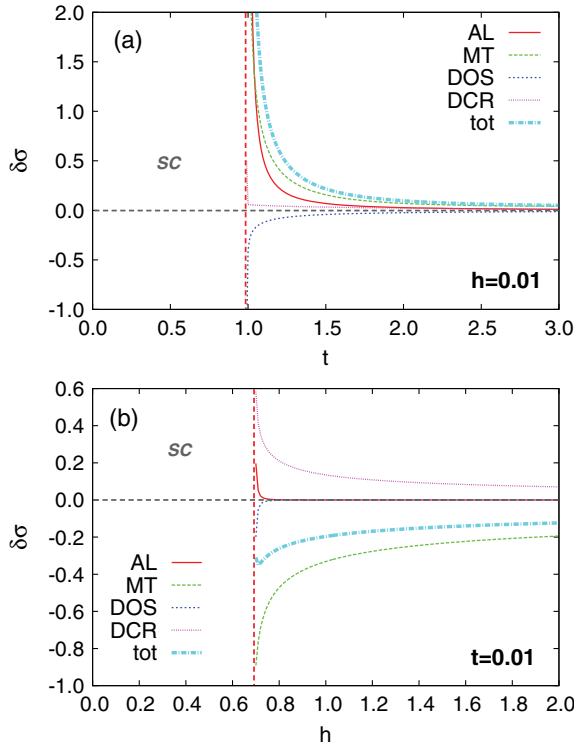


FIG. 16. Fluctuation-conductivity contributions: AL, MT, DOS, DCR, and total (tot) for $T_{c0}\tau = 10^{-3}$ and $T_{c0}\tau_\phi = 5$. (a) The temperature dependence at low field $h = 0.01$, and (b) the field dependence at low temperature $t = 0.01$. From Glatz, Varlamov, and Vinokur, 2011a.

magnetic field $h = 0.01$ [Fig. 14(a)] and temperature $t = 0.01$ [Fig. 14(b)]. Figure 14(a) reproduces the asymptotic expressions near T_{c0} given in Table II, and one can see that the contribution from diagrams 7–10 is negligible. However, in the quantum regime the latter becomes the dominating contribution [Fig. 14(b)], rendering the total fluctuation conductivity negative. It is canceled only very close to the QPT by the MT contribution.

Despite Eq. (55) being a closed expression, its specific evaluation in the most general case requires sophisticated numerical summation and integration. We describe the more technical aspect of fluctuation spectroscopy at the end of this review in Sec. XI.

2. Observation of fluctuation conductivity in experiments

The usefulness of the fluctuation-spectroscopy approach was shown for several experimental systems. Here we review a few of them in some detail.

a. Indium oxide films

In Glatz, Varlamov, and Vinokur (2011a) resistivity measurements of thin disordered indium oxide films, presented by Steiner and Kapitulnik (2005), were fitted by Eq. (55). Figure 17 shows the low-temperature data for one sample [referred to as “weak” in Steiner and Kapitulnik (2005)] of a film with thickness 30 nm, transition temperature $T_{c0} = 3.35$ K, and critical magnetic field $B_{c2}(0) = 13$ T. The resistivity was measured, depending on magnetic field, for low-temperature values $T = 200, 300, 400,$ and 500 mK. The theoretical expression for $\sigma_{xx}^{(fl)}$ is plotted using fitting parameter values $B_{c2}(0) = 13.7$ T, $T_{c0}\tau_\phi = 5 \pm 1$, and the experimentally found value of $T_{c0} = 3.35$ K. Overall, the fitted $\sigma_{xx}^{(fl)}$ curves show good agreement with the results of the measurements.

As mentioned, τ_ϕ usually depends on temperature, such that for a better fit one needs first to analyze FC data at constant

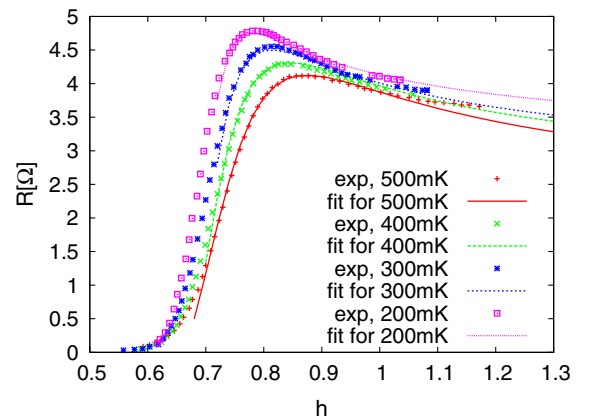


FIG. 17. Comparison to resistivity measurements in thin indium oxide films. The experimental data were taken from Fig. 4(a) of Steiner and Kapitulnik (2005) for the “weak” sample with thickness 30 nm, $T_{c0} = 3.35$ K, and $B_{c2}(0) = 13$ T. The resistivity R for temperatures 0.2, 0.3, 0.4, and 0.5 K was fitted using Eq. (55) with the experimentally found T_{c0} . For $B_{c2}(0)$ a slightly larger value of 13.7 T and $T_{c0}\tau_\phi = 5 \pm 1$ were used. From Glatz, Varlamov, and Vinokur, 2011a.

temperatures to extract $\tau_\phi(T)$ and then fit temperature-dependent data. This way one can obtain precise values for the parameters T_{c0} , $H_{c2}(0)$, and $\tau_\phi(T)$, which would be difficult to determine otherwise. In many cases it is useful to choose the parameter

$$\delta = \pi\hbar/(8k_B T\tau_\phi) \quad (60)$$

as a fitting parameter, since often $\tau_\phi \propto T^{-1}$, such that δ becomes temperature independent. This parameter is related to γ_ϕ in Eq. (55) by $\gamma_\phi = \tau\delta$.

b. Fluctuations in ultrathin TiN films

A rather detailed fluctuation-spectroscopy study was presented by [Baturina et al. \(2012\)](#), showing how one can extract the real BCS critical temperature from a measurement. In particular, it was demonstrated how an omission of the Maki-Thompson contribution leads to incorrect values of T_{c0} . In that work, the conductivity measured in thin (≤ 5 nm) TiN films was analyzed and we review the work here in some depth.

In thin films, σ in Eq. (59) refers to the conductance rather than to conductivity and the WL and ID corrections can be written as

$$\sigma^{(WL)} + \sigma^{(ID)} = \sigma_{00} A \ln [k_B T\tau/\hbar], \quad (61)$$

with $A = ap + A^{(ID)}$. Here $\sigma_{00} = e^2/(2\pi^2\hbar)$, $a = 1$ if spin-orbit scattering is neglected ($\tau_\phi \ll \tau_{so}$) or $a = -1/2$ when scattering is relatively strong ($\tau_\phi \gg \tau_{so}$), p is the exponent in the temperature dependence of the phase coherence time $\tau_\phi \propto T^{-p}$, and A_{ID} is a constant depending on the Coulomb screening and which in all cases remains of the order of unity ([Finkel'shtein, 1983](#)). At low temperatures where electron-electron scattering dominates one gets $p = 1$ and at higher temperatures, where the electron-phonon interaction becomes relevant, $p = 2$. This is in agreement with experimental observations ([Bruynseraede et al., 1983](#); [Gershenson, Gubankov, and Zhuravlev, 1983](#); [Raffy et al., 1983](#); [Bergmann, 1984](#); [Gordon, Lobb, and Tinkham, 1984](#); [Santhanam and Prober, 1984](#); [Brenig et al., 1986](#); [Gordon and Goldman, 1986](#); [Wu and Lin, 1994](#)), where $1 \leq p \leq 2$, with $p = 1$ at $T < 10$ K.

In Fig. 18(c) the ratio T_{\max}/T_{c0} as a function of δ [see Eq. (60)] is plotted for the three most common experimental situations where $A = 3, 2$, and 0.5 , corresponding to three sets of parameters (a, p, A_{ID}) in Eq. (61): $(1, 2, 1)$, $(1, 1, 1)$, and $(-1/2, 1, 1)$. It is noteworthy that the maximum lies in the domain where the SFs are dominated by the Maki-Thompson contribution and that the maximum itself arises from the competition between the WL + ID and MT processes. In general, T_{\max}/T_{c0} vs δ curves relate the quantity T_{\max} , which is the only characteristic point in the $R(T)$ dependence, to the transition temperature T_{c0} and as such can serve as a set of calibrating curves for an easy determination of T_{c0} , since A can be estimated from the analysis of the resistance behavior at high temperatures.

In Fig. 19(a), the temperature dependences of the resistance per square for four TiN films with different room temperature

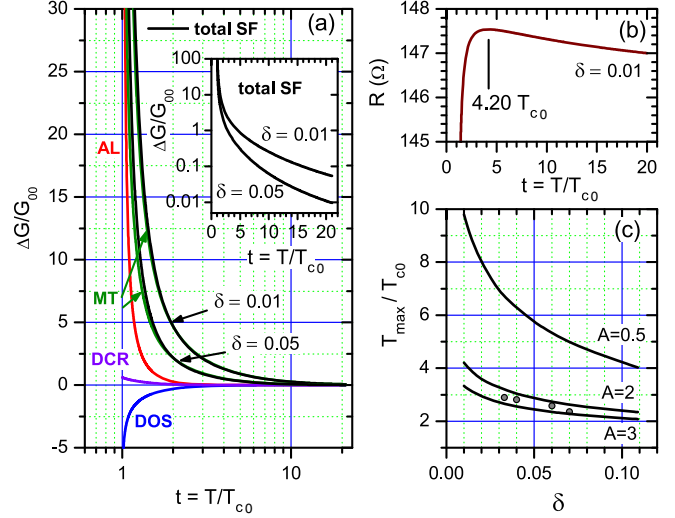


FIG. 18. (a) Temperature dependences of superconducting-fluctuation contributions to conductance [in units of $G_{00} = \sigma_{00} = e^2/(2\pi^2\hbar)$]. The curves for AL, DOS, and DCR processes are universal functions of reduced temperature $t = T/T_{c0}$, the MT contribution is presented for $\delta = 0.01$ and 0.05 . The solid black lines are the sum of all SF contributions Eq. (55). The inset shows the same total SF contribution on a logarithmic scale. (b) Resistance vs reduced temperature (see details in the text). (c) The set of the curves T_{\max}/T_{c0} vs δ for different coefficients A from Eq. (61). The circles represent the measured T_{\max} , T_{c0} , and δ obtained by fitting the experimental data. From [Baturina et al., 2012](#).

resistances are shown and in Fig. 19(b) the temperature behavior of the conductance. Solid fitting lines in Figs. 19(a) and 19(b) account for all quantum contributions.

The fitting captures all major features of the observed dependences: their nonmonotonic behavior, the position and the height of R_{\max} , and the gradual decrease in the resistance perfectly matching the experimental points down to values $R \ll R_{\max}$ [without any additional assumptions about mesoscopic inhomogeneities ([Ioffe and Larkin, 1981](#); [Caprara et al., 2011](#))]. In this study three fitting parameters δ , A , and T_{c0} were used. Note that varying δ and A significantly shifts the temperature position and the value of R_{\max} , it does not change the position of T_{c0} noticeably. It demonstrates the fact that $\sigma_{xx}^{(n)}$ does not depend on the pair-breaking parameter δ in the close vicinity of T_{c0} [see the inset of Fig. 18(a) where the curves for different δ merge].

At this point it is instructive to review the approaches for inferring T_{c0} from the experimental data that were frequently used in the past. From Fig. 19(c) one sees that T_c lies at the “foot” of the $R(T)$ curve where $R(T) \approx (0.08-0.13)R_{\max}$. Therefore, the determination of T_{c0} as the temperature where $R(T)$ drops to $0.5R_N$ (let alone to $0.9R_N$) significantly overestimates T_{c0} . Another frequently used procedure ([Fiory, Hebard, and Glaberson, 1983](#)) is based on the assumption that the effect of quantum corrections can be reduced to the AL term only, i.e., that the resistance obeys the relation $R^{-1} = R_N^{-1} + R_{AL}^{-1}/(T/T_{c0} - 1)$, where $R_{AL}^{-1} = e^2/(16\hbar) = 1.52 \times 10^{-5} \Omega^{-1}$. This implies that a range of temperatures near T_{c0} exists, where the plot $[(R^{-1} - R_N^{-1})^{-1}/R_{AL}]$ vs T can be approximated by a straight line with a

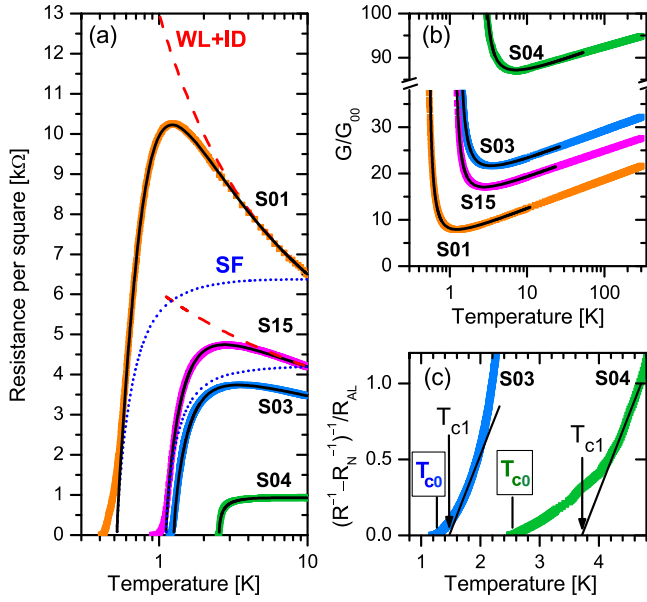


FIG. 19. (a) Resistance per square vs temperature for four different TiN film samples, labeled S_{xx} . Solid lines: fits accounting for all corrections. Dashed lines (marked as WL + ID): separate contribution of the sum of weak localization and interaction in the diffusion channel to the resistance of the samples S01 and S15. Dotted lines (SF): contribution of superconducting fluctuations. (b) The same data as in (a), but extended to room temperatures and replotted as the dimensionless conductance ($G/G_{00} = \sigma/\sigma_{00}$). The semilogarithmic scale representation reveals a logarithmic decrease of the conductance with temperature due to the WL and ID effects. (c) Reduced conductance $(R^{-1} - R_N^{-1})^{-1}/R_{AL}$ ($R_{AL}^{-1} = e^2/16\hbar$ and $R_N = R_{max}$) vs T . The linear fit to the AL expression (solid lines) is often used for the determination of T_{c0} and generally gives incorrect (much too high) values of the critical temperature, shown here for samples S03 and S04 (marked by arrows). The correct values of T_{c0} obtained through fluctuation spectroscopy are framed and marked by vertical bars. From Baturina *et al.*, 2012.

slope of 1. The intersection of this line with the T axis would have defined T_{c0} . Utilizing this approach for the data of the two samples plotted in Fig. 19(c) yields temperatures of the intersections marked as T_{c1} . One sees, however, that this procedure also gives too high values for the superconducting critical temperatures.

We remark that the used fluctuation spectroscopy does not explain all features of the measured conductance curves, e.g., possible effects of Berezinskii-Kosterlitz-Thouless (BKT) physics (Beasley, Mooij, and Orlando, 1979; Halperin and Nelson, 1979) even above T_{c0} , glassy behavior (Feigel'man, Ioffe, and Mézard, 2010; Sacépé *et al.*, 2011), or spatial inhomogeneities in the films (Caprara *et al.*, 2013) are not taken into account. In fact, the BKT transition was studied as well by Baturina *et al.* (2012) and it was shown that in the analyzed samples the BKT transition temperature follows the universal relation found by Beasley, Mooij, and Orlando (1979). However, the effect of the BKT transition on corrections to conductivity above T_{c0} is negligible in this case.

In conclusion, Baturina *et al.* (2012) showed that the real microscopic parameters for thin superconducting films

obtained by fluctuation spectroscopy can be significantly different than qualitative estimations.

c. Transverse magnetoresistance above $H_{c2}(0)$

Fluctuation spectroscopy can also be used to analyze the transverse magnetoresistance observed in the layered organic superconductor κ -(BEDT-TTF) $_2X$ above $H_{c2}(0)$ at low temperatures (Pratt *et al.*, 1993; Kartsovnik *et al.*, 1999; Zuo, Schlueter, and Williams, 1999) and explain its nonmonotonic behavior. The motion of FCPs in the z direction in such a system has a hopping character and the quasiparticle spectrum can be assumed to have the form of a corrugated cylinder. Close to T_{c0} the fluctuation magnetoconductivity tensor in this model was already studied in detail by Dorin *et al.* (1993). In this work it was demonstrated that the transverse paraconductivity in that case is suppressed by the square of the small anisotropy parameter $(\xi_z/\xi_x)^2$, while the dependence on the reduced temperature ϵ is considerably more singular than that of the in-plane paraconductivity. In terms of the Ginzburg-Landau FCP lifetime (1), it can be written as

$$\sigma_{zz}^{(AL)}(\epsilon) = \frac{4e^2\xi_z^4}{\pi^2\xi_x^2s^3}T_{c0}^2\tau_{GL}^2(\epsilon), \quad (62)$$

where s is the interlayer distance. In principle this result could be obtained even from the Drude formula applied to the FCP charge transfer [see how Eq. (9) for $\sigma_{xx}^{(AL)}(\epsilon)$ was obtained] combined with the above speculations regarding the hopping of FCPs along the z axis (Lerner, Varlamov, and Vinokur, 2008). This general approach, which does not involve the GL scheme, allows one to map Eq. (62) on the case of the QPT by just replacing $\tau_{GL}(\epsilon) \rightarrow \tau_{QF}(\tilde{h})$:

$$\sigma_{zz}^{(AL)}(\tilde{h}) = \frac{4e^2\xi_z^4}{\xi_x^2s^3}T_{c0}^2\tau_{QF}^2(\tilde{h}) = \frac{4e^2\xi_z^4}{\xi_x^2s^3}\left(\frac{\gamma_E}{\pi}\right)^2\frac{1}{\tilde{h}^2}.$$

The negative contribution appearing from the diffusion coefficient renormalization competes with the positive $\sigma_{zz}^{(AL)}(\tilde{h})$. The only difference between the in-plane [see Eqs. (57) and (58)] and the z -axis components of this one-particle contribution consists in the anisotropy factor $\langle v_z^2 \rangle / v_x^2 = \xi_z^2 / \xi_x^2$. As a result one gets

$$\sigma_{zz}^{(DCR)} = -\frac{2e^2}{3\pi^2}\frac{\xi_z^2}{s\xi_x^2}\ln\frac{1}{\tilde{h}}$$

and the total fluctuation correction to the z -axis magnetoconductivity at zero temperature above $H_{c2}(0)$ can be written as

$$\sigma_{zz}^{(fl)} = \frac{2e^2\xi_z^2}{3\pi^2\xi_x^2s}\left[1.94\left(\frac{\xi_z}{s}\right)^2\frac{1}{\tilde{h}^2} - \ln\frac{1}{\tilde{h}}\right]. \quad (63)$$

Glatz, Varlamov, and Vinokur (2011a) used Eq. (63) for the analysis of data taken from Kartsovnik *et al.* (1999) on the magnetoresistance of the layered organic superconductor κ -(BEDT-TTF) $_2Cu(NCS)_2$ at the temperature $T = 1.7$ K, much below $T_{c0} \approx 9.5$ K, but at magnetic fields above

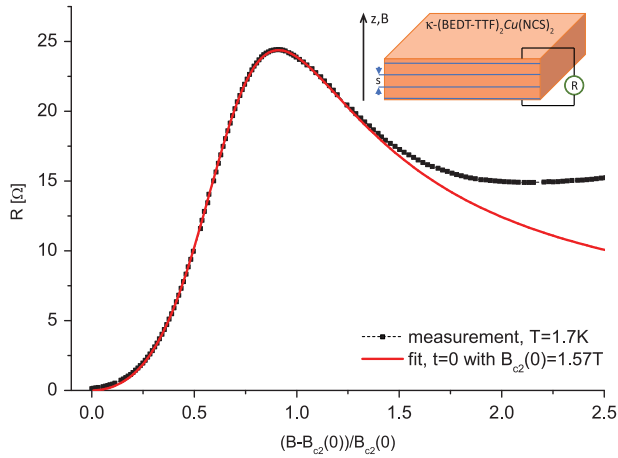


FIG. 20. Comparison to resistivity measurements of the layered organic superconductor κ -(BEDT-TTF) $_2$ Cu(NCS) $_2$. The material has a transition temperature of $T_{c0} \approx 9.5$ K, $B_{c2}(0) \approx 1.57$ T, and $\tau = 1.7$ ps. This experimental curve is taken at $T = 1.7$ K and fitted by Eq. (63), which is in perfect agreement with the experiment. The inset shows a sketch of the measurement setup. From Glatz, Varlamov, and Vinokur, 2011a.

$B_{c2}(0) \approx 1.57$ T. In this measurement the magnetic field and current were applied perpendicular to the layers. The experimental curve was fitted by $0.23(0.18/\tilde{h}^2 + \ln \tilde{h})$; see Fig. 20. For the material parameters of this compound, they reported $\tau = 1.7$ ps, $\xi_z = 0.3$ – 0.4 nm, and $s = 1$ nm. The fitting shown in Fig. 20 corresponds to the ratio $\xi_z/s = 0.32$ and looks rather convincing.

The discrepancy appearing between the theoretical and experimental curves in the high-field region was attributed to the large normal-state magnetoresistance, reflecting the specifics of the cyclotron orbits on the multiconnected Fermi surface of the compound (due to the low crystal symmetry it is quite difficult to fit).

VI. FLUCTUATION HALL CONDUCTIVITY

A. Fluctuation Hall effect and the special role of particle-hole asymmetry

It is known that interacting electronic systems with simple band structure do not exhibit the Hall effect without impurity scattering (Aronov, Hikami, and Larkin, 1995). So how does the presence of superconducting fluctuations lead to a nonzero Hall resistance?

The FCP contribution to the Hall effect was first mentioned by Abrahams, Prange, and Stephen (1971), where the effect of the magnetic field on fluctuations above T_{c0} was studied in the framework of the time-dependent GL theory. They recognized that the nonzero fluctuation correction to the Hall conductivity appears only if an additional term proportional to frequency is included in the nonstationary GL equation. They have introduced an imaginary part of the diffusion coefficient without going into a detailed discussion about its origin. Ullah and Dorsey (1991) extended the phenomenological consideration of the effect of fluctuations on the Hall

conductivity for the wide range of magnetic fields by applying the Hartree approximation. They attributed the imaginary part, which is responsible for particle-hole asymmetry, to the coefficient in front of the time derivative in the time-dependent GL equation, which is mathematically equivalent to the approach taken by Abrahams, Prange, and Stephen (1971). Later, Aronov and Rapoport (1992) expressed the parameter characterizing particle-hole asymmetry of superconducting fluctuations through the derivative of the critical temperature with respect to the quasiparticle chemical potential, $\partial T_{c0}/\partial \mu$ at the Fermi level, without any assumptions concerning the microscopic nature of superconductivity.

Simultaneously with Abrahams *et al.*, Fukuyama, Ebisawa, and Tsuzuki (1971) approached the problem of the fluctuation Hall conductivity in the framework of a microscopic theory. They found that the fluctuation correction to σ_{xy} , as in the case of the intrinsic effect in a normal metal, is proportional to $\partial \rho_e / \partial E|_{E=\mu}$, i.e., it differs from zero only when the electron-hole asymmetry is taken into account.

Finally, Aronov, Hikami, and Larkin (1995) demonstrated that, due to the requirement of the gauge invariance of the time-dependent GL theory, the only form in which the particle-hole asymmetry can manifest itself in the fluctuation propagator (32) is through the appearance of the term $(i\Omega_k/\pi^2)\partial \ln T_{c0}/\partial \mu$ side by side with the modulus of the boson frequency $|\Omega_k|$.

In addition to the small particle-hole asymmetry factor, the fluctuation correction to the Hall conductivity contains the small parameter $G_{(d)}$ related to the weakness of superconducting fluctuations. This explains why the first experimental evidence of the pronounced effect of fluctuations on the Hall conductivity was reported only when high-temperature superconductors came into the focus of investigations (Galffy and Zirngiebl, 1988; Artemenko, Gorlova, and Latyshev, 1989; Forro and Hamzić, 1989; Iye, Nakamura, and Tamegai, 1989; Hagen *et al.*, 1990). In these materials, the Ginzburg-Levanyuk number can be as large as 10^{-2} due to their effectively two-dimensional structure. Moreover, the fluctuation Hall conductivity acquires a stronger singularity upon approaching T_{c0} [$\propto \epsilon^{-2}$ (Varlamov and Livanov, 1990; Ullah and Dorsey, 1991) instead of $\propto \epsilon^{-3/2}$ (Fukuyama, Ebisawa, and Tsuzuki, 1971) for 3D superconductors]. As a result, the Hall resistance exhibits a distinct deviation from the linear temperature dependence expected in the normal state, up to temperatures of about $2T_{c0}$ (Paalanen, Hebard, and Ruel, 1992; Hagen *et al.*, 1993; Graybeal, Luo, and White, 1994; Samoilov, 1994; Smith *et al.*, 1994; Lang *et al.*, 1995; Liu *et al.*, 1997; Kokubo, Aarts, and Kes, 2001). At temperatures near T_{c0} , a sign reversal of the Hall conductivity was observed.

Note that the electron-hole asymmetry in the band structure is not the only effect that can lead to the appearance of a nonzero fluctuation correction to Hall conductivity. It has been shown (Angilella *et al.*, 2003) that its sign and the value can depend on the topological structure of the Fermi surface. Evidence for a universal behavior of the Hall conductivity as a function of doping, which can change the topology of the Fermi surface, has been reported in the cuprate superconductors (Nagaoka *et al.*, 1998).

B. Microscopic theory of fluctuation Hall effect

Formally, similar to the diagonal component of conductivity, the fluctuation correction to the Hall conductivity is described by the same ten diagrams depicted in Fig. 14, but with one of the vertices being $e\hat{v}_y$ instead of $e\hat{v}_x$. Historically, the AL process, corresponding to an independent channel of charge transfer, was studied the most, since it is the dominant contribution in the GL regime, domains I–III near T_{c0} (Abrahams, Prange, and Stephen, 1971; Fukuyama, Ebisawa, and Tsuzuki, 1971; Inoue *et al.*, 1979; Ullah and Dorsey, 1990, 1991; Varlamov and Livanov, 1990; Aronov and Rapoport, 1992).

First we discuss the physical meaning of the Hall resistivity ρ_{xy} . In the case of only one type of carriers, it depends on their concentration n and turns out to be independent of the electron diffusion coefficient $\rho_{xy} = H/(en)$. The fluctuation processes of MT and DCR types contribute to the diffusion coefficient, so their expected contribution to the Hall resistivity is zero. For the Hall conductivity in a weak field one can write

$$\begin{aligned}\sigma_{xy} &= \rho_{xy}\sigma_{xx}^2 = \rho_{xy}\sigma_{xx}^{(n)2} + 2\rho_{xy}\sigma_{xx}^{(n)}\sigma_{xx}^{(fl)} \\ &= \sigma_{xy}^{(n)}\left(1 + 2\frac{\sigma_{xx}^{(fl)}}{\sigma_{xx}^{(n)}}\right).\end{aligned}\quad (64)$$

This means the relative fluctuation correction to the Hall conductivity is twice as large as the fluctuation correction to the diagonal component. This qualitative consideration was confirmed by a direct calculation of the MT diagram (Fukuyama, Ebisawa, and Tsuzuki, 1971).

A complete theory of the fluctuation Hall effect was recently developed by Michaeli, Tikhonov, and Finkel'stein (2012). In agreement with Aronov, Hikami, and Larkin (1995), they introduced the particle-hole asymmetry parameter $\zeta = -(1/2)\partial \ln T_{c0}/\partial \mu$ in the propagator of superconducting fluctuations as follows:

$$\begin{aligned}\tilde{L}_n^{-1}(\Omega_k) &= -\rho_e \left[\ln \frac{T}{T_{c0}} + \psi \left(\frac{1}{2} + \frac{|\Omega_k| + \Omega_H(n+1/2)}{4\pi T} \right) \right. \\ &\quad \left. - \psi \left(\frac{1}{2} \right) + \zeta \Omega_k \right].\end{aligned}\quad (65)$$

The fact that the term linear in Ω_k appears outside the argument of the polygamma function is related to the smallness of ζ and the condition $|\Omega_k| \leq \tau^{-1}$ which allows one to expand the ψ function with respect to $\zeta\Omega_k$ and to arrive at Eq. (65), which results in the total contribution from the aforementioned ten diagrams being proportional to $\zeta\Omega_H$.

Michaeli, Tikhonov, and Finkel'stein (2012) supported this qualitative statement and demonstrated that the sum of the contributions of the two DOS diagrams, 5 and 6 in Fig. 14, the MT diagram and all DCR diagrams is equal to zero for all H and T above the transition line $H_{c2}(T)$ (their combined effect can be reduced to a renormalization of the diffusion coefficient). It is therefore sufficient to consider only the AL contribution and the two remaining DOS contributions, 3 and 4.

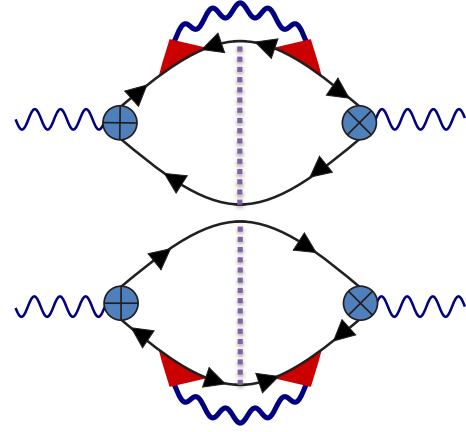


FIG. 21. Two additional Feynman diagrams giving leading-order contributions to the Hall conductivity. The solid lines represent the electron Green's function, the wavy lines represent the fluctuation propagator, and the red (dark gray) triangles represent electron scattering at impurities. In addition, the dotted purple (gray) lines take into account the flux enclosed by the paths of all charged excitations. The x and y vertices are marked by $+$ and \times , respectively. All other diagrams are similar to the conductivity diagrams of Fig. 14, but with different vertices.

Michaeli, Tikhonov, and Finkel'stein (2012) also considered two usually disregarded diagrams, shown in Fig. 21, which also contribute a leading-order correction to the Hall conductivity. This additional contribution is proportional to the cyclotron frequency of quasiparticles $\omega_c^{(qp)}$. It turns out to be dominant at high temperatures $T \gg T_{c0}$. Note that the correction to the diagonal component of fluctuation conductivity $\sigma_{xx}^{(fl)}$ from these two diagrams contains an additional small prefactor $T\tau$ and does not contribute to the leading order.

C. Asymptotic analysis and comparison to experiments

1. Region close to the line $H_{c2}(T)$

In the vicinity of the superconducting phase transition line at small enough magnetic fields $h \ll t$, the leading correction to σ_{xy} is produced by the AL diagram:

$$\sigma_{xy}^{(fl)}(h, t) = \frac{2e^2\zeta T_{c0}\rho(0)}{\pi} \text{sgn}(h)t \sum_n (n+1) \frac{[\tilde{L}_n(0) - \tilde{L}_{n+1}(0)]^3}{[\tilde{L}_{n+1}(0) + \tilde{L}_n(0)]^2}.\quad (66)$$

This correction is negative due to the fact that $\zeta < 0$ for a superconducting film with three-dimensional electrons and a simple electron spectrum, and has a nonmonotonic dependence on the applied magnetic field, reaching a peak at $h^* = 1.3e$ in the close vicinity of T_{c0} .

The experimental results of Breznay *et al.* (2012) for the fluctuation correction to the Hall conductivity in ultrathin disordered films of TaN_x , calculated by subtracting the normal (linear in magnetic field) component from the total measured conductivity, are in excellent agreement with a fitting based on the AL correction, Eq. (66), which is dominant over a wide range of magnetic fields and temperatures in a region around the transition, as shown in Fig. 22.

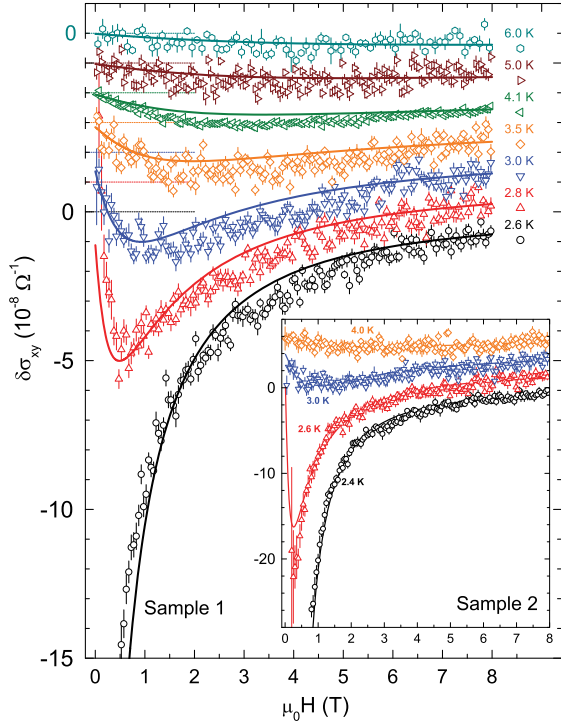


FIG. 22. Experimental results for fluctuation Hall conductivity in two samples of TaN_x as a function of the applied magnetic field for a range of temperatures near $T_c(H)$. The fitting is done in accordance with Eq. (66). From Breznay *et al.*, 2012.

In another recent experimental study Breznay and Kapitulnik (2013) also observed a significant fluctuation contribution to the Hall resistance (less the normal linear contribution) at $T > T_c(H)$. The results indicate the existence of a peak Hall resistance due to superconducting fluctuations

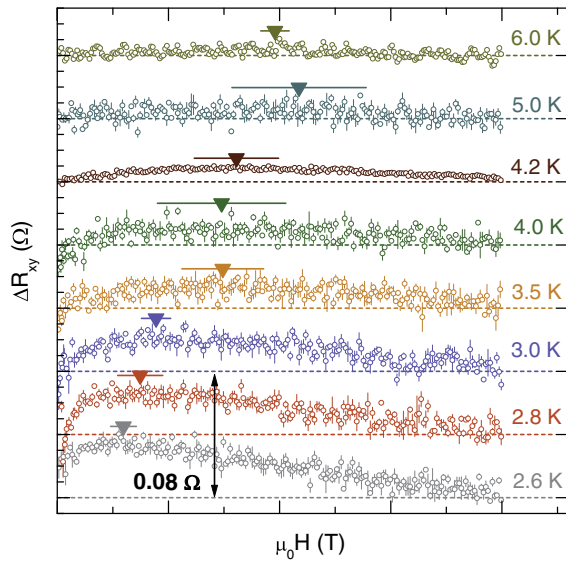


FIG. 23. Experimental results for fluctuation Hall resistance in a TaN thin film as a function of applied magnetic field for a range of temperatures above $T_c(H)$ with marked peak at H^* . The normal-state contribution has been subtracted from R_{xy} . The curves are offset vertically for clarity, and a vertical scale bar of 0.08Ω is indicated. From Breznay and Kapitulnik, 2013.

observed at some H^* above the $H_c(T)$ line; see Fig. 23. This peak at H^* , as a function of temperature above the transition, starts to form at T_{c0} and shifts toward larger fields until at a temperature $\sim T \sim 2T_{c0}$ the Hall effect from superconducting fluctuations becomes too weak and the peak is smeared out.

2. Limit of weak fields

In the GL domains I and II, the sum over Landau levels in Eq. (66) can be replaced by a continuous integral, yielding the following complete correction to Hall conductivity:

$$\sigma_{xy}^{(n)} = \frac{\zeta \Omega_H e^2}{96} \frac{\text{sgn}(h)}{(\epsilon + h)^2}. \quad (67)$$

Note that the divergence of the Hall conductivity near T_{c0} , $\sigma_{xy}^{(n)} \sim 1/(\epsilon + h)^2$, is stronger than the one for the contribution to longitudinal conductivity $\sigma_{xx}^{(n)} \sim 1/(\epsilon + h)$.

Close to the $H_{c2}(0)$ line, in domain III, it is sufficient to consider only the contribution of the lowest Landau level, which yields

$$\sigma_{xy}^{(n)} = \frac{2\zeta T_{c0} e^2}{\pi} \frac{\text{sgn}(h)}{\epsilon + h}. \quad (68)$$

In the region of high temperatures and low fields, domain VIII, $t \gg 1 \gg h$, the contribution from the two diagrams shown in Fig. 21 dominates over the AL and DOS corrections, resulting in

$$\sigma_{xy}^{(n)} = \frac{\zeta \omega_c^{(qp)} e^2}{4\pi^2} \text{sgn}(h) \left[\ln \ln \frac{1}{T_{c0}\tau} - \ln \ln t \right]. \quad (69)$$

3. Limit of strong fields

In the vicinity of $H_{c2}(0)$, all of the previous terms produce comparable contributions to the Hall conductivity. In the regime of classical fluctuations and classical-to-quantum transition (domains V and VI), the complete correction takes the form

$$\sigma_{xy}^{(n)} = \frac{2e^2}{\pi} \frac{\text{sgn}(h)}{\tilde{h}} \left(\zeta T - \frac{21T}{8\epsilon_F} \right). \quad (70)$$

Note that the first term in Eq. (70) is in full agreement with Eq. (68), where $1/(\epsilon + h)$ in domain III turns into $1/\tilde{h}$ in domain VI. The second term in Eq. (70) comes from the anomalous MT contribution and does not contribute to the leading-order correction at weak fields.

In the quantum regime (domain IV), the fluctuation correction to Hall conductivity becomes

$$\sigma_{xy}^{(n)} = \frac{e^2}{2\pi^2} \text{sgn}(h) \ln \tilde{h} \left(\frac{2\zeta \Omega_H}{3} - \omega_c^{(qp)} \tau \right). \quad (71)$$

The results for the different domains of the phase diagram are summarized in Table III.

TABLE III. Asymptotic expressions for fluctuation corrections to the Hall conductivity in different domains of the phase diagram.

Domain	$\sigma_{xy}^{(fl)}$
I, II	$\frac{\zeta\omega_H e^2}{96} \frac{\text{sgn}(h)}{(e+h)^2}$
III	$\frac{2\zeta T_{c0} e^2}{\pi} \frac{\text{sgn}(h)}{e+h}$
IV	$\frac{e^2}{2\pi^2} \text{sgn}(h) \ln \tilde{h} \left(\frac{2\zeta\omega_H}{3} - \omega_c^{(qp)} \tau \right)$
V, VI	$\frac{2e^2}{\pi} \frac{\text{sgn}(h)}{h} \left(\zeta T - \frac{21T}{8e_F} \right)$
VIII	$\frac{\zeta\omega_c^{(qp)} e^2}{4\pi^2} \text{sgn}(h) \left[\ln \ln \frac{1}{T_{c0}\tau} - \ln \ln \tau \right]$

VII. FLUCTUATION NERNST-ETTINGSHAUSEN EFFECT

A. General expression for the fluctuation Nernst-Ettingshausen coefficient

The theoretical description of fluctuation contributions to the thermoelectric and thermomagnetic coefficients remains complex and controversial. Initially, the fluctuation contribution to the Seebeck coefficient in the 3D superconductor was studied by Maki (1973) in the framework of the time-dependent Ginzburg-Landau equation, and it was found to be nonsingular and negligibly small. After the discovery of an anomaly in the Seebeck coefficient behavior close to T_{c0} in monocrystals of $\text{YBa}_2\text{Cu}_3\text{O}_{7-\delta}$ (Howson *et al.*, 1990), the problem was revisited both phenomenologically (Ullah and Dorsey, 1991) and microscopically (Reizer and Sergeev, 1994). Both papers confirmed Maki's conclusion that the fluctuation correction to the Seebeck coefficient is proportional to the degree of particle-hole asymmetry. Yet, they found that in the 2D case it logarithmically depends on the closeness to T_{c0} : $S_{(2)}^{(fl)} \sim (T/E_F) \ln [T_{c0}/(T - T_{c0})]$.

The fluctuation NE effect was initially studied in the framework of the GL approach by Ullah and Dorsey (1991). They demonstrated that the FCP contribution to the NE coefficient, despite being very similar to the thermoelectric coefficient, does not contain the smallness induced by the particle-hole asymmetry (T/E_F) and close to the transition exhibits a much stronger temperature dependence $\nu_{(2)}^{(fl)} \sim T_{c0}/(T - T_{c0})$.

The discovery of the giant Nernst signal in underdoped phases of high-temperature superconductor $\text{La}_{2-x}\text{Sr}_x\text{CuO}_4$ (LSCO) (Xu *et al.*, 2000; Wang, Li, and Ong, 2006) (see Fig. 24) (with critical temperatures around 30 K) triggered great interest, both of theorists and experimentalists. They reported an anomalously enhanced Nernst signal at temperatures as high as 150 K and attributed this phenomenon to the specific physics of HTS. Since the NE effect in type-II superconductors below T_{c0} is related to the entropy transport by moving vortices they hypothesized the presence of strong phase fluctuations in the pseudogap phase. Such fluctuations do not destroy the pseudogap but the Meissner effect. Later this idea was supported theoretically by Tan and Levin (2004), Podolsky, Raghu, and Vishwanath (2007), and Raghu *et al.* (2008), while Hartnoll *et al.* (2007) attributed the anomalously

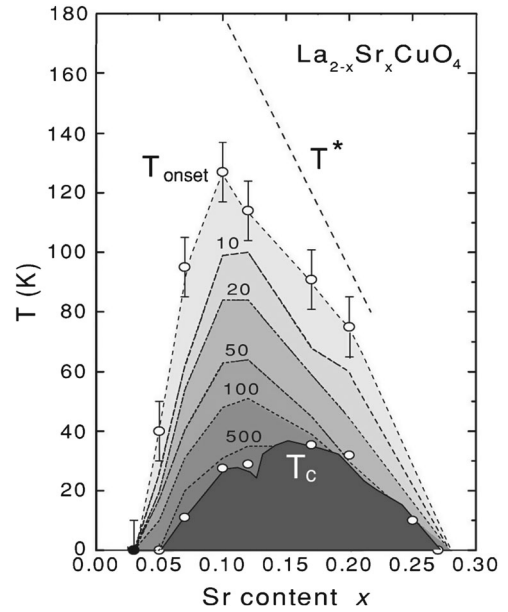


FIG. 24. The phase diagram of LSCO showing the Nernst region between T_{c0} and T_{onset} (numbers on the contour curves indicate the value of the Nernst coefficient ν in nV/KT). The curve of T_{onset} vs x has end points at $x = 0.03$ and 0.26 and peaks conspicuously near 0.10 . The dashed line is T^* estimated from heat capacity measurements. From Wang, Li, and Ong, 2006.

large NE effect to the proximity of the system to a quantum critical point.

Inspired by the new experimental findings by Ong's group, Ussishkin, Sondhi, and Huse (2002), Ussishkin (2003), and Ussishkin and Sondhi (2004) revisited the problem of the calculation of the NE coefficient in the fluctuation regime. In these papers, besides reproducing the linear response theory results of Ullah and Dorsey (1991), they emphasized the importance of the fluctuation magnetization currents flowing in the sample subject of applied magnetic field and gradient of temperature. Taking into account their contribution to the heat flow, they demonstrated that this results in a thrice lower value of the NE coefficient compared to what was predicted in the vicinity of T_{c0} by Ullah and Dorsey (1991).

Later, giant Nernst signals were also discovered in superconducting films (Pouret, Aubin *et al.*, 2006; Pouret *et al.*, 2007), which are well described by the usual BCS model. Therefore, they provided an indication that superconducting fluctuations are likely to be a key to understanding the underlying physics of the giant thermomagnetic response. Next we concentrate on the properties of a conventional type-II superconductor, abstaining from the specifics of underdoped phases of HTS.

The complete microscopic analysis of the fluctuation NE signal through the whole phase diagram was performed by Serbyn *et al.* (2009) in the framework of the Matsubara diagrammatic technique, while the quantum kinetic approach was developed by Michaeli and Finkel'stein (2009a, 2009b). It was shown in these papers that the role of magnetization currents turns out to be even more important in the regime of quantum fluctuations. Indeed, the restriction of the straightforward calculus of the Kubo-like response contribution to

the heat flow (Mahan, 2000) results in the violation of the third law of thermodynamics which can be rectified only by taking into account the fluctuating Meissner magnetization above $H_{c2}(0)$.

1. Definition of the NE coefficient

Let us review the definition of transport coefficients and consider a conductor placed in a magnetic field \mathbf{H} , subjected to an applied temperature gradient ∇T . The electric and heat transport currents in it are related to the applied weak-enough electric field and temperature gradient by means of the relations

$$\mathbf{j}_{\text{tr},\alpha}^{(e)} = \sigma^{\alpha\delta}(\mathbf{H})\mathbf{E}_\delta + \beta^{\alpha\delta}(\mathbf{H})\nabla_\delta T, \quad (72)$$

$$\mathbf{j}_{\text{tr},\alpha}^{(h)} = \gamma^{\alpha\delta}(\mathbf{H})\mathbf{E}_\delta - \kappa^{\alpha\delta}(\mathbf{H})\nabla_\delta T, \quad (73)$$

where $\beta^{\alpha\beta}(\mathbf{H})$, $\gamma^{\alpha\beta}(\mathbf{H})$ and $\kappa^{\alpha\beta}(\mathbf{H})$ are thermoelectricity and heat conductivity tensors (here we use two superscripts for tensors and subscripts for vector components). Thermoelectric tensors $\beta^{\alpha\beta}$ and $\gamma^{\alpha\beta}$ are connected by the Onsager relation $\gamma^{\alpha\beta}(\mathbf{H}) = -T\beta^{\alpha\beta}(-\mathbf{H})$. Let us mention that the validity of the Onsager relation follows from the principle of the symmetry of transport coefficients, which is based on the invariance of the quantum mechanical equations with respect to time reversal.

The off-diagonal components of the tensor $\beta^{\alpha\beta}$ in the absence of a magnetic field are equal to zero. If besides a temperature gradient ∇T also a magnetic field \mathbf{H} is applied to the sample, a potential difference $V^{(\text{NE})}$ appears along the y axis. The circuit in this direction is supposed to be broken. The corresponding open-circuit conditions are $\nabla_x T \neq 0$, $\mathbf{j}_{\text{tr},x}^{(h)} = \mathbf{j}_{\text{tr},x}^{(e)} = \mathbf{j}_{\text{tr},y}^{(e)} = 0$; see Fig. 25. This so-called Nernst-Ettingshausen (or Nernst) effect¹⁰ is well pronounced in semiconductors but is usually small in good metals. It is characterized by the NE coefficient which can be expressed by means of the conductivity and thermoelectric tensors¹¹:

$$\nu = \frac{E_y}{(-\nabla_x T)H} = \frac{1}{H} \frac{\beta^{xy}\sigma_{xx} - \beta^{xx}\sigma_{xy}}{(\sigma_{xx})^2 + (\sigma_{xy})^2}. \quad (74)$$

Usually, when the Hall component of conductivity $\sigma_{xy} \ll \sigma_{xx}$, while both β^{xx} and β^{xy} are of the same order, Eq. (74) directly relates the NE coefficient to the off-diagonal component of the thermoelectric tensor

$$\nu(T, H) = R_\square \beta^{xy}(T, H)/H, \quad (75)$$

where $R_\square = (\sigma_{xx})^{-1}$ is the sheet resistance of the film. In the case under consideration, the validity of approximation (75) is even more justified, considering the excess of the off-diagonal thermoelectricity compared to the diagonal one.

¹⁰The Nernst-Ettingshausen effect is closely related to the Ettingshausen effect, which is just the opposite: it consists of the appearance of a temperature gradient in a conductor placed in a magnetic field, when an electric current is applied.

¹¹The Nernst signal is related to the NE coefficient through the simple relation $\mathfrak{N} = \nu H$.

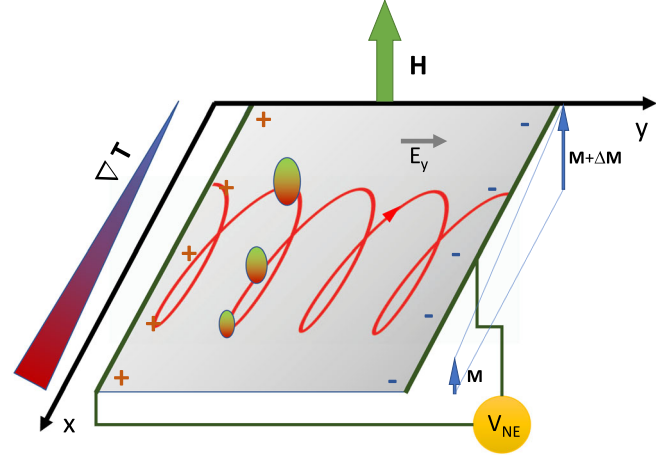


FIG. 25. Schematic representation of the FCP motion in a superconducting film subjected to a temperature gradient along its x axis. The concentration and size of FCPs vary with temperature. The local magnetization parallel to the external magnetic field varies along the x axis as well. The spatial inhomogeneity of the magnetization leads to a transformation of the FCP trajectories from circular to trochoidal, which is why the magnetization currents appear. To compensate for these currents a voltage is induced in the y direction that provides a sizable contribution to the fluctuation NE coefficient.

2. Onsager relations and magnetization currents

It is well known that the absence of free-electron magnetism in the classical theory is explained by the compensation of the total current created by the electrons moving along closed trajectories in the bulk of the sample by the current of the electrons moving along the open “hopping” trajectories close to its surface. In quantum theory such a compensation does not occur (Teller, 1931) and Landau diamagnetism (Landau, 1930) takes place. In the middle of the 20th century a lively debate concerning the fulfillment of reciprocal Onsager relations in metals and semiconductors subjected to a magnetic field and gradient of temperature was taking place [see Obratsov (1964) and references therein]. Obratsov demonstrated the fact that microscopic surface currents inducing electron magnetization can contribute considerably to the density of the macroscopic current when a temperature gradient is applied to the sample. Taking corresponding contributions to the heat and electric currents flowing in the system into account restores the fulfillment of the reciprocal Onsager relations and validity of the third law of thermodynamics.

The contribution to the electric current can be easily expressed using Ampere’s law as

$$\mathbf{j}^{\text{mag}} = \frac{c}{4\pi} \nabla \times \mathbf{B},$$

where $\mathbf{B} = \mathbf{H} + 4\pi\mathbf{M}$, \mathbf{H} is the spatially homogeneous external magnetic field, and \mathbf{M} is the local value of magnetization. In the presence of a temperature gradient $\nabla_x T$ one can express the magnetization current as (Obratsov, 1964; Ussishkin, Sondhi, and Huse, 2002)

$$\mathbf{j}_y^{\text{mag}} = -c(dM_z/dT)\nabla_x T,$$

and the thermoelectric tensor $\beta^{\alpha\delta}(\mathbf{H})$ in Eq. (72) acquires besides its kinetic part $\tilde{\beta}^{\alpha\delta}(\mathbf{H})$ also a magnetization contribution $\beta_M^{\alpha\delta} = \epsilon^{\alpha\beta\zeta} c dM_\zeta/dT$:

$$\beta^{\alpha\delta}(\mathbf{H}) = \tilde{\beta}^{\alpha\delta}(\mathbf{H}) + \epsilon^{\alpha\beta\zeta} c \frac{dM_\zeta}{dT} \quad (76)$$

with $\epsilon^{\alpha\beta\zeta}$ being the Levi-Civita symbol. In the case of NE geometry the open-circuit condition holds $\mathbf{j}_{\text{tr},y}^{(e)} = 0$ and in full analogy to the classical Hall effect, the magnetization current in the y direction is compensated for by the current induced through the Nernst-Ettingshausen voltage $E_y^{\text{NE}} = R_{\square} j_y^{\text{mag}}$.

The transport heat current (73) is also affected by magnetization currents. In the presence of a magnetic field, the measurable transport heat current $\mathbf{j}_{\text{tr}}^{(h)}$ differs from the microscopic heat current $j^{(h)}$ by the circular magnetization current $\mathbf{j}_M^{(h)} = c\mathbf{M} \times \mathbf{E}$ (Larkin and Varlamov, 2009). As a result, the thermoelectric tensor $\gamma^{\alpha\delta}$ relating $\mathbf{j}_{\text{tr}}^{(h)}$ with the applied electric field can be found as the sum of the kinetic $\tilde{\gamma}^{\alpha\delta}$ and thermodynamic $\gamma_M^{\alpha\delta} = \epsilon^{\alpha\delta\zeta} c M_\zeta/T$ contributions

$$\gamma^{\alpha\delta} = \tilde{\gamma}^{\alpha\delta} + \epsilon^{\alpha\delta\zeta} c M_\zeta/T. \quad (77)$$

The reciprocal Onsager relations in this interpretation acquire the form

$$\tilde{\gamma}^{\alpha\delta}(H) + \epsilon^{\alpha\delta\zeta} \frac{c M_\zeta(H)}{T} = -T \left[\tilde{\beta}^{\alpha\delta}(-\mathbf{H}) + \epsilon^{\alpha\delta\zeta} c \frac{dM_\zeta(-\mathbf{H})}{dT} \right]. \quad (78)$$

Hence, in order to find the NE coefficient [see Eq. (75)] one can calculate $\tilde{\gamma}^{\alpha\delta}(-H)$ instead of $\tilde{\beta}^{\alpha\delta}(\mathbf{H})$ and obtain

$$\nu(T, H) = -R_{\square} \frac{\tilde{\gamma}^{\text{xy}}(H) + c M_z(H)/T}{TH}. \quad (79)$$

This way turns out to be much more straightforward using the microscopic approach.

3. Microscopic expression for fluctuation NE coefficient

Here we review the microscopic calculation of the NE coefficient. In the spirit of the Kubo formalism one can relate the electron heat current $\mathbf{j}_{\text{tr}}^{(h)}$ to the value of the heat current operator averaged over quantum and thermal states applied to the one-electron Green's function. Expansion of the latter in the electric field relates the tensor $\gamma^{\alpha\delta}(\mathbf{H})$ to the loop of two-electron Green's functions separated by the heat and electromagnetic field vertexes (analogously to the loop for the electromagnetic field operator for the conductivity tensor):

$$\tilde{\gamma}^{\alpha\delta} = -\lim_{\omega \rightarrow 0} \frac{\text{Im} \tilde{Q}_{\alpha\delta}^R(-i\omega + 0)}{\omega}.$$

The electric-heat-current correlation function $\tilde{Q}_{\alpha\delta}(\omega_k)$ is calculated first at bosonic Matsubara frequencies $\omega_k = 2\pi T k$ and then analytically continued to real frequencies.

The fluctuation part of the electric-heat-current correlation function $\tilde{Q}_{\alpha\delta}^{(\text{n})}(\omega_k)$ is graphically represented by the same ten diagrams of Fig. 14, but taken with vertices as in Fig. 26. These were analyzed in detail by Serbyn *et al.* (2009). They found that in the case of the NE effect, the Maki-Thompson contribution becomes exactly zero. The contribution of the DOS diagrams turns out to be less singular than the contribution corresponding to the diagrams containing three Cooperons (DCR, see Fig. 26). The positive AL term dominates in the GL region and competes with the negative DCR contribution everywhere else. The fluctuation magnetization was discussed in Sec. IV. Finally, the general expression for the NE coefficient of 2D superconductors valid beyond the line $H_{c2}(T)$ takes the form

$$\begin{aligned} \nu^{(\text{n})} = & \frac{\beta_0 R_{\square}}{8H} \left[\eta \sum_{m=0}^{M_t} (m+1) \sum_{k=0}^{\infty} \left\{ \left(\frac{3}{\mathcal{E}_m} + \frac{1}{\mathcal{E}_{m+1}} \right) (\mathcal{E}'_m - \mathcal{E}'_{m+1}) + [\eta(2m+1) + k] \frac{\mathcal{E}''_m}{\mathcal{E}_m} + [\eta(2m+3) + k] \frac{\mathcal{E}''_{m+1}}{\mathcal{E}_{m+1}} \right\} \right. \\ & + 4\pi^2 \sum_{m=0}^{M_t} (m+1) \int_{-\infty}^{\infty} \frac{dx}{\sinh^2 \pi x} \left\{ \frac{\eta \text{Im} \mathcal{E}_m \text{Im}(\mathcal{E}_m + \mathcal{E}_{m+1}) + [\eta(m+1/2) \text{Im} \mathcal{E}_m + x \text{Re} \mathcal{E}_m] \text{Im}(\mathcal{E}_{m+1} + \eta \mathcal{E}'_m - \mathcal{E}_m)}{|\mathcal{E}_m|^2} \right. \\ & + \frac{\eta \text{Im} \mathcal{E}_{m+1} \text{Im}(\mathcal{E}_m + \mathcal{E}_{m+1}) + [\eta(m+3/2) \text{Im} \mathcal{E}_{m+1} + x \text{Re} \mathcal{E}_{m+1}] \text{Im}(\mathcal{E}_{m+1} + \eta \mathcal{E}'_{m+1} - \mathcal{E}_m)}{|\mathcal{E}_{m+1}|^2} + 4x \text{Im} \ln \frac{\mathcal{E}_m}{\mathcal{E}_{m+1}} \\ & \left. \left. - 2 \frac{\text{Im}(\mathcal{E}_m + \mathcal{E}_{m+1}) (\text{Im} \mathcal{E}_m \text{Im} \mathcal{E}_{m+1} + \text{Re} \mathcal{E}_m \text{Re} \mathcal{E}_{m+1})}{|\mathcal{E}_{m+1}|^2 |\mathcal{E}_m|^2} \left[\eta \left(m + \frac{3}{2} \right) \text{Im} \mathcal{E}_{m+1} - \eta \left(m + \frac{1}{2} \right) \text{Im} \mathcal{E}_m + x \text{Re}(\mathcal{E}_{m+1} - \mathcal{E}_m) \right] \right\} \right], \quad (80) \end{aligned}$$

where $\eta = 4h/(\pi^2 t)$ and $\beta_0 = k_B e/\pi \hbar = 6.68$ nA/K is the quantum of thermoelectric conductance.

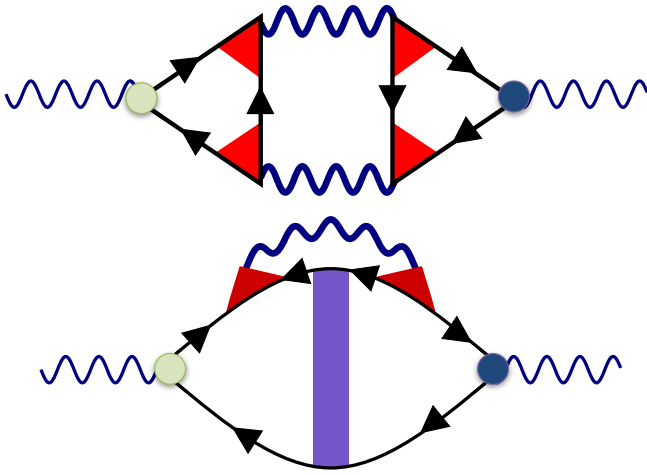


FIG. 26. The Aslamazov-Larkin (top) and DCR (bottom) diagrams for the thermoelectric response $\tilde{\gamma}^{xy}$. The DCR diagram has a symmetric counterpart. The green and blue (light and dark gray) circles correspond to the different heat and electric vertices, the triangular and rectangular blocks represent impurity interaction, and the wavy lines denote the fluctuation propagator.

B. Asymptotic analysis

The effect of SF on the Nernst-Ettingshausen coefficient is demonstrated in Fig. 27, where a surface plot of $\nu^{(n)}(T, H)$ according to Eq. (80) is shown. We start with its asymptotic expressions, which are summarized in Table IV.

Close to the critical temperature T_{c0} , where fluctuations have thermal character (GL domains I–III), only the AL contribution is essential, which takes magnetization currents into account. In the limit of vanishingly small magnetic fields $h \ll \epsilon$ (domain I), the numerical factor in the coefficient of the

NE signal slightly varies in Reizer and Sergeev, 1994; Ussishkin, Sondhi, and Huse, 2002; Ussishkin, 2003; Michaeli and Finkel'stein, 2009b; Serbyn *et al.*, 2009). This difference between GL and microscopic approaches may signal, e.g., a problem with the definition of the heat currents within the time-dependent Ginzburg-Landau theory and diagrammatics. The exact origin of this discrepancy presently remains unclear. In the limit of relatively strong fields in the GL region $\epsilon \ll h$ (domain II) and approaching the transition line $H - H_{c2}(T) \ll H_{c2}(T)$ (domain III), the NE signal diverges.

Next we look at the low-temperature regime close to the upper critical field $H_{c2}(0)$ (domains IV–VI in Fig. 9). Here the role of the magnetization term becomes crucial: The cancellation of the $1/T$ divergence by magnetization currents ensures that the third law of thermodynamics holds, and the total NE coefficient remains finite in the $T \rightarrow 0$ limit. In the purely quantum limit of vanishing temperature and away from $H_{c2}(0)$ ($t \ll \tilde{h}$, domain IV), $\nu^{(n)}$ is negative, linear in temperature, and diverges as \tilde{h}^{-1} approaching the transition point. One can see from Table IV that it coincides with our qualitative estimation in Eq. (22). This change of sign in the thermoelectric response is similar to the negative fluctuation conductivity close to the quantum phase transition in the vicinity of $H_{c2}(0)$ found in Galitski and Larkin (2001a) (compare insets in Figs. 15 and 27). The sign change is due to the DCR contribution, which is larger than the positive AL term in this region. In the quantum-to-classical crossover region, where H approaches $H_{c2}(T)$ but remains finite [$t^2/\ln(1/t) \ll \tilde{h} \ll t$, domain V], the NE coefficient becomes positive and less singular. Increasing the temperature one goes over into the region of thermal fluctuations. Moving further along the line $H_{c2}(T)$ [$\tilde{h} \ll t^2/\ln(1/t)$, domain VI], one sees that the NE signal grows. Equation (80) allows for one to

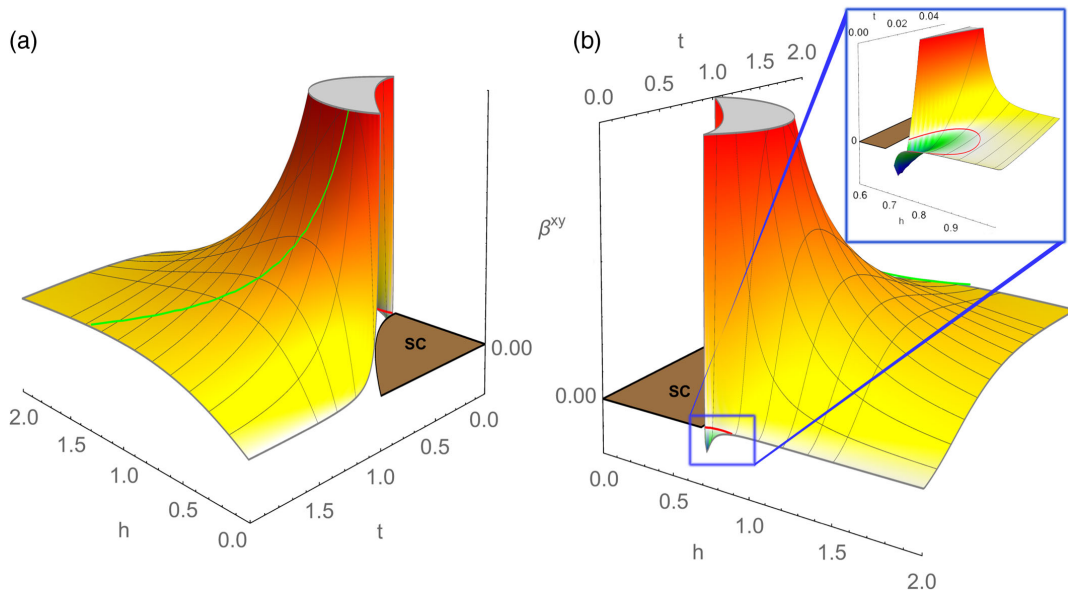


FIG. 27. The magnetic field and temperature dependence of the fluctuation part of the Nernst coefficient. (a) A view from the $h = 0$ plane with the ghost field line in green (light gray) indicating the maximum of the Nernst coefficient for constant t . (b) A view from the $t = 0$ plane with a zoom close to the quantum fluctuation region at $h = h_{c2}$. The red (dark gray) line indicates the contour where the Nernst coefficient becomes zero.

TABLE IV. Asymptotic expressions for fluctuation corrections to the NE coefficient in different domains of the phase diagram.

Domain	$\frac{H}{\beta_0 R_{\square}} \nu^{(fl)}$
I	$\frac{2eH\xi_{GL}^2(T)}{3c} = \frac{2eH\xi_c^2}{3c} \frac{1}{e}$
II	$1 - (\ln 2)/2$
III	$\frac{1}{e+h}$
IV	$-\frac{2\gamma_E}{9} \frac{t}{h}$
V	$\ln \frac{t}{h}$
VI	$\frac{8\gamma_E^2}{3} \frac{t^2}{h(t)}$
VII	$\frac{1}{h(t)} \left[1 + \frac{2h_{c2}(t)\psi'(\frac{1}{2} + \frac{2h_{c2}(t)}{\pi^2 t})}{\pi^2 t \psi'(\frac{1}{2} + \frac{2h_{c2}(t)}{\pi^2 t})} \right]$
VIII	$\frac{4e\xi_c^2}{3\pi^2} \frac{H}{c} \frac{1}{t \ln t}$
IX	$\frac{\pi^2}{48} \frac{t}{h \ln h}$

study the full classical region just above the transition line, which covers a wide range of temperatures and magnetic fields ($\tilde{h} \ll 1$, domain VII). Close to T_{c0} , the expression obtained matches the expression valid in domain III [here $\tilde{h}(t) = e + h$], while in the limit $T \rightarrow 0$ it matches the asymptotic expression, provided that $\tilde{h} \ll t^2 / \ln(1/t)$.

Finally, we address the “nonsingular” domains VIII and IX far from the transition line. In these limits, the Kubo contribution $\tilde{\gamma}^{xy}$ diverges as $[\ln \ln(1/T_{c0}\tau) - \ln \ln \max(h, t)]$, with $1/(T_{c0}\tau)$ playing the role of an ultraviolet cutoff of the Cooperon modes. Remarkably, the same divergence with opposite sign occurs in the magnetization contribution γ_M^{xy} . Hence, the total expression for $\nu^{(fl)}$ remains finite (see Table IV). We see that even far from the transition, the fluctuation Nernst signal can be comparable or even parametrically larger than the Fermi-liquid terms. In fact, it is conceivable that in some materials the Cooper channel contribution to thermal transport dominates even in the absence of any superconducting transition (e.g., if it is “hidden” by another order).

C. Fluctuation spectroscopy: Analysis of Nernst signal measurements

As mentioned, numerous experimental studies of the last two decades have revealed an anomalously strong thermomagnetic signal, in the normal state of both high-temperature superconductors (Xu *et al.*, 2000; Wang *et al.*, 2001, 2002; Capan *et al.*, 2002; Wen *et al.*, 2003; Xu *et al.*, 2005; Wang, Li, and Ong, 2006; Li and Greene, 2007; Tafti *et al.*, 2014) and conventional superconducting films (Pourret, Aubin *et al.*, 2006; Pourret *et al.*, 2007); see Fig. 28. In experiments on $\text{La}_{2-x}\text{Sr}_x\text{CuO}_4$ HTS compounds, the NE signal \mathfrak{N} exceeded the background value by 100 times close to the superconducting transition and a sizable effect remained even up to 130 K, well above the transition temperature T_{c0} . Surprisingly, in experiments on the conventional superconductor $\text{Nb}_{0.15}\text{Si}_{0.85}$ (Pourret, Aubin *et al.*, 2006; Pourret *et al.*, 2007) the value of the excess signal transcended the expected magnitude

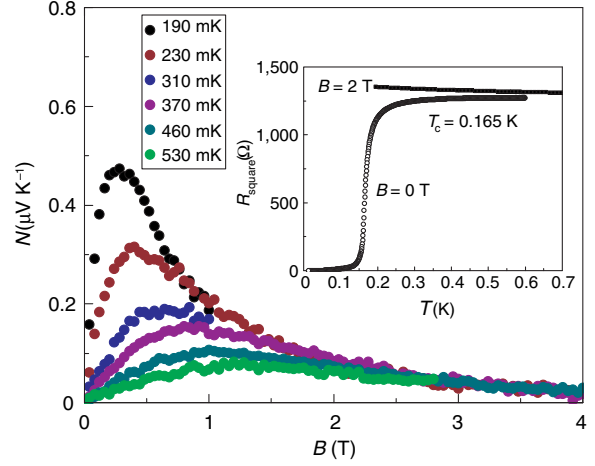


FIG. 28. Nernst signal (labeled N in the figure, \mathfrak{N} in the text) measured in a $\text{Nb}_{0.15}\text{Si}_{0.85}$ film as a function of the magnetic field for temperatures ranging from 0.19 to 5.8 K, for a sample with $T_{c0} = 0.165$ K. A finite Nernst signal is present for $T > T_{c0}$. With increasing temperature, this signal decreases in magnitude and becomes more linear in field. From Pourret, Aubin *et al.*, 2006.

according to the classical Sondheimer theory (Sondheimer, 1948) not by 100 but by a few thousand times. Such observations were especially striking in view of the previously recorded data on the magnitude of the Seebeck coefficient in the normal state of superconductors, undergoing a weak singular decrease close to T_{c0} but remaining on the same order of magnitude as in the normal phase (Howson *et al.*, 1990; Lowe, Regan, and Howson, 1993; Ri *et al.*, 1994). These and further similar experiments have sparked the interest in thermomagnetic phenomena beyond the superconducting state.

One of the reasons for this interest is that the measured fluctuation effects exceed Sondheimer’s evaluation of the normal phase quasiparticle contribution by orders of magnitude. Close to the critical temperature and in sufficiently weak magnetic fields the experimental findings are in good agreement (Behnia and Aubin, 2016) with results obtained in the simple GL approximation (Ullah and Dorsey, 1991; Ussishkin, Sondhi, and Huse, 2002). Moreover, since the fluctuation Nernst signal can be observed in a wide temperature range, one can compare experimental data with the predictions of the microscopic theory (Michaeli and Finkel’stein, 2009a; Serbyn *et al.*, 2009) in detail.

1. Giant Nernst signal in NbSi

In Fig. 29 a comparison between the theory of Serbyn *et al.* (2009) and the magnitude of the experimentally measured Nernst coefficient (Pourret, Aubin *et al.*, 2006) in weak fields is plotted for a $\text{Nb}_{0.15}\text{Si}_{0.85}$ film of thickness $d = 12.5$ nm in a wide range of temperatures up to $30T_{c0}$. The dashed line corresponds to the theoretically calculated Nernst coefficient (Serbyn *et al.*, 2009). A diffusion coefficient of 0.087 cm^2/s , which is 60% of that reported by Pourret, Aubin *et al.* (2006), is used for the fitting. Far from the transition temperature ($\epsilon > 2$), the superconducting coherence length $\xi(T)$ becomes shorter than d and the 3D nature of the diffusion manifests

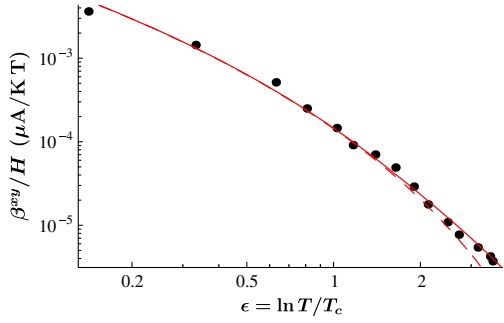


FIG. 29. Comparison with experiment. Circles: experimental data for the fluctuation part of the NE coefficient vs $\epsilon = \ln T/T_{c0}$ obtained for the 12.5-nm-thick $\text{Nb}_{0.15}\text{Si}_{0.85}$ film (Pourret, Aubin *et al.*, 2006). Dashed line: theoretical prediction for the strictly 2D geometry. Solid line: theoretical prediction for the sample with 2D-3D crossover taken into account. The only adjustable parameter in this fit is the diffusion coefficient, here $0.087 \text{ cm}^2/\text{s}$. From Serbyn *et al.*, 2009.

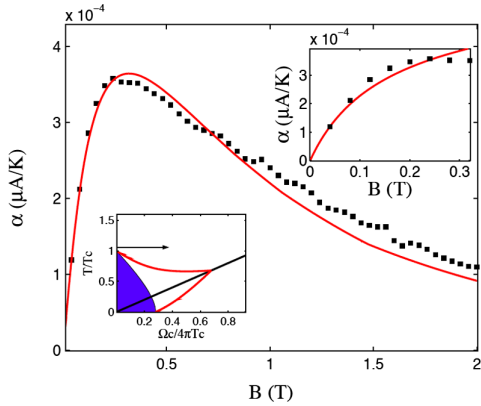


FIG. 30. Comparison with experiment. The Nernst signal (labeled α , \mathfrak{N} in the text) as a function of the magnetic field measured at $T = 410 \text{ mK}$. The black squares correspond to the experimental data of Pourret, Aubin *et al.* (2006) while the solid line describes the theoretical result of Michaeli and Finkel'stein (2009a). The arrow on the phase diagram illustrates the direction of the measurement. In the inset the low magnetic field data are fitted with the theoretical curve. From Michaeli and Finkel'stein, 2009a

itself. Taking this fact into account noticeably improves the fitting (see the solid line in Fig. 29).

In Fig. 30 an excellent agreement between the theory of Michaeli and Finkel'stein (2009a) and the measurements of the Nernst signal (performed on the same $\text{Nb}_{0.15}\text{Si}_{0.85}$ film) as a function of the magnetic field is demonstrated.

2. Analysis of the ghost critical field

The characteristic feature of the fluctuation Nernst signal is its nonmonotonic behavior as a function of the magnetic field. One can see from the first row of Table IV that close to T_{c0} , the Nernst signal is proportional to the magnetic field and quadratically dependent on the GL coherence length. As long as the magnetic field is relatively small, the effective size of FCPs remains to be determined by $\xi_{\text{GL}}(\epsilon)$ and is fixed by

temperature. However, when the magnetic field increases and consequently the magnetic length $\ell_{\text{H}}^{\text{FCP}} = \sqrt{c/2eH}$ of the FCPs becomes comparable to $\xi_{\text{GL}}(\epsilon)$, the former gradually takes on the role of the characteristic size of FCP. Such field-induced shrinking of the fluctuations characteristic scale is well known since the early studies of fluctuating diamagnetism (Schmid, 1969; Prange, 1970; Gollub *et al.*, 1973; Skocpol and Tinkham, 1975; Behnia and Aubin, 2016). As a result, the Nernst signal reaches its maximum at some field $H^*(T)$ and decreases when the magnetic field further increases.

Pourret, Aubin *et al.* (2006) were the first who measured such isothermal curves (see Fig. 31) and also determined the temperature dependence $H^*(T)$ for the temperatures several times exceeding T_{c0} . They identified $H^*(T)$ with the field when $\ell_{\text{H}}^{\text{FCP}} = \sqrt{c/(2eH^*)} \sim \xi_{\text{GL}}(\epsilon)$ and, following Kapitulnik, Palevski, and Deutscher (1985), called the curve $H^*(\epsilon)$ as the “mirror field” [others called it the “ghost critical field”]; in the vicinity of T_{c0} it is indeed symmetrical to the line $H_{c2}(\epsilon)$. Moreover, recalling that ϵ in the microscopic theory is the asymptotic expression of the $\ln T/T_{c0}$, Pourret, Aubin *et al.* (2006) extended their fitting also to temperatures beyond the GL region.

The study of the temperature dependence of $H^*(T)$ acquired special significance for HTS compounds. Recently, Tafti *et al.* (2014) and Yamashita *et al.* (2015) proposed using it for the precise determination of the second critical field $H_{c2}(0)$, often inaccessible for direct measurements because of its large value. The analysis of the experimental data obtained on the HTS compound $\text{Pr}_{2-x}\text{Ce}_x\text{CuO}_4$ led Tafti *et al.* (2014) to propose for the temperature dependence of the ghost critical field a phenomenological expression:

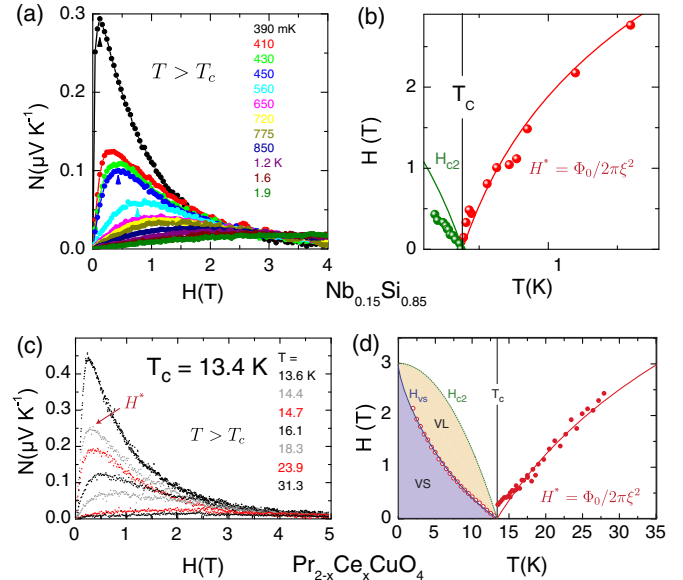


FIG. 31. Nernst signal (labeled N in the plots, \mathfrak{N} in the text) (a) in the conventional superconductor $\text{Nb}_{0.15}\text{Si}_{0.85}$ and (c) in the HTS $\text{Pr}_{2-x}\text{Ce}_x\text{CuO}_4$ measured above critical temperature (Pourret, Aubin *et al.*, 2006; Tafti *et al.*, 2014) and the related temperature dependences of the corresponding maxima, labeled H^* (the “ghost critical field”) in (b) and (d), respectively. From Behnia and Aubin, 2016.

$$H^*(T) = H_{c2}(0) \ln \frac{T}{T_{c0}}. \quad (81)$$

The prefactor $H_{c2}(0)$ was chosen as a single empirical parameter that characterizes the strength of the superconductivity. They stated that “the characteristic field scale encoded in superconducting fluctuations above T_{c0} ” is equal to the field needed to kill superconductivity at $T = 0$ K, i.e., a straightforward empirical procedure for measuring of the fundamental field scale for superconductivity from superconducting fluctuations above T_{c0} was proposed.

The complete expression, Eq. (80), unfortunately does not allow one to extract the temperature dependence of the ghost field $H^*(T)$ analytically. Nevertheless, due to its specific scaling form, the temperature dependence of the magnetic field corresponding to the maximum of the Nernst signal can be expressed in a very generic way (Kavokin and Varlamov, 2015)

$$H^*(T) = H_{c2}(0) \left(\frac{T}{T_{c0}} \right) \varphi \left(\ln \frac{T}{T_{c0}} \right), \quad (82)$$

where $\varphi(x)$ is some smooth function which satisfies the condition $\varphi(0) = 0$.

Note that Eq. (82) coincides with Eq. (81) only in the particular case of $\varphi(x) = x \exp(-x)$. In the case of any other analytical function $\varphi(x)$, the magnetic field corresponding to the maximum of the NE signal $H^*(T)$ would increase mainly linearly with the growth of temperature.

Let us recall that the heuristic justification of Eq. (81) is based on the statement that the maximum in the NE signal magnetic field dependence occurs where the FCP size $\xi_{GL}(T)$ is of the order of its magnetic length $\ell_{H^*}^{FCP} = (c/2eH^*)^{1/2}$. Close to the critical temperature this indeed yields

$$H^* \sim H_{c2}(0)(T - T_{c0})/T_{c0} \approx H_{c2}(0) \ln \frac{T}{T_{c0}}.$$

Far from T_{c0} Pouret, Aubin *et al.* (2006), Tafti *et al.* (2014), and Yamashita *et al.* (2015) extended the GL expression as

$$\xi_{GL}(T) = \xi_{BCS} \left/ \sqrt{\ln \frac{T}{T_{c0}}} \right.,$$

which brings them to Eq. (81). We believe that this extension misses some justification, and the microscopically obtained Eq. (80) has to be investigated for its extrema.

However, it is possible to numerically extract the ghost field from Eq. (80). The result is shown in Fig. 32. In addition to this numerically extracted curve, scaled experimental data from Chang *et al.* (2012) on Eu-LSCO and Tafti *et al.* (2014) on doped PCCO are plotted. The latter is in fact better fitted by the maximum of Eq. (80) than the phenomenological curve (81) in its lower temperature range. The former data set also shows a rather linear behavior at higher temperatures with a slope of 0.35.

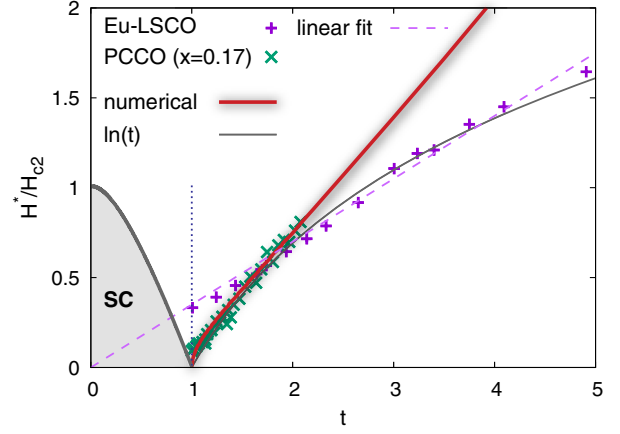


FIG. 32. Temperature dependence of the ghost field scaled to H_{c2} from experiments (+ and \times), numerically obtained from Eq. (80) [thick solid red (dark gray) line], and $\ln(t)$ (thin gray line). The experimental data on Eu-LSCO (+) are taken from Chang *et al.* (2012) [Fig. 3(b)] and the data on PCCO at doping level $x = 0.17$ (\times) from Tafti *et al.* (2014) (Fig. 10). The data on Eu-LSCO are also fitted to a line through zero (slope 0.35) for comparison (dashed line).

VIII. FLUCTUATION PSEUDOGAP AND LOW-BIAS ANOMALY

A. Fluctuation depletion of the electron DOS

According to the microscopic BCS theory (Bardeen, Cooper, and Schrieffer, 1957a, 1957b), the superconducting state is characterized by a gap in the quasiparticle spectrum centered around the Fermi level, which vanishes along the transition line $H_{c2}(T)$. However, it was predicted as early as in 1970 (Abrahams, Redi, and Woo, 1970) that thermal fluctuations result in a noticeable suppression of the DOS in a narrow energy range around the Fermi level even in the normal state of a superconductor [see Fig. 33(a)]. More specifically, in the case of a disordered thin film, the fluctuation correction to the DOS assumes the form (Abrahams, Redi, and Woo, 1970)

$$\frac{\delta\rho_{(2)}^{(n)}(E, T)}{\rho_e} = \frac{4.6\text{Gi}_{(2)}k_B^2T^2}{[E - (1/2)\tau_{GL}^{-1}]^2} \times \left[\frac{E - (1/2)\tau_{GL}^{-1}}{E + (1/2)\tau_{GL}^{-1}} - \ln \frac{E + (1/2)\tau_{GL}^{-1}}{\tau_{GL}^{-1}} \right], \quad (83)$$

where ρ_e is the electron density of states per one spin of a normal metal at the Fermi level, $\text{Gi}_{(2)} = 1.3\hbar^2/p_F^2ls$ is the Ginzburg-Levanyuk number for a 2D film of thickness s , l is the electron mean free path, and τ_{GL} is the Ginzburg-Landau time.

One can see that Eq. (83) is a sign-changing function and its integral over the complete energy range must be equal to zero:

$$\int_0^\infty \delta\rho^{(n)}(E, T)dE = 0. \quad (84)$$

Equation (84) is merely the sum rule: the superconducting interaction cannot create new states, it just redistributes the

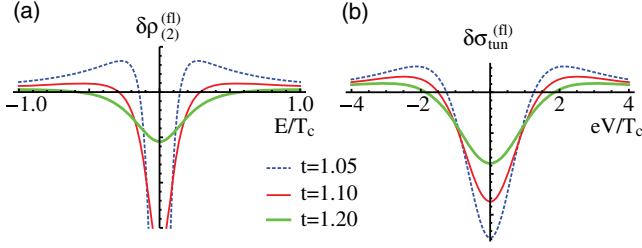


FIG. 33. (a) Theoretical curves of the fluctuation correction to the single particle DOS $\delta\rho_{(2)}^{(f)}$ vs energy E for 2D superconductors above critical temperature ($t = T/T_{c0} = 1.05, 1.1, 1.2$). (b) The pseudogap in the tunneling conductivity obtained by applying Eq. (86) to the fluctuation correction (83). From Glatz, Varlamov, and Vinokur, 2014.

existing ones over the energy spectrum. In particular, a sharp dip [$\delta\rho_{(2)}^{(f)}(0, \epsilon) \sim -\text{Gi}_{(2)}\rho_e/\epsilon^2$] is formed at the Fermi level, which is a precursor effect of the superconducting gap. At the same time, the electron states corresponding to the fluctuation pairing move to higher energies. Yet it is clear that these pairings are restricted to energies not much larger than $\Delta E_s \sim k_B(T - T_{c0})$, where the maximum of Eq. (83) is formed [see Fig. 33(a)].

B. Fluctuation pseudogap in tunneling conductivity: Phenomenological approach

Tunneling spectroscopy is the tool of choice for investigating the quasiparticle spectrum. Therefore, the ability to analyze voltage-current characteristics obtained by a superconducting electrode in the fluctuation regime (N + SF) is of integral importance, as the domain is key to revealing the microscopic mechanisms of high-temperature superconductivity and the superconductor-insulator transition.

Giaever and Megerle (1961) (GM) related the quasiparticle tunneling current to the densities of electron states of the left and right electrodes and to the difference of the equilibrium distribution functions in both of them:

$$I^{(f)}(V) = -\frac{\hbar}{eR_N\rho_L(0)\rho_R(0)} \times \int_{-\infty}^{\infty} [n_F(E + eV) - n_F(E)]\rho_L(E + eV)\rho_R(E)dE. \quad (85)$$

Here R_N is the tunnel-junction resistance, $n_F(E)$ is the Fermi distribution function, and $\rho_{L,R}$ is the energy dependent density of states of the left (right) electrode, respectively. Assuming the left electrode is a normal metal with constant density of states ρ_L and the right electrode is a thin superconducting film above its critical temperature, one can write an explicit expression for the excess tunneling conductivity in terms of $\delta\rho_{(2)}^{(f)}(E, T)$ and the derivative of the Fermi function. Combining the latter with the sum rule (84), one finds

$$\delta\sigma_{\text{tun}}^{(f,GM)}(V) = \frac{\hbar}{4TeR_N\rho_e} \int_{-\infty}^{\infty} \tanh^2 \frac{E + eV}{2k_B T} \delta\rho_{(2)}^{(f)}(E) dE \quad (86)$$

and arrives at the disappointing conclusion that the predicted strong and narrow singularity in the density of states, Eq. (83), manifests itself in the observable tunneling conductivity only as a wide [$eV^{(pg)} \sim T_{c0} \sim \Delta_{\text{BCS}}$ instead of $\Delta E_s \sim k_B(T - T_{c0})$] and weak in the magnitude [$\ln(k_B T \tau_{\text{GL}}/\hbar) \sim \ln[T_{c0}/(T - T_{c0})]$ instead of $T_{c0}^2/(T - T_{c0})^2$] pseudogap structure, resembling that one in the superconducting phase (Varlamov and Dorin, 1983); see Fig. 33(b). The strong divergence of Eq. (83) at zero energy in the process of integration in Eq. (86) is completely eliminated due to the presence of $\tanh^2(E/2k_B T)$. As a result, only a weakly singular dip as a function of temperature at zero voltage and two bumps of $\delta\sigma_{\text{tun}}^{(f)}(V)$ are reminiscent of the proximity to the superconducting transition.

This kind of pseudogap was repeatedly observed in experiments with both conventional (Belogolovskii, Khachaturov, and Chernyak, 1986; Sacépé *et al.*, 2010) and high-temperature (Jacobs, Katterwe, and Krasnov, 2016) superconductors. However, in such nontrivial superconducting systems such as HTS materials or strongly disordered superconducting films close to the superconductor-insulator transition, multiple other mechanisms of pseudogap formation are possible (Perali *et al.*, 2002; Chen *et al.*, 2005; Bennemann and Ketterson, 2008; Sacépé *et al.*, 2011; Palestini *et al.*, 2012).

C. General expression for the fluctuation tunneling conductivity

The GM phenomenology accounts for the depletion of single-electron DOS due to superconducting fluctuations, but it is not sufficient to uncover quantum coherent effects similar to Andreev reflection of injected electrons on a SF domain in a biased electrode. In order to correctly describe such effects, one can employ the Matsubara temperature Green's function technique. This quantitative theory was developed by Glatz, Varlamov, and Vinokur (2014) and is capable of adequately describing high resolution scanning tunneling microscopy (STM) and scanning tunneling spectroscopy (STS) data side by side with the pseudogap, thus uncovering subtle features of the tunneling spectra.

A low-transparency junction can be described by the tunnel Hamiltonian

$$\hat{\mathcal{H}}_T = \sum_{\mathbf{p}, \mathbf{k}, \sigma} (T_{\mathbf{p}, \mathbf{k}} \hat{a}_{\mathbf{p}, \sigma}^+ \hat{b}_{\mathbf{k}, \sigma} + T_{\mathbf{p}, \mathbf{k}}^* \hat{b}_{\mathbf{k}}^+ \hat{a}_{\mathbf{p}}), \quad (87)$$

where $\hat{a}_{\mathbf{p}, \sigma}^+$ and $\hat{b}_{\mathbf{k}, \sigma}$ are the creation and annihilation operators in the left and right electrodes, correspondingly. The summations are performed over the electron states \mathbf{p} , \mathbf{k} in the corresponding electrodes, and spin components σ , and $T_{\mathbf{p}, \mathbf{k}}$ is the tunnel matrix element between states \mathbf{p} and \mathbf{k} . The transparency of the barrier is determined by the averaged value of $|T_{\mathbf{p}, \mathbf{k}}|^2$. The tunneling current can be identified as the time derivative of the particle number operator in one of the electrodes $\hat{N}_L = \sum_{\mathbf{p}, \sigma} \hat{a}_{\mathbf{p}, \sigma}^+ \hat{a}_{\mathbf{p}, \sigma}$ averaged over the statistical ensemble:

$$I^{(f)}(V, T) = e \left\langle \frac{d\hat{N}_L}{dt} \right\rangle = -\frac{ie}{\hbar} \langle [\hat{N}_L, \hat{\mathcal{H}}_T] \rangle. \quad (88)$$

The procedure of ensemble averaging with the density matrix is described in detail by Richardson (1997). The tunneling current is then determined by the loop (correlator) of two exact one-electron Green's functions G_L and G_R of the electrodes (Varlamov and Dorin, 1983):

$$K(\omega_k) = 4T \sum_{\epsilon_n} \sum_{\mathbf{q}, \mathbf{p}} |T_{\mathbf{p}, \mathbf{q}}|^2 G_L(\mathbf{p}, \epsilon_n + \omega_k) G_R(\mathbf{q}, \epsilon_n). \quad (89)$$

Here the summations are performed over all momenta and fermionic frequencies $\epsilon_n = 2\pi T(n + 1/2)$. The external bosonic frequency $\omega_k = 2\pi T k$ ($k = 0, 1, 2, \dots$) accounts for the potential difference between the electrodes, and the factor 4 is due to the summation over the spin degrees of freedom. The current is then given by

$$I^{(\text{fl})}(t, h, v_t) = -\frac{2eT_{c0}Sh}{\pi^3 \sigma_n R_N} \sum_{m=0}^{M_t} \sum_{k=0}^{\infty} \frac{\text{Im} \mathcal{E}'_m(k - iv_t)}{\mathcal{E}_m(k)} + \frac{eT_{c0}Sh}{\pi^3 \sigma_n R_N} \sum_{m=0}^{M_t} \left\{ \frac{\text{Im} \mathcal{E}'_m(-iv_t)}{\mathcal{E}_m(0)} + \sinh\left(\frac{\pi}{2} v_t\right) \int_{-\infty}^{\infty} dz \frac{\text{Re} \mathcal{E}_m(iz) [\text{Re} \mathcal{E}'_m(iz - iv_t) - \text{Re} \mathcal{E}'_m(iz)] + \text{Im} \mathcal{E}_m(iz) [\text{Im} \mathcal{E}'_m(iz - iv_t) + \text{Im} \mathcal{E}'_m(iz)]}{\sinh(\pi z) \sinh[\pi(z - v_t/2)] [\text{Re}^2 \mathcal{E}_m(iz) + \text{Im}^2 \mathcal{E}_m(iz)]} \right\}, \quad (91)$$

with the dimensionless voltage $v = 2eV/\Delta_{\text{BCS}}$ used in the parameter

$$v_t = v/(2\gamma_E t) = eV/(\pi T),$$

$\Delta_{\text{BCS}} = \pi T_{c0}/\gamma_E$ the value of the BCS gap, and cutoff $M_t = 1/(tT_{c0}\tau)$.

Note that the AL and MT fluctuation contributions, which are essential for the majority of the phenomena discussed in this review, manifest themselves only in second order ($\sim |T_{\mathbf{p}, \mathbf{k}}|^4$) in the barrier transparency (Larkin and Varlamov, 2009).

D. Fluctuation pseudogap: Asymptotic analysis

We start the analysis of Eq. (91) in the strong pair-breaking regime, when its second term is suppressed and the effect of fluctuations is manifested by the pseudogap structure in tunnel conductivity, already discussed qualitatively in the framework of the phenomenological approach.

1. Tunnel conductivity in weak magnetic field

Close to T_{c0} , in domains I–III, in sufficiently weak magnetic fields $H \ll H_{c2}(0)$, the most singular term in Eq. (91) arises from zero frequency bosonic mode $k = 0$. The summation over Landau levels can be performed in terms of polygamma functions $\psi^{(n)}(x)$, and one finds an expression valid for any combination of ϵ and $h \ll 1$:

$$I^{(\text{fl})}(\epsilon, h, v_t) = -\frac{eTS}{2\pi^3 \sigma_n R_N} \left[\ln \frac{1}{2h} - \psi\left(\frac{1}{2} + \frac{\epsilon}{2h}\right) \right] \times \text{Im} \psi'\left(\frac{1}{2}(1 - iv_t)\right). \quad (92)$$

$$I^{(\text{fl})}(V) = -e \text{Im} K^R(\omega_k \rightarrow -ieV), \quad (90)$$

where the superscript R means that the correlator $K(\omega_k)$ is continued to the plane of complex voltages in such a way that it remains an analytic function in the upper complex half plane.

The fluctuation correction to the tunneling current is presented graphically by the diagram shown in Fig. 34(b). The details of its calculation are reported by Glatz, Varlamov, and Vinokur (2014), where the complete expression valid for arbitrary temperatures, magnetic fields, and voltages was derived:

Equation (92) reproduces the results of Varlamov and Dorin (1983) and Reizer (1993). The corresponding contribution to the tunneling conductance is

$$\sigma_{\text{tun}}^{(\text{fl})}(\epsilon, h, v_t) = \frac{Se^2}{4\pi^4 \sigma_n R_N} \left[\ln \frac{1}{2h} - \psi\left(\frac{1}{2} + \frac{\epsilon}{2h}\right) \right] \times \text{Re} \psi''\left(\frac{1}{2}(1 - iv_t)\right), \quad (93)$$

which gives the pseudogap structure in the limit of the zero field (domain I)

$$\sigma_{\text{tun}}^{(\text{fl})}(\epsilon, v_t) = \frac{Se^2}{4\pi^4 \sigma_n R_N} \ln \frac{1}{\epsilon} \text{Re} \psi''\left(\frac{1}{2}(1 - iv_t)\right). \quad (94)$$

A corresponding plot for the tunneling resistance is shown in Fig. 38 for different values of ϵ . The value of the pseudogap follows from the maximum of Eq. (94), which appears for $v_t = 1$. This gives

$$eV_{\text{max}}(\epsilon, h = 0) = \gamma_E \Delta_{\text{BCS}}(1 + \epsilon). \quad (95)$$

Far from T_{c0} , in domain VIII, one can restrict the consideration to the study of the temperature dependence of the magnitude of the fluctuation contribution to the differential conductivity at zero voltage. When $T \gg T_{c0}$ one can approximate the sums in Eq. (91) by integrals. For the k integration it was assumed that the main k dependence is due to the nominator and it can be omitted in the argument of the ψ function. Cutting off the double logarithm divergence at the upper limit in the usual way, one finds

$$\sigma_{\text{tun}}^{(\text{fl})}(t \gg 1, v_t = 0) = -\frac{Se^2}{4\pi^2 \sigma_n R_N} \left(\ln \ln \frac{1}{T_{c0}\tau} - \ln \ln t \right), \quad (96)$$

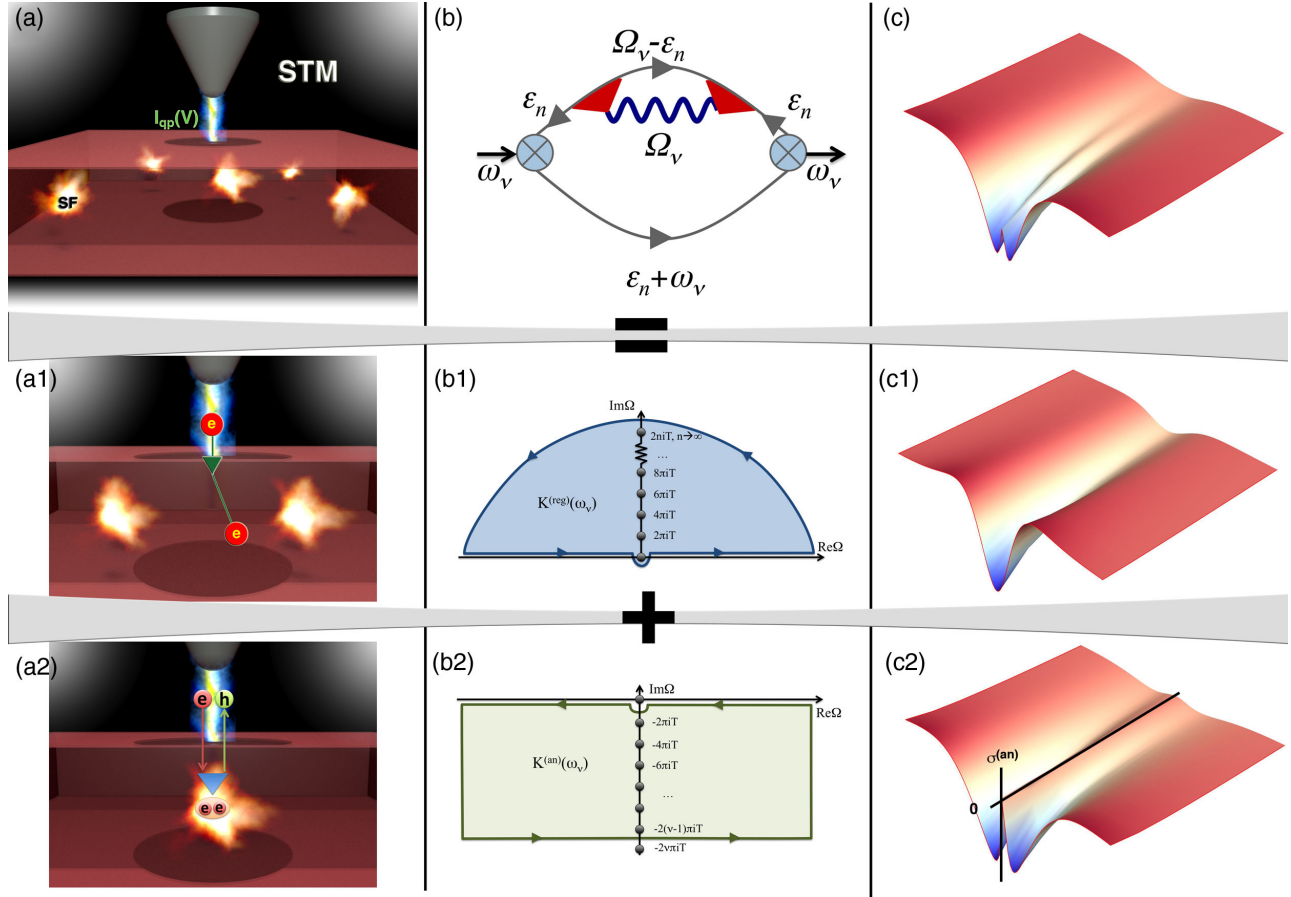


FIG. 34. (a) Schematic STM setup of a N-I(N + SF) tunnel experiment. (a1) An injected electron pair ($2e$) thermalizes in the electrode, which reduces the density of states due to superconducting fluctuations. (a2) Andreev-like reflections of injected electrons in the region of superconducting fluctuations. (b) The (Matsubara) diagram describing the fluctuation contribution to tunneling current. (b1), (b2) Two contours in the plane of complex voltage describing both corresponding tunneling processes shown in (a1) and (a2). (c) Surface plot of the total tunneling conductivity, Eq. (91), depending on voltage and temperature. The corresponding theoretical expression is valid throughout the whole phase diagram of temperature and magnetic field with a wide pseudogap structure and narrow low-bias anomaly (LBA). (c1) Pseudogap anomaly related to the renormalization of the one-electron density of states due to superconducting fluctuations in the electrode. It directly corresponds to the process pictured in (a1) and contour (b1). (c2) LBA contribution of the tunneling conductivity due to process (a2), resulting from contour (b2). From Glatz, Varlamov, and Vinokur, 2014.

which is again in complete agreement with Varlamov and Dorin (1983). This double logarithmic behavior in the wide range of temperatures up to $14T_{c0}$ was observed by Sacépé *et al.* (2010).

2. Vicinity of the line $H_{c2}(T)$

In the vicinity of the line $H_{c2}(T)$, the LLL approximation, Eq. (39), for the $\mathcal{E}_0(k)$ can be applied. It is valid along the line $H_{c2}(T)$ where $t \ll h_{c2}(t)$. The summation in the first term of Eq. (91) can be performed using

$$\sum_{k=0}^{\infty} \frac{1}{k + \alpha} \frac{1}{(k + \beta)^2 + \gamma^2} = -\frac{1}{\gamma} \text{Im} \frac{\psi(\beta + i\gamma) - \psi(\alpha)}{\beta + i\gamma - \alpha} - \frac{1}{2\alpha\beta^2 + \gamma^2},$$

which gives an expression for the regular part [first term in Eq. (91)] of the fluctuation tunneling current valid for low enough temperatures along the line $h_{c2}(t)$:

$$I^{(n)}[t \ll h_{c2}(t), \tilde{v}_t] = -\frac{2eST_{c0}h}{\pi^3 \sigma_n R_N} \frac{\tilde{v}_t}{1 + \tilde{v}_t^2} \left\{ \ln \sqrt{1 + \tilde{v}_t^2} + \left[\ln \left(\frac{4h}{\pi^2 t} \right) - \psi \left(\frac{4h}{\pi^2 t} \tilde{h} \right) \right] - \frac{\arctan \tilde{v}_t}{\tilde{v}_t} \right\}. \quad (97)$$

Here we introduced the dimensionless voltage

$$\tilde{v}_t = \frac{V}{V_0(t, \tilde{h})}.$$

The value

$$V_0(t, \tilde{h}) = \frac{\Delta_{\text{BCS}}}{2e} [1 + 2\gamma_{Et} - \tilde{h}/h_{c2}(t)] \quad (98)$$

determines the voltage at which the differential conductivity crosses zero in the considered domain of the phase diagram [see Figs. 35(g) and 35(h)] as we will see later.

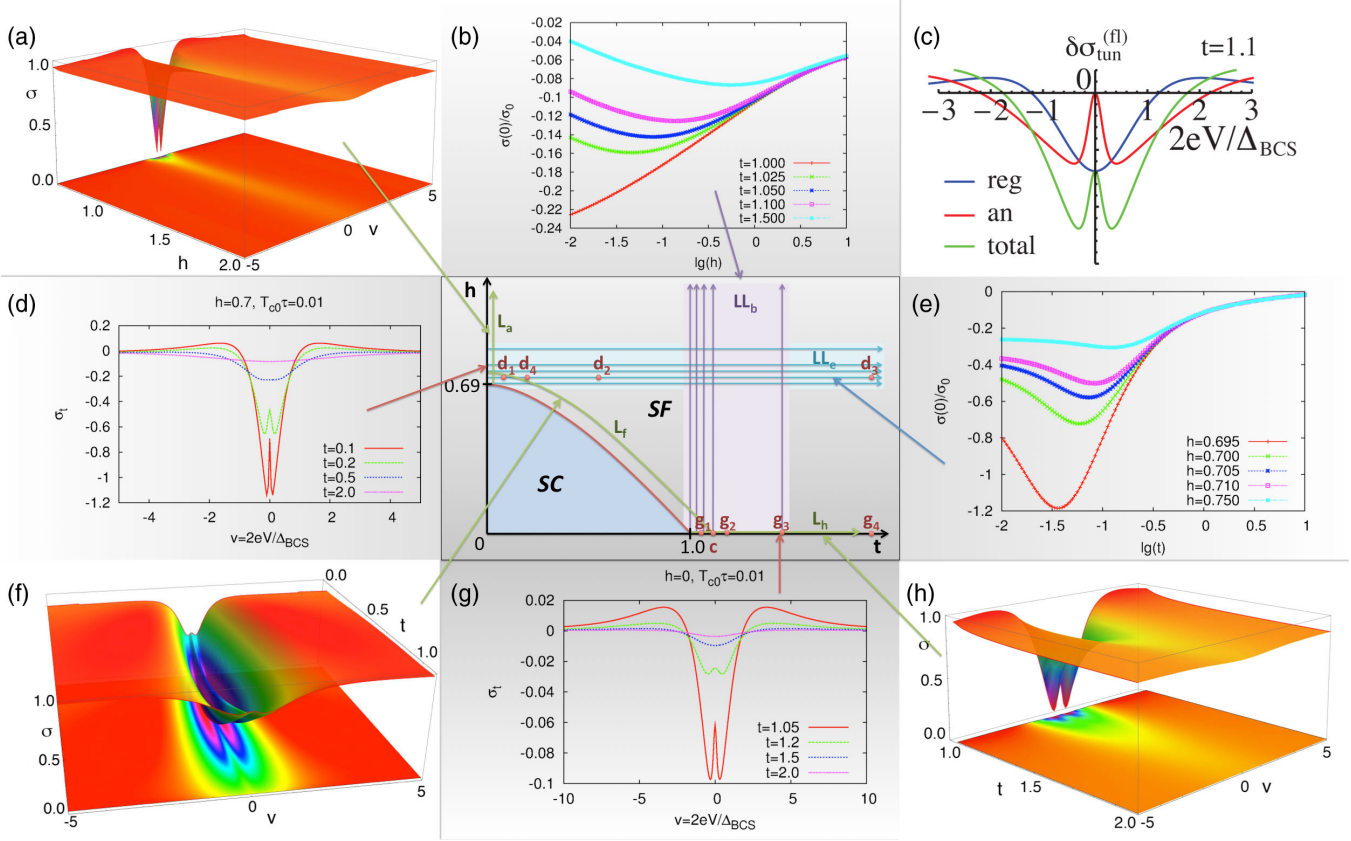


FIG. 35. Various plots of the tunneling conductance for different cuts and points in the t - h plane. The cut lines and points are indicated in the t - H phase diagram in the central panel. Points are labeled by the panel letter, lines by “L,” and panel letter subscript. (a) Low-temperature ($t = 0.05$) dependence of the conductivity as a surface plot depending on voltage v and magnetic field $h > h_{c2}(0) = 0.69$ (cut line L_a). (b) Zero-bias conductivity at fixed temperatures as a function of $\ln(h)$ (cut lines LL_b). (c) $t = 1.1$ plot of the components (pseudogap “reg” and LBA “an”) of the tunneling conductivity (point c). (d) Tunnel conductance for $h = 0.7$ at different temperatures depending on v (points d_1 – d_4). (e) Zero-bias conductivity at fixed magnetic field as a function of $\ln(t)$ (cut lines LL_e). (f) Conductivity as a surface plot depending on voltage and closely following the superconducting transition line in the t - h plane (cut line L_f). (g) Tunnel conductance for $h = 0$ at different temperatures depending on v (points g_1 – g_4). (h) Zero-field ($h = 0$) dependence of the conductivity as a surface plot depending on voltage v and temperature $t > t_c = 1$ (cut line L_h) [the same parameters as used for column (c) of Fig. 34]. From Glatz, Varlamov, and Vinokur, 2014.

Close to $H_{c2}(0)$, in the region of quantum fluctuations $t \ll \tilde{h}$, the argument of the ψ function in Eq. (97) becomes large despite the smallness of \tilde{h} , and the ψ function can therefore be approximated by its logarithmic asymptotic expression:

$$I^{(fl)}(\tilde{h}, \tilde{v}_t) = -\frac{e\Delta_{\text{BCS}}S}{4\pi^2\sigma_n R_N} \frac{\tilde{v}_t}{1 + \tilde{v}_t^2} \ln \frac{\sqrt{1 + \tilde{v}_t^2}}{\tilde{h}}.$$

The corresponding tunneling conductivity up to logarithmic accuracy is given by

$$\sigma_{\text{tun}}^{(fl)}(\tilde{h}, \tilde{v}_t) = \frac{dI}{dV} \approx -\frac{e^2 S}{2\pi^2\sigma_n} \frac{1}{[1 - 8\gamma_E \tilde{h}/\pi^2] (1 + \tilde{v}_t^2)^2} \ln \frac{\sqrt{1 + \tilde{v}_t^2}}{\tilde{h}}.$$

At zero temperature one just needs to replace \tilde{v}_t by v . One sees that this expression has a pseudogap structure similar to Eq. (94). The corresponding value of the pseudogap close to H_{c2} is given by

$$eV_{\text{max}}(t = 0, h = \pi^2/(8\gamma_E)) = \frac{\sqrt{3}}{2} \Delta_{\text{BCS}}. \quad (99)$$

Comparing Eq. (99) to Eq. (95), one notices that the fluctuation pseudogap is determined by Δ_{BCS} in both cases, but the numerical coefficients depend on the shape of the fluctuation correction of tunneling conductivity.

In the region of high fields $H \gg H_{c2}$ and low temperatures, the sums in Eq. (91) can be approximated by integrals, which gives for the value of the differential conductivity at zero voltage:

$$\sigma_{\text{tun}}^{(fl)}(h \gg 1, v = 0) = -\frac{e^2 S}{4\pi^2\sigma_n R_N} \left(\ln \ln \frac{1}{T_{c0}\tau} - \ln \ln h \right).$$

One can see that this dependence is exactly the same as the one in the case of high temperatures with reversed roles of the reduced temperature and field.

E. Weak pair breaking: Low-bias anomaly

The second term in Eq. (91) describes the anomalous process of Andreev reflection of injected, energetically non-relaxed electrons at a fluctuation-induced superconducting domain in the biased electrode; see Figure 34(a2). In order to participate in fluctuation Cooper pairing, the injected electron “extracts” an electron-hole pair from the vacuum with momentum opposite to its own and forms a Cooper pair with the electron, while the remaining hole returns along its previous trajectory; see Fig. 34(a2). This quantum coherent contribution cannot be accounted for by the phenomenological method, but can be derived only within the microscopic diagrammatic approach. This anomalous tunneling process gives rise to an additional current, which like the regular one is proportional to the first powers of the Ginzburg-Levanyuk number and barrier transparency and is cubic in voltage V near zero bias. The additional current becomes relevant only sufficiently close to the superconducting transition. As a result, a peculiar LBA appears near the superconducting transition line $H_{c2}(T)$.

It turns out that the discussed LBA in the I - V characteristics appears only in the case where the energy (or phase) relaxation time τ_ϕ of an electron injected into the explored electrode is long enough $T_{c0}\tau_\phi \gg \hbar/k_B$. The shape of the LBA close to the critical temperature [$\hbar\tau_\phi^{-1} \lesssim k_B(T - T_{c0}) \ll k_B T_{c0}$] for low voltages $eV \lesssim k_B(T - T_{c0})$ can be found analytically:

$$\sigma_{\text{tun}}^{(fl)} = -\frac{7\zeta(3)e^2 S}{2\pi^4 \hbar \sigma_n R_N} \left[\ln \frac{T_{c0}}{T - T_{c0}} + \frac{3\tau_\phi}{8\pi \hbar k_B} \frac{(eV)^2}{(T - T_{c0})} \right]. \quad (100)$$

When $k_B(T - T_{c0})$ decreases to the value $\hbar\tau_\phi^{-1}$, the growth of the LBA ceases. One can show that close to the transition temperature T_{c0} , the dip in the tunneling conductivity develops on the scale $eV_{\text{LBA}}^{(th)} \sim \Delta_{\text{BCS}}^{1/2} \sqrt{\hbar\tau_\phi^{-1}(T - T_{c0})/T_{c0}} \ll \Delta_{\text{BCS}}$. At zero temperature, close to the second critical field $H_{c2}(0)$, fluctuations acquire a quantum nature and the corresponding voltage scale becomes $eV_{\text{LBA}}^{(QF)} \sim \Delta_{\text{BCS}}^{1/2} \sqrt{\hbar\tau_\phi^{-1}[H - H_{c2}(0)]/H_{c2}(0)} \ll \Delta_{\text{BCS}}$. From Eq. (100), one can see that the intensity of the LBA is directly proportional to the energy relaxation length $\ell_\phi = v_F \tau_\phi$, which is in complete agreement with the physical picture of this non-trivial quantum coherence effect presented: the anomalous Cooper pair formation takes place only in a volume of size $S\ell_\phi$ near the contact area, where the injected electrons are nonthermalized.

F. Epilogue of the theoretical analysis

Graphical representations of the full fluctuation contribution to tunneling conductivity as a function of magnetic field, temperature, and voltage are presented in Figs. 34(c) and 35. One can see that as external parameter values depart from the transition line, the amplitude of the LBA rapidly decays.

Remarkably, both complimentary physical processes shown in Figs. 34(a1) and 34(a2) are straightforwardly expressed in terms of a graphic mathematical language: the calculation of the diagram of Fig. 34(b) is reduced to the evaluation of the

integrals of the electron Green’s functions in the linked electrodes along two contours in the complex frequency plane shown in Fig. 34(b1) and 34(b2), respectively. The upper contour corresponds to the conventional GM tunneling, while the lower one describes the contribution due to Andreev reflection from superconducting fluctuations. Accordingly, the fluctuation part of the tunneling conductance shown in Fig. 34(c) exhibits both, the pseudogap anomaly due to fluctuation depletion of the one-electron DOS [Fig. 34(c1)] coming from the integration over the contour of Fig. 34(b1) and the Andreev reflection induced LBA [Fig. 34(c2)], arising from the integration over the contour of panel (b2).

One should remark that the latter contribution is zero at zero-bias voltage [see Fig. 35(c)]. An important feature of this novel Andreev process is that it appears in the lowest (first-) order approximation with respect to tunneling-barrier transparency. Its additional smallness, related to the strength of fluctuations G_i , can be noticeably compensated by the presence of a small factor $(T - T_{c0})$ in the denominator of the second term of Eq. (100), which makes the effect strongly temperature dependent close to the transition point.

The LBA, which appears already in first order of the transparency, differs qualitatively from the well-known Andreev conductance of a superconducting microconstriction (Blonder, Tinkham, and Klapwijk, 1982). This occurs below the transition temperature and rapidly disappears when going from the metallic toward the tunneling regime. The reason for this discrepancy is that the fluctuation-induced superconducting regions in the biased electrode are not separated by any barrier from the surrounding normal phase and thus the process of Andreev reflection does not involve any additional tunneling process.

Figure 35 shows the plots of fluctuation contributions to the tunneling conductivity for different parts of the temperature-magnetic field phase diagram of the superconducting film. The central panel (the h - t phase diagram) depicts the parameter combinations or ranges for the 2D graphs or 3D surface plots arranged around it in Figs. 35(a)–35(h). In accordance with the theoretical speculations the strength of the singularity in the low-voltage behavior of the tunneling conductance smears out when moving away from the transition line [Figs. 35(a)–35(d), 35(g), and 35(h)]. We point out that the LBA is most pronounced roughly halfway between the “end points” of the transition line; see Fig. 35(f).

G. Fluctuation spectroscopy: Analysis of experiments

There have been impressive developments in STM and STS studies of superconductivity triggered by investigations of the pseudogap state and vortex state in high-temperature cuprates (Micklitz and Norman, 2009; Scherpelz *et al.*, 2013), observations of the pseudogap in 2D disordered films of conventional superconductors (Sacépé *et al.*, 2010) (Fig. 36), investigations of the superconductor-insulator transition (Sacépé *et al.*, 2008), measurements of the tunneling conductivity close to the superconducting transition in intrinsic Josephson junctions in slightly overdoped $\text{Bi}_{2-y}\text{Pb}_y\text{Sr}_2\text{CaCu}_2\text{O}$ crystals (Krasnov *et al.*, 2011; Jacobs, Katterwe, and Krasnov, 2016) (Fig. 37), and many others.

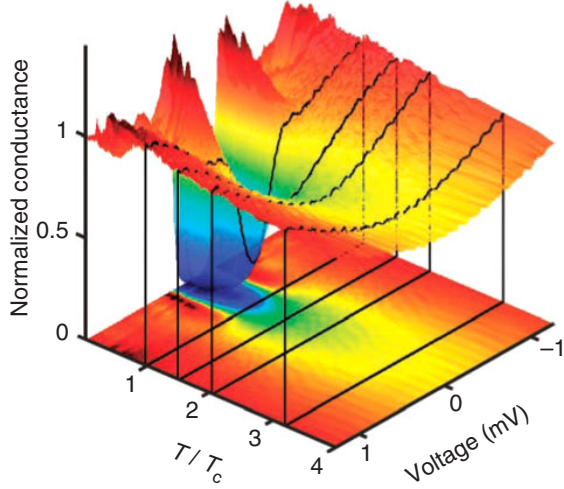


FIG. 36. Pseudogap in the density of states. Three-dimensional plot of the tunneling conductance $G(V, T/T_{c0})$ normalized by the conductance measured at high voltage and low temperature as a function of bias voltage and normalized temperature T/T_{c0} for a superconducting TiN film. Black lines mark the spectra measured at $T/T_{c0} = 1, 1.5, 2,$ and 3 , illustrating that the pseudogap state grows more pronounced and extends over a wider temperature range as the disorder increases. The suppression of the density of states of the TiN₃ sample remains visible up to $T = 14T_{c0}$. From Sacépé *et al.*, 2010.

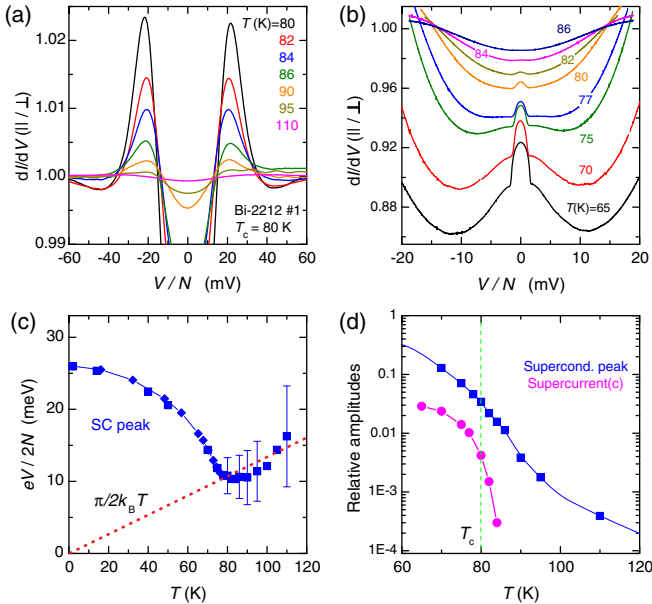


FIG. 37. (a) Tunneling curves above T_{c0} at $H = 10$ T for the Bi-2212 crystal. (b) Low-bias parts of the curves for the Bi-2212 crystal. The zero-bias maximum which below T_{c0} they attribute to an interlayer Josephson current remains also above the critical temperature. (c) Temperature dependences of the superconducting peak voltage for Bi-2212 crystal. (d) Amplitudes of the SC peak and the LBA. From Jacobs, Katterwe, and Krasnov, 2016.

1. Observation of the fluctuation pseudogap

In the inset of Fig. 38, the result of measurements of the differential resistance in a Al-I-Sn tunnel junction at temperatures slightly above the critical temperature of the Sn electrode is presented. This experiment was conducted (Belogolovskii, Khachaturov, and Chernyak, 1986) to check the proposed theory (Varlamov and Dorin, 1983), plotted as the main graphs in Fig. 38. The nonlinear differential resistance was measured at low voltages, which allowed the observation of the fine structure of the zero-bias anomaly. It is worth mentioning that the experimentally measured positions of the minima are $eV \approx \pm 3T_{c0}$, while the theoretical prediction following from Eq. (92) is $eV = \pm \pi T_{c0}$. Similar results on an aluminum film with two regions of different superconducting transition temperatures were reported by Park, Isaacson, and Parpia (1995). Observations of pseudogap anomalies in tunneling experiments at temperatures above T_{c0} were reported by Tao, Lu, and Wolf (1997), Watanabe, Fujii, and Matsuda (1997, 2000), Renner *et al.* (1998), Suzuki, Karimoto, and Namekawa (1998), Cucolo, Cuoco, and Varlamov (1999), and Matsuda, Sugita, and Watanabe (1999) using a variety of experimental techniques.

The pseudogap in the density of states of a superconducting TiN₃ film was thoroughly measured in a wide range of temperatures above T_{c0} by Sacépé *et al.* (2010). They observed how the pseudogap state becomes more pronounced and extends over a wider temperature range when increasing the disorder. The suppression of the density of states of the TiN₃ sample remains noticeable up to $T = 14T_{c0}$. The temperature dependence of the minimum of the tunnel conductivity was found to be well described by the double logarithmic behavior in Eq. (96), which indicates that its origin can be attributed to SFs.

A pseudogap, attributed to SFs, was also observed in slightly overdoped high-temperature superconductors (Jacobs, Katterwe, and Krasnov, 2016). The experimental data presented in this work [see Fig. 37(c)] confirm the

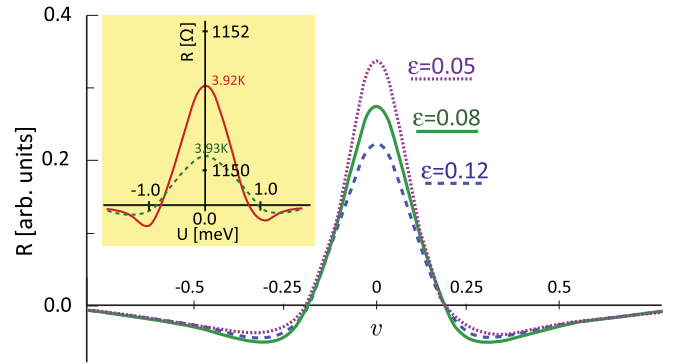


FIG. 38. Theoretical prediction for the fluctuation-induced pseudogap structure in the tunnel-junction resistance [see Eq. (92)] as a function of dimensionless voltage v for different reduced temperatures $\epsilon = 0.05, 0.08,$ and 0.12 . The inset shows a fit to experimentally observed differential resistance as a function of voltage in an Al-I-Sn junction ($R_N = 1149.4 \Omega$) just above the transition temperature ($T_{c0} = 3.88$ K) at two different temperatures $T = 3.92$ (red) and $T = 3.93$ (dashed green). From Belogolovskii, Khachaturov, and Chernyak, 1986.

prediction of a linear temperature dependence of the pseudogap (Varlamov and Dorin, 1983); see Eq. (95).

2. Observation of the low-bias anomaly

At the same time, the LBA gives rise to a new fluctuation-spectroscopy tool for determining microscopic material parameters, including the energy relaxation time τ_ϕ , the critical temperature T_{c0} , and the magnetic field $H_{c2}(0)$, by measuring the tunneling conductance and fitting the experimental data with the complete expression for the fluctuation tunneling current, Eq. (91). Remarkably, all the information about these parameters is encoded in merely the distance between the LBA dips and the height of the central peak in the conductivity curve. An observation of the described LBA in a dc experiment is indicative of the appearance of fluctuation Cooper pairs during the time of the experiment at the point below the STM tip. Recent tunneling current measurements of N-I-S junctions indeed indicate the presence of the LBA (Jacobs, Katterwe, and Krasnov, 2016); see Fig. 37(b). Since the characteristic lifetime of fluctuation Cooper pairs is $\hbar/k_B(T - T_{c0})$, a time-resolved STM measurement utilizing ac currents with frequencies in the range of 1–10 GHz promises to make it possible, in principle, to “visualize” them directly in real time.

IX. EFFECT OF FLUCTUATIONS ON THE NMR RELAXATION RATE

A. General expression for the fluctuation NMR relaxation rate

Nuclear magnetic resonance spin-lattice relaxation occurs through the interaction of nuclei with low-frequency excitations (Slichter, 1990). It is an important process for studying dynamics of nuclei in novel materials (Rigamonti, Borsa, and Carretta, 1998). In the vortex phase of type-II superconductors at low temperatures, localized superconducting regions of size ξ_{BCS} separate magnetic flux lines, provided the applied magnetic field is below H_{c2} , but well above H_{c1} . In the vortex phase the spin-lattice relaxation is mainly due to low-energy intravortex and intervortex excitations, which are possibly connected by a spin diffusion process (Slichter, 1990). Flux line diffusion can be an additional relaxation mechanism in the vortex liquid phase (Corti *et al.*, 1996).

The effect of superconducting fluctuations on the NMR relaxation rate was studied in many works (Maniv and Alexander, 1977; Kuboki and Fukuyama, 1989; Heym, 1992; Randeria and Varlamov, 1994; Carretta *et al.*, 1996; Eschrig, Rainer, and Sauls, 1999; Gorniy *et al.*, 1999; Mitrović *et al.*, 1999, 2002; Mosconi, Rigamonti, and Varlamov, 2000; Prando *et al.*, 2010). It can be observed in a wide range of temperatures and magnetic fields beyond the second critical field line $H_{c2}(T)$. It is well known that the density of quasiparticle excitations, which enters quadratically into the NMR relaxation rate W , is suppressed by SFs (Abrahams, Redi, and Woo, 1970; Di Castro *et al.*, 1990). However, a second mechanism of how fluctuations affect spin-lattice relaxation exists. This relaxation process is of quantum nature and consists in fluctuation “self-pairing” of an electron on a self-intersecting trajectory after a spin-flip scattering event on a nucleus (Maniv and Alexander, 1977; Kuboki and Fukuyama, 1989; Larkin and Varlamov, 2009; Glatz, Galda, and Varlamov,

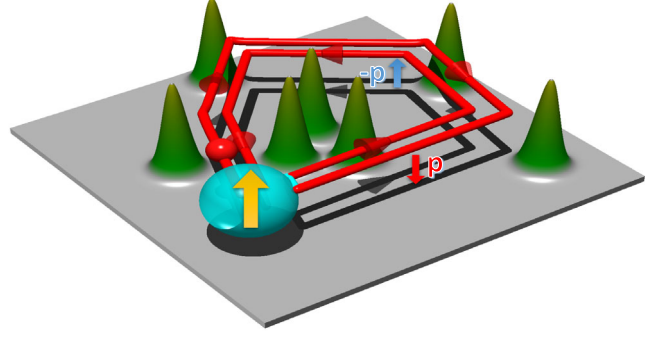


FIG. 39. The MT spin-lattice relaxation mechanism is due to self-pairing of electrons on self-intersecting trajectories involving spin-flip scatterings on the investigated nucleus [cyan (light gray)]. Initially, an electron moves along the trajectory \mathbf{p} (clockwise) and due to several impurity scattering events (green, Gaussian potential peaks) it returns to the departure point. As a result of the electron’s interaction with the nucleus, its spin and momentum flip and it returns along almost the same trajectory $-\mathbf{p}$ (counterclockwise). During this process, the electron effectively interacts with itself in the past, which is possible only due to “fast” motion of the electron along its trajectory, and the retarded character of the electron-phonon interaction.

2015); see Fig. 39. This process of MT type represents a new channel of NMR relaxation and leads to an increase of the relaxation rate W . Note that the effect of this relaxation process is of opposite sign than that of the DOS contribution.

As described in Sec. II, a dynamic state with clusters of coherently rotating FCPs is formed above the $H_{c2}(T)$ line at low temperatures. Therefore, it is important to analyze the effect of this fluctuation analog of the vortex state on the magnetic field dependence of the relaxation rate near $H_{c2}(T)$. Lascialfari, Rigamonti, and Zucca (2005) studied the ^{11}B NMR relaxation rates in a single crystal of superconducting YNi_2B_2 ($T_{c0} = 15.3$ K). They observed an anomalous peak in $W(H)$ at low enough temperatures (2 and 4 K) in fields close to $H_{c2}(T)$, which was tentatively attributed to quantum fluctuations of magnetic flux lines. Next we review the effects of superconducting fluctuations, both of thermal and quantum nature, on the NMR relaxation mechanisms.

The NMR relaxation rate W is determined by the imaginary part of the static limit of the dynamic spin susceptibility integrated over all momenta:

$$W = T \lim_{\omega \rightarrow 0} \frac{A}{\omega} \text{Im} \int (d\mathbf{k}) \chi_{\pm}^R(\mathbf{k}, -i\omega), \quad (101)$$

where A is a positive constant involving the gyromagnetic ratio, and $\chi_{\pm}^R(\mathbf{k}, \omega) = \chi_{\pm}(\mathbf{k}, \omega_\nu \rightarrow -i\omega + 0^+)$ is the dynamic spin susceptibility, calculated as

$$\chi_{\pm}(\mathbf{k}, \omega_\nu) = \int_0^{1/T} d\tilde{\tau} e^{i\omega_\nu \tilde{\tau}} \langle \hat{T}_{\tilde{\tau}} (\hat{S}_+(\mathbf{k}, \tilde{\tau}) \hat{S}_-(-\mathbf{k}, 0)) \rangle. \quad (102)$$

Here \hat{S}_{\pm} are the spin raising and lowering operators, $\tilde{\tau}$ is the imaginary time, $\omega_\nu = 2\pi T\nu$ ($\nu = 0, 1, 2, \dots$) are bosonic Matsubara frequencies corresponding to the external field, and the angle brackets denote thermal and impurity averaging in the usual way.

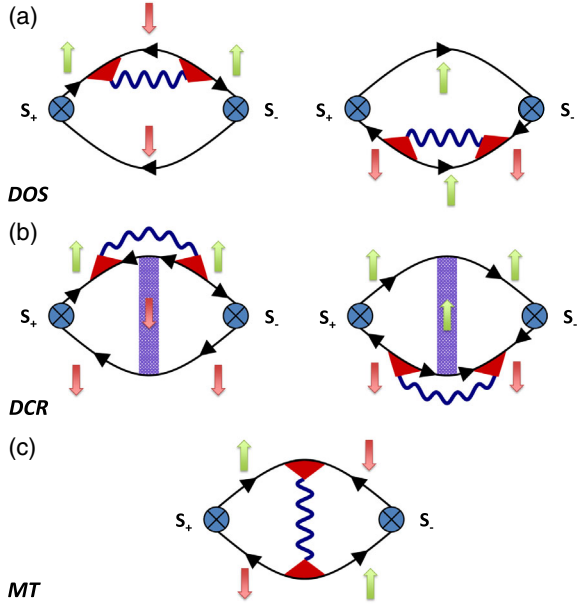


FIG. 40. Spin susceptibility diagrams. The solid lines correspond to free-electron Green's functions, the wavy lines correspond to the fluctuation propagator, and the dashed triangles and rectangles represent electron scattering at impurities. The two diagrams (a) correspond to the DOS correction, the diagrams (b) represent the renormalization of the diffusion coefficient (DCR), and the diagram (c) corresponds to the MT process. From Glatz, Galda, and Varlamov, 2015.

For noninteracting electrons, $\chi_{\pm}^{(0)}(\mathbf{k}, \omega_{\nu})$ is determined by the usual loop diagram with the $\hat{S}_{\pm}(\mathbf{k}, \tilde{\tau})$ operators playing the role of external vertices (electron interaction with the external field), leading to the well-known Korringa law $W_0 = 4\pi A T \rho_e^2$.

The first-order fluctuation correction to χ_{\pm} in dirty superconductors at magnetic fields $H > H_{c2}(T)$ can be calculated as the standard loop of two Green's functions "dressed" (see Fig. 40) with a fluctuation propagator (32) and impurity vertices (30) and (31). Figure 40 shows the diagrams for fluctuation corrections to spin susceptibility. The two diagrams in Fig. 40(a) represent the effect of fluctuations on the single-particle self-energy, leading to a decrease in corresponding DOS at the Fermi

level. Consequently, in accordance with the Korringa law, SFs reduce the relaxation rate W with respect to its normal value. This opens a type of fluctuation spin gap on the approach of the transition line $H_{c2}(T)$ from the normal phase.

Figure 40(b) contains four-leg Cooperon impurity blocks, which account for the corrections to the NMR relaxation rate due to DCR processes. An analogous contribution is a dominant correction to fluctuation conductivity in the regime of quantum fluctuations (Glatz, Varlamov, and Vinokur, 2011a). However, in the case of spin susceptibility, these contributions are strongly suppressed due to the additional integration over external momenta (Randeria and Varlamov, 1994), which makes them proportional to the square of the small Ginzburg-Levanyuk number.

The MT process shown in Fig. 40(c) has one important difference from the corresponding diagram for conductivity. Because of the particular spin assignments on the free-electron Green's function, the MT diagram for spin susceptibility is a nonplanar graph containing a single fermion loop. Yet, the MT diagram for conductivity is a planar graph with two fermion loops (Larkin and Varlamov, 2009). Since the number of loops determines the sign of the fluctuation correction (Abrikosov *et al.*, 1965), the contribution of the MT diagram to spin susceptibility bears the opposite sign to that for conductivity (Kuboki and Fukuyama, 1989). Therefore, MT spin-lattice relaxation processes result in an increase of W with respect to the Korringa value.

The sign of the MT contribution is not the only difference between the first-order corrections to fluctuation conductivity and spin susceptibility. Because of the presence of the spin-flip operators $\hat{S}_{\pm}(\mathbf{k}, \tilde{\tau})$ as external vertices in the diagram for spin susceptibility, the Aslamazov-Larkin process is completely absent from the corrections to the NMR relaxation rate. It is impossible to consistently assign spin labels to the central fermion lines for spin-singlet pairing (Maniv and Alexander, 1977).

When collecting the DOS and MT contributions in one expression and normalizing the result by the normal Korringa relaxation rate in metals, one finds (Glatz, Galda, and Varlamov, 2015) the following expression for $W^{(n)}$ valid in the whole phase diagram (with the restrictions discussed previously):

$$\frac{W^{(n)}(t, h)}{W_0} = \frac{\text{Gi}_{(2)}}{7\zeta(3)} \left(\frac{h}{t}\right) \sum_{m=0}^M \left[\sum_{k=-\infty}^{\infty} \frac{8\mathcal{E}_m''(t, h, |k|)}{\mathcal{E}_m(t, h, |k|)} + 4\pi \int_{-\infty}^{\infty} \frac{dz}{\sinh^2(\pi z)} \frac{\text{Im}\mathcal{E}_m'(t, h, iz)\text{Im}\mathcal{E}_m(t, h, iz)}{\text{Re}^2\mathcal{E}_m(t, h, iz) + \text{Im}^2\mathcal{E}_m(t, h, iz)} \right. \\ \left. + \frac{\pi}{\gamma_{\phi}/\pi^2 + \eta(m + 1/2)} \int_{-\infty}^{\infty} \frac{dz}{\sinh^2(\pi z)} \frac{\text{Im}^2\mathcal{E}_m(t, h, iz)}{\text{Re}^2\mathcal{E}_m(t, h, iz) + \text{Im}^2\mathcal{E}_m(t, h, iz)} \right]. \quad (103)$$

1. Asymptotic analysis

a. Vicinity of T_{c0} (domains I-III)

First we present the limiting behavior of $W^{(n)}$ in the thermal and quantum regimes in Eq. (103). Close to T_{c0} and for magnetic fields not too high ($h \ll 1$) but arbitrary with respect to reduced temperature $\epsilon = (T - T_{c0})/T_{c0} \ll 1$ and phase-breaking rate $\gamma_{\phi} \ll 1$, one obtains

$$\frac{W^{(n)}(\epsilon, h \ll 1)}{W_0} = -3\text{Gi}_{(2)} \left\{ \left[\ln \frac{1}{h} - \psi \left(\frac{\epsilon}{2h} + \frac{1}{2} \right) \right] \right. \\ \left. - \frac{\pi^4}{168\zeta(3)} \frac{1}{\epsilon - \gamma_{\phi}} \left[\psi \left(\frac{\epsilon}{2h} + \frac{1}{2} \right) - \psi \left(\frac{\gamma_{\phi}}{2h} + \frac{1}{2} \right) \right] \right\}. \quad (104)$$

TABLE V. Asymptotic expressions for the total relative correction to the NMR relaxation rate in different domains; see Fig. 9. The first column gives the domain according to that figure and is determined by the t and h regions given in Fig. 9.

Domain	$\delta W^{(n)}/W_0$
I	$3\text{Gi}_{(2)}\left[\frac{\pi^4}{168\zeta(3)}\frac{1}{e-\gamma_\phi}\ln\frac{e}{\gamma_\phi}-\ln\frac{1}{e}\right]-\text{Gi}_{(2)}\frac{h^2}{2e^2}\left[\frac{\pi^4}{168\zeta(3)}\frac{\gamma_\phi+\epsilon}{\gamma_\phi^2}-1\right]$
II	$3\text{Gi}_{(2)}\left[\frac{\pi^6}{672\zeta(3)}\frac{1}{h}-\ln\frac{1}{h}\right]$
III	$3\text{Gi}_{(2)}\left\{\frac{\pi^4}{168\zeta(3)}\frac{2h}{(\epsilon+h)(\gamma_\phi+h)}-\ln\frac{1}{h}\right\}$
I–III	Equation (104)
IV	$-\frac{4\pi^2\text{Gi}_{(2)}}{7\zeta(3)}\left[\ln\frac{1}{h}+\frac{\pi^4 t^3 \gamma_\phi}{192h_{c2}^2(0)h^2}\right]$
V	$-\frac{4\pi^2\text{Gi}_{(2)}}{7\zeta(3)}\ln\frac{1}{h}$
VI–VII	$-\frac{4\pi^2\text{Gi}_{(2)}}{7\zeta(3)}\left[\ln\frac{1}{h(t)}+\frac{\pi^2 t^2 \gamma_\phi}{16h_{c2}^2(t)h(t)}\right]$
IV–VII	Equation (105)
VIII	$-\frac{2\pi^2\text{Gi}_{(2)}}{7\zeta(3)}\left[\ln\ln\frac{1}{T_{c0}t}-\ln\ln t\right]$
IX	$-\frac{2\pi^2\text{Gi}_{(2)}}{7\zeta(3)}\left[\ln\ln\frac{1}{T_{c0}t}-\ln\ln h\right]$

As with fluctuation corrections to conductivity discussed in Sec. V, one can split the limiting cases into nine domains, according to Fig. 9. In the limit of weak field near T_{c0} , $h \ll \epsilon \ll 1$ (domain I), the first term in the corresponding correction (see Table V) reproduces the zero-field result from Maniv and Alexander (1977), Kuboki and Fukuyama (1989), Heym (1992), and Randeria and Varlamov (1994), while the second term provides the magnetic field dependence first calculated by Mosconi, Rigamonti, and Varlamov (2000). One can see that the MT contribution dominates when the pair breaking is weak, i.e., in weak fields SFs increase the NMR relaxation rate.

As the phase-breaking grows, the role of the first term in domain I of Table V weakens, and the contribution of fluctuations can change sign. The MT trajectories shorten, and the negative contribution of superconducting fluctuations due to the suppression of the quasiparticle DOS becomes the dominant one. Since $\gamma_\phi \lesssim 1$, the effect of the magnetic field on $W^{(n)}$ is always negative.

In the case $1 \gg h \gg \max\{\epsilon, \gamma_\phi\}$, domain II, the MT contribution dominates (Mosconi, Rigamonti, and Varlamov, 2000): here intrinsic pair breaking is weak while the effect of the magnetic field on the motion of Cooper pairs is not yet strong enough.

2. Region close to the line $H_{c2}(T)$ (domains IV–VII)

Next we discuss the domain of the phase diagram above the second critical field at relatively low temperatures, where fluctuations manifest themselves in the form of vortex clusters. The general formula (103) allows one to obtain explicit analytical expressions. For instance, the main contribution along the line $H_{c2}(T)$, where $t \ll h_{c2}(t)$, comes from the lowest Landau level of the FCP motion. Performing the summation over bosonic frequencies and the integration in Eq. (103), one finds

$$\frac{W^{(n)}(t \ll h_{c2}(t))}{W_0} = -\frac{4\pi^2\text{Gi}_{(2)}}{7\zeta(3)}\left\{\ln\frac{1}{h}+\frac{2\tilde{h}\gamma_\phi}{\pi^2}\left[\psi'\left(\frac{4h_{c2}(t)\tilde{h}}{\pi^2 t}\right)-\frac{\pi^2 t}{4h_{c2}(t)\tilde{h}}-\frac{1}{2}\left(\frac{\pi^2 t}{4h_{c2}(t)\tilde{h}}\right)^2\right]\right\}. \quad (105)$$

In domain IV, the regime of quantum fluctuations is realized at very low temperatures $t \ll \tilde{h}$ and just above $H_{c2}(0)$. Quantum fluctuations suppress the NMR relaxation due to decrease of the quasiparticle density of states. At higher temperatures $\tilde{h} \ll t \ll h_{c2}(t)$, superconducting fluctuations become thermal in nature, while the DOS suppression of the NMR relaxation remains dominant.

Figure 41 presents the results of numerical analysis based on Eq. (103) for different pair-breaking rates γ_ϕ . For small enough pair breaking, superconducting fluctuations result in the increase of the NMR relaxation rate in a large domain of the phase diagram. Increasing the pair breaking leads to the suppression of the MT contribution, and for $\gamma_\phi \sim 1$ the effect of quasiparticle DOS suppression on $W^{(n)}$ dominates in the entire phase diagram.

Note that even in the absence of pair breaking $\gamma_\phi \rightarrow 0$ the MT relaxation process is suppressed by strong magnetic fields below some crossover temperature T_0^* , at which point the fluctuation correction $W^{(n)}$ becomes negative. In the case of a 2D superconductor, $T_0^* \approx 0.6T_{c0}$. This results in an opening of a fluctuation spin gap in the

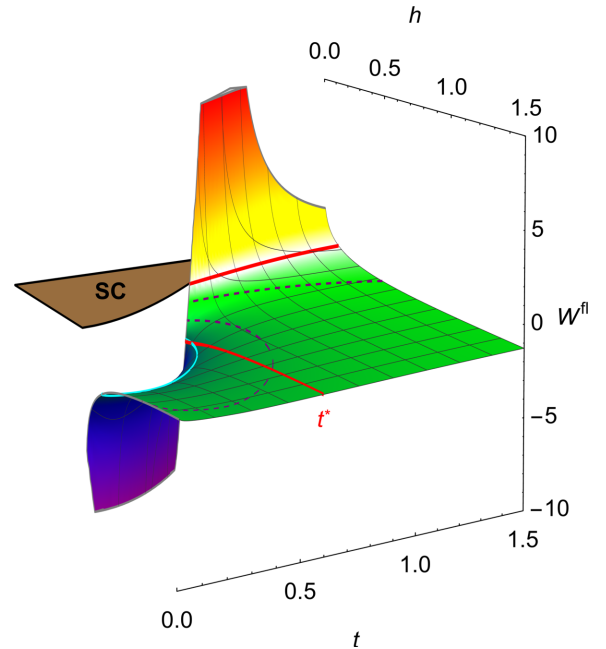


FIG. 41. The temperature and magnetic field dependence of the relaxation rate $W^{(n)}$ in the case of very weak pair breaking $\gamma_\phi = 0.003$. The thick isoline [red (dark gray)] represents a zero relaxation rate, while the dashed isolines correspond to relaxation rate values of -1 and -2 . The mesh line t^* [red (dark gray)] marks the critical temperature for $\gamma_\phi \rightarrow 0$, while the light [cyan (light gray)] contour line indicates the value of $W^{(n)}$ at $h_{c2}(t^*)$ (-3.04). From Glatz, Galda, and Varlamov, 2015.

magnetic field dependence of W at strong magnetic fields $H \gtrsim H_{c2}(T_0^*)$.

Above the crossover temperature T_0^* , the field dependence of $W^{(fl)}$ shows a nonmonotonic behavior as a result of the two competing contributions; see Fig. 41. The total correction is positive (for not too strong pair breaking γ_ϕ) close to the line $h_{c2}(t)$; it then decreases rapidly reaching a minimum negative value at some intermediate distance from $h_{c2}(t)$ before increasing up to zero when sufficiently far from the superconducting region.

Below the crossover temperature, the total correction increases monotonically as a function of the magnetic field. For $t \ll h_{c2}(t)$, in the regime of both quantum and thermal fluctuations, the numerical analysis is in full agreement with the asymptotic expressions (see Table V) confirming the negative sign of the total correction.

3. Suppression of the fluctuation contribution to the NMR rate beyond the GL region

The analysis based on Eq. (103) in the entire temperature range along $H_{c2}(T)$ allows one to identify the temperature $T^*(\gamma_\phi)$ at which the DOS and MT relaxation mechanisms fully compensate each other, such that the fluctuation correction $W^{(fl)}$ completely vanishes (in the leading order of perturbation theory). The asymptotic crossover temperature T_0^* is then defined as $T^*(0)$, i.e., the temperature below which the negative DOS contribution always dominates, regardless of the values of γ_ϕ and h .

B. Fluctuation spectroscopy: Analysis of the NMR relaxation rate

At the end of the 1990s and into the 2000s a deep controversy related to the magnetic field dependence of the fluctuation contribution to W existed. The theory predicted, as in the case with magnetoconductivity, that the positive MT contribution is suppressed by magnetic field, while the magnetic-field-dependent part of the negative DOS contribution grows with increasing magnetic field. However, in contrast to the magnetoconductivity, which can be measured extremely precisely, the NMR relaxation rate experiments are much more sophisticated. The result of the competition between these field-dependent corrections to W depends on a number of parameters (γ_ϕ, τ). The results were found to be qualitatively different in experiments on HTS materials performed by various groups. The reasons for this discussion were the absence of a strong positive AL contribution, possible d pairing, killing the MT contribution (Kuboki and Fukuyama, 1989), a small magnitude of the sum of MT and DOS effects even in the case of s pairing, the lack of the precise values of γ_ϕ, τ leading to contradicting theoretical predictions (Randeria and Varlamov, 1994; Carretta *et al.*, 1996; Eschrig, Rainer, and Sauls, 1999; Mosconi, Rigamonti, and Varlamov, 2000), and the difference in the quality of samples and experimental methods (Zimmermann *et al.*, 1991; Brinkmann, 1995; Carretta *et al.*, 1996, 2000; Gorny *et al.*, 1999; Mitrović *et al.*, 1999; Zheng *et al.*, 1999, 2000; Larkin and Varlamov, 2009).

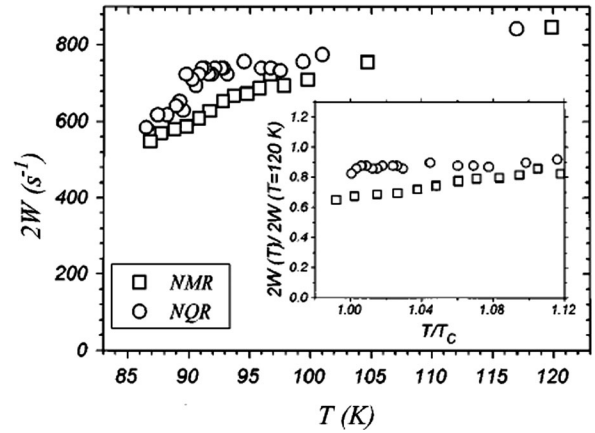


FIG. 42. ^{63}Cu relaxation rates $2W(0)$ in zero field from the NQR relaxation and $2W(H)$ in a field of 5.9 T (from NMR relaxation of the $-1/2 \rightarrow 1/2$ line) in the oriented powders of $\text{YBa}_2\text{Cu}_3\text{O}_{7-\delta}$, with $T_{c0} = 90.5$ K and $T_{c0}(H) = 87.5$ K. The relaxation rates, normalized with respect to $W(H) = W(0)$ for temperatures well above T_{c0} , are reported in the inset as a function of T/T_{c0} . From Carretta *et al.*, 1996.

The first attempt to reveal the role of the SF in the NMR-NQR (nuclear quadrupole resonance) spin-lattice relaxation rate was carried out by Carretta *et al.* (1996). Since the AL fluctuation correction is zero (for s -wave superconductors), the idea was to focus on the magnetic field dependency on MT and DOS contributions to the relaxation rate. ^{63}Cu NQR (i.e., with zero external magnetic field) measurements of W in YBCO were compared to the corresponding ones in the presence of an external magnetic field. The positive MT contribution to W near T_{c0} was correctly assumed to be strongly quenched by the field, while the negative DOS term was expected to be more robust. A small dip with respect to the Korringa behavior on approaching T_{c0} from above was observed (see Fig. 42). The studies carried out subsequently by others did not confirm the DOS dip, at least not of comparable strength. The role of impurities or defects was suspected to affect the results. Some clarification was provided by the detailed estimate of the effect of external magnetic field on the DOS contribution (Mosconi, Rigamonti, and Varlamov, 2000). Other NMR-NQR studies were carried out for ^{17}O NMR measurements (Mitrović *et al.*, 1999).

Taking into account a nonzero frequency of an ac field, the effect of amplitude fluctuations in clean superconductors was considered by Fay *et al.* (2001). The results obtained in the limit of zero frequency correspond to those of Randeria and Varlamov (1994) in the clean case. Moreover, Fay *et al.* (2001) took the effect of BKT vortex-antivortex fluctuations on the relaxation rate into account.

X. FURTHER DEVELOPMENTS OF FLUCTUATION SPECTROSCOPY

In this review, we focused on a unique approach for the description of the fluctuation phenomena in conventional, dirty 2D superconductors, valid in the wide range of temperatures and magnetic fields beyond the line $H_{c2}(T)$, including the domains of thermal and quantum fluctuations, and the crossover between them. It allows one to study

the effect of fluctuations on thermodynamic and transport characteristics of a superconductor both analytically and numerically. This approach helps to visualize it in the form of 3D surfaces spanning the entire $t-h$ parameter space above the superconducting transition and to extract from the experimental data such important characteristics as the critical temperature, second critical field, phase-breaking time, etc. In this section we discuss several extensions of the above approach.

A. Extension of fluctuation spectroscopy on quasi-two-dimensional superconductors

First we present an extension of the presented approach to quasi-two-dimensional layered superconductors by taking the transverse motion of FCPs into account. Close to T_{c0} , properties of a quasi-two-dimensional superconductor can be described well in the framework of the phenomenological Lawrence-Doniach (LD) model (Lawrence and Doniach, 1971), which provides a generalization of the Ginzburg-Landau functional. In the case of a magnetic field applied perpendicular to the coupled superconducting layers, it takes the form

$$\mathcal{F}^{(LD)}[\Psi] = \sum_l \int d^2 r \left[\alpha T_{c0} \epsilon |\Psi_l|^2 + \frac{b}{2} |\Psi_l|^4 + \frac{1}{4m} |(\nabla_{\parallel} - 2ie\mathbf{A}_{\parallel})\Psi_l|^2 + \mathcal{J} |\Psi_{l+1} - \Psi_l|^2 \right].$$

Here Ψ_l is the order parameter of the l th superconducting layer, and the phenomenological constant \mathcal{J} is proportional to the energy of the Josephson coupling between two adjacent planes. The gauge with $A_z = 0$ is chosen. In the immediate vicinity of T_{c0} , the LD functional reduces to the GL one with the effective mass $M = (4\mathcal{J}s^2)^{-1}$ along the z direction. One can relate the value of \mathcal{J} to the coherence length along the z direction, or, more conveniently, with the parameter characterizing the degree of three dimensionality of the system $r = 4\xi_z^2/s^2$: $\mathcal{J} = \alpha T_{c0} r/2$ (Larkin and Varlamov, 2009).

This generalization can also be done in the microscopic approach by accounting for transversal motion in the propagator and Cooperons

$$\Omega_H \left(n + \frac{1}{2} \right) \rightarrow \Omega_H \left(n + \frac{1}{2} \right) + \frac{\mathcal{J}}{2} (1 - \cos q_z s)$$

and performing an additional integration over transverse momenta in the final equations. This procedure was performed by Glatz, Galda, and Varlamov (2015) in order to fit the experimental data of Lascialfari, Rigamonti, and Zucca (2005). It allowed one to study the evolution of the crossover temperature $T^*(r)$ as a function of the effective dimensionality of the sample.

B. Fluctuations in two-band superconductors

The specifics of underdoped cuprates attracted the interest to consider fluctuations in these materials in terms of an effective two-gap model (Perali *et al.*, 2000). The latter was

motivated by the strong anisotropy of the band dispersion and introduced two weakly coupled bands in order to preserve a substantial distinction between the superconducting order parameter in different regions of the momentum space. This approach allows for different fluctuation regimes for pairings in different k -space regions. The strongly bound pairs forming at high temperature T^* can experience large fluctuations until the system is stabilized by the coupling with less bound, BCS-like states, leading to a coherent superconducting state at $T_{c0} < T^*$. The temperatures T_{c0} and T^* merge around or above optimum doping. Such a model shares similarities with the fermion-boson models for cuprates (Ranninger, Robin, and Eschrig, 1995; Geshkenbein, Ioffe, and Larkin, 1997), to which it reduces in the strong-coupling limit. An important conclusion of Perali *et al.* (2000) was that in the case of two very different but interacting bands, the effective Ginzburg-Levanyuk number, mainly determined by the large band, remains small. As a result, the system is stabilized with respect to fluctuations, allowing for a coherent superconducting phase.

Since the discovery of superconductivity in MgB_2 (Xi, 2008), the properties of multiband superconductors returned to the spotlight of attention after half a century of oblivion (Moskalenko, 1959; Suhl, Matthias, and Walker, 1959). Further discovery of multiband high-temperature superconductivity in iron-based materials gave an even stronger boost to this field; see the experimental (Johnston, 2010; Paglione and Greene, 2010; Stewart, 2011) and theoretical (Hirschfeld, Korshunov, and Mazin, 2011; Chubukov, 2012) reviews.

Superconducting properties of magnesium diboride are strongly influenced by multiband effects. Among the anomalies found in MgB_2 was the unusually narrow temperature range of applicability of the standard Ginzburg-Landau theory (Koshelev and Golubov, 2004; Koshelev, Varlamov, and Vinokur, 2005; Komendová *et al.*, 2011). The Cooper pairs of different kinds, formed by electrons of π bands and by electrons of σ bands, respectively, behave themselves as the unique condensate only very close to T_{c0} . Because of the large difference in the c -axis coherence lengths of σ and π bands, the condensates of different kinds split already at temperatures parametrically close to T_{c0} : $|T - T_{c0}|/T_{c0} \gtrsim \xi_{\sigma z}^2/\xi_{\pi z}^2 + S_{\pi\sigma} \ll 1$ (here $S_{\pi\sigma} \ll 1$ is the relative interband interaction constant). Evidently, this particularity should manifest itself in fluctuation properties.

The theory generalizing the microscopic theory of fluctuations to a two-band superconductor and deriving the related nonlocal GL functional was developed by Koshelev, Varlamov, and Vinokur (2005). It was strongly focused on the application to magnesium diboride, in which the main differences between the bands are the strength of intraband coupling constants and the values of the c -axis coherence length. As a result, the very early manifestation of the short-wavelength fluctuations in the π band (where superconducting interaction is weaker) was predicted. The predictions of the theory have not been confirmed experimentally (Ferrando *et al.*, 2007), likely because fluctuations in magnesium diboride are extremely weak. The Ginzburg-Levanyuk number for clean MgB_2 can be estimated as $\text{Gi}_{(3)} \approx 1.5 \times 10^{-6}$ (Koshelev, Varlamov, and Vinokur, 2005).

In contrast, the iron pnictides are multiband *semimetals* and, as a consequence, are characterized by fairly strong fluctuations. Depending on the compound, the estimates for the Ginzburg-Levanyuk number range from 3×10^{-5} to 5×10^{-3} (Koshelev and Varlamov, 2014). It is likely that the behavior of superconducting fluctuations in iron-based superconductors at sufficiently low temperatures is influenced by multiband effects. Unfortunately, the partial coherence lengths for different bands are not known at present. However, multiband effects are noticeable in the fluctuation properties of $\text{FeSe}_{0.5}\text{Te}_{0.5}$ (Klein *et al.*, 2010; Serafin *et al.*, 2010).

The study of short-wavelength and dynamic fluctuations in the vicinity of the upper critical field line for a two-band superconductor was performed by Koshelev and Varlamov (2014). As mentioned, multiband effects are more pronounced when the bands have significantly different coherence lengths. The transition to the superconducting state is mainly determined by the properties of the rigid condensate of the “strong” band, while the “weak” band with a large coherence length of the Cooper pairs causes the nonlocality in fluctuation behavior and breakdown of the simple Ginzburg-Landau picture. Usually, the effect of a magnetic field on fluctuations becomes essential when the magnetic length ℓ_H^{FCP} reaches the value of the fluctuation Cooper pair size. Since the coherence lengths of different bands together with the gaps in the multiple-band superconductor can differ strongly, one can expect that the short-wavelength fluctuation modes in them will be excited at very different fields, as it was found in the temperature dependences of paraconductivity and fluctuation heat capacity for MgB_2 (Koshelev, Varlamov, and Vinokur, 2005). As expected, the multiband electronic structure does not change the functional forms of dominating divergences of the fluctuating corrections when the magnetic field approaches the upper critical field. The temperature dependence of the coefficients, however, is modified. A nontrivial consequence of the developed theory consists of the fact that the large in-plane coherence length sets the field scale at which the upper critical field has an upward curvature (see Fig. 43). They also observed that the apparent transport transition displaces to lower temperatures with respect to the thermodynamic transition. Even though this effect exists already in the single-band

case at sufficiently high fields, it may be strongly enhanced in multiband materials.

C. Fluctuations in clean superconductors in strong fields

In the limit of a clean superconductor, when the electron mean free path considerably exceeds the BCS coherence length ($T_{c0}\tau \gg 1$), Eqs. (30)–(32) for Cooperons and the fluctuation propagator, obtained in the diffusion approximation for the electron motion, are no longer applicable. Moreover, it is known that in the ultraclean case, when the electron mean free path considerably exceeds the coherence length of FCPs, $\xi_{\text{GL}}(\epsilon)$, the DOS and MT contributions cancel each other (Livanov, Savona, and Varlamov, 2000).

The AL contribution for the case of a clean 2D superconductor in the absence of a magnetic field was analyzed in a wide range of temperatures by Reggiani, Vaglio, and Varlamov (1991). They demonstrated that in the temperature dependence of $\sigma_{(2)}^{\text{(AL)}} = (e^2/\hbar)f(\ln t)$ the low-temperature ($\ln t \ll 1$) asymptotic $f(x) = x^{-1}/16$ is replaced at high temperatures ($\ln t \gg 1$) by $f(x) = 0.12x^{-3}$. This statement was checked experimentally multiple times and it was found that the high-temperature regime already starts at an argument value of $x = 0.25$ (Cimberle *et al.*, 1997; Caprara *et al.*, 2005).

The compensation of the MT, DOS, and DCR contributions in a clean superconductor occurs at the level of the Green’s function blocks, i.e., before the integration over FCP momentum, or, more generally, the summation over its quantum numbers. This suggests that in the clean limit the AL diagram is the only remaining one, even in the case of a strong magnetic field (Galitski and Larkin, 2001a). This is why in order to study the effect of fluctuations on physical properties of a clean superconductor in an entire phase diagram, the required elements of the Feynman diagrams have to be found for arbitrary temperatures and in the presence of the magnetic field, while taking into account their nonlocal structure.

The role of the magnetic field here is twofold. First, the superconducting transition itself is governed by the magnetic field. The other effects are the de Haas–van Alphen (in thermodynamic properties) and Shubnikov–de Haas oscillations (in transport coefficients) due to the quantization of the

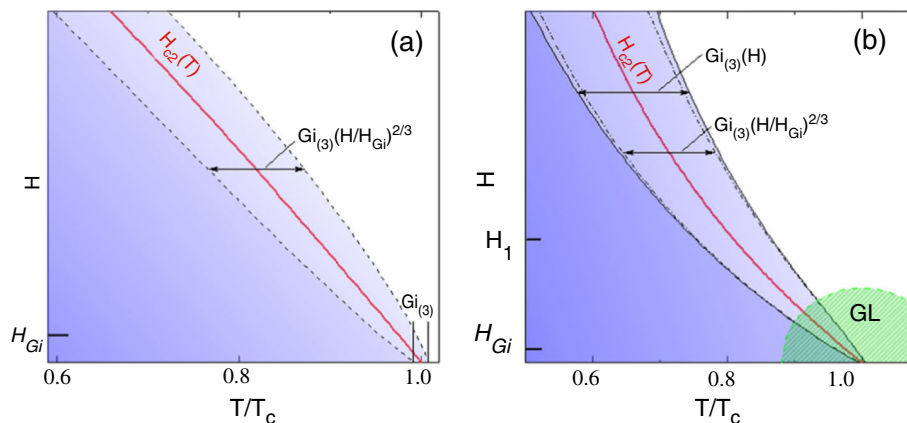


FIG. 43. Field dependences for the fluctuation region for (a) single-band and (b) two-band superconductors. $H_{\text{Gi}} \equiv \tilde{H}_{c2}(0)G_{i(3)}$ is the typical value of the magnetic field, and $G_{i(3)}(H)$ is the width of the fluctuation region. From Koshelev and Varlamov, 2014.

energy levels. However, if $\omega_c \tau \ll 1$ and $T \gg \omega_c \sim T_{c0}^2/E_F$, the oscillation terms are exponentially small and can be neglected.

The method for the analysis of fluctuation effects in the clean case, requiring one to deal with nonlocal operators, is based on the Helfand-Werthamer theory. In the seminal paper [Helfand and Werthamer \(1966\)](#), evaluated the matrix element λ_0 for the Cooperon in a magnetic field, which determines the upper critical field $H_{c2}(T)$. They proved the following mathematical statement, which is referred to as the Helfand-Werthamer theorem. Let us consider an operator \mathcal{O} and suppose that its kernel in coordinate representation has the following form:

$$\mathcal{O}(\mathbf{r}, \mathbf{r}') = \tilde{\mathcal{O}}(\mathbf{r} - \mathbf{r}') \exp\left(-2ie \int_{\mathbf{r}}^{\mathbf{r}'} \mathbf{A}(\mathbf{s}) d\mathbf{s}\right). \quad (106)$$

Then, the operator can be written as

$$\hat{\mathcal{O}} = \int \tilde{\mathcal{O}}(\mathbf{r}) \exp(-i\mathbf{r}\hat{\boldsymbol{\pi}}) d^d \mathbf{r},$$

where $\hat{\boldsymbol{\pi}} = [\hat{\mathbf{p}} - 2ie\mathbf{A}(\mathbf{r})]$ is the kinetic momentum, which can be expressed in terms of creation and annihilation operators in Landau representation. One can see that all the operators involved in these calculations satisfy the Helfand-Werthamer theorem. Namely, the particle-particle bubbles, current vertex, and the four Green's function blocks of the AL diagram in coordinate representation can be written as a product of a function of the coordinate difference and the gauge factor. Magnetic field effects can be treated semiclassically, which means that the factor $\tilde{\mathcal{O}}(\mathbf{r} - \mathbf{r}')$ in Eq. (106) can be considered in zero field.

A corresponding approach was realized by [Kurkijärvi, Ambegaokar, and Eilenberger \(1972\)](#) and [Galitski and Larkin \(2001a\)](#) in the studies of fluctuation diamagnetism and conductivity in clean superconductors.

D. Fluctuation spectroscopy of artificial nanosolids

Nanosolids are artificially designed arrays of nanocrystals composed of small crystals ranging in size from 2 to 100 nm (they are also called *granular systems*). Because of the electron confinement effect, nanocrystals can be viewed as quantum dots and the behavior of their physical properties lies in between that of molecules and bulk materials. The study of transport properties of granular metals has gained significant attention ([Goldman and Marković, 1998](#); [Beloborodov et al., 2007](#)) since the groundbreaking experiments on the superconductor-insulator transition in granular samples ([Haviland, Liu, and Goldman, 1989](#)). Altering the nanocrystal composition and size allows one to modify bulk material properties, in particular, enabling the study of the interplay between electron correlations and mesoscopic effects of disorder.

A clear experimental signature of granularity in a superconducting system was given by [Lerner, Varlamov, and Vinokur \(2008\)](#). Nanosolids are characterized by the following two one-electron transport mechanisms: the intragrain diffusion (with diffusion coefficient \mathcal{D}_g) and the intergrain tunneling (with effective diffusion coefficient $\mathcal{D}_T = \Gamma a^2$,

where Γ is the electron tunneling rate between nanograins and a is the average grain size). Typically, $\mathcal{D}_g \gg \mathcal{D}_T$ and these two mechanisms result in the appearance of two different Ginzburg-Landau lengths. The first one $\xi_{GL,g}(\epsilon) = (\mathcal{D}_g/T_{c0}\epsilon)^{1/2}$ is a result of intragrain pairing, while the second $\xi_{GL,T}(\epsilon) = (\mathcal{D}_T/T_{c0}\epsilon)^{1/2}$ corresponds to pairing across (intergrain) grains. As a consequence, there are three distinct temperature regimes in the vicinity of the critical temperature. In the first one, far from T_{c0} , where $\epsilon > \mathcal{D}_g a^{-2} T_{c0}^{-1} = E_{Th}/T_{c0}$ (E_{Th} is the Thouless energy), the pairing has an intergrain nature. In this region the FCPs of each grain are independent and their motion has 3D character, corresponding to a critical exponent of the paraconductivity of $-1/2$. When temperature approaches T_{c0} and $\xi_{GL,g}(\epsilon)$ becomes larger than the grain size, while $\xi_{GL,T}(\epsilon)$ remains smaller, the pairing still has the intergrain nature, but the size of FCPs in this temperature range ($\Gamma/T_{c0} \ll \epsilon \ll E_{Th}/T_{c0}$) exceeds the grain diameter. Here each grain acts as its own zero-dimensional (0D) superconductor for which the paraconductivity is expected to be proportional ϵ^{-2} . However, an intergrain FCP transport requires two electrons to hop within one GL lifetime $\tau_{GL} \sim \epsilon^{-1}$ such that the AL contribution in a quasi-0D array of grains should in fact be $\sim \epsilon^{-3}$. Finally, in the immediate vicinity of the critical temperature $\epsilon \ll \Gamma/T_{c0}$, the coherence length $\xi_{GL,T}(\epsilon)$ exceeds the grain size and the pairing involves electrons of different grains such that the system becomes effectively 3D and the critical exponent of the paraconductivity is $-1/2$, the same as in region $E_{Th}/T_{c0} < \epsilon$. This qualitative picture was supported by the rigorous calculations of [Lerner, Varlamov, and Vinokur \(2008\)](#). Another type of dimensional double crossover of fluctuation conductivity as a function of temperature was predicted for multilayer superconducting films by [Varlamov and Yu \(1991\)](#).

Recently [Klemencic et al. \(2017\)](#) presented measurements for the resistance versus temperature in a series of boron-doped nanocrystalline diamond (BNCD) films with different grain sizes, varied by changing the film thickness. Upon extracting the fluctuation conductivity near to the critical temperature, they indeed observed three distinct scaling regions (3D intragrain, quasi-0D, and 3D intergrain, see Fig. 44), confirming the prediction of [Lerner, Varlamov, and Vinokur \(2008\)](#). The location of the crossovers between these scaling regions allowed them to determine the tunneling energy and the Thouless energy for each film.

The tunneling energy, or Γ , is an energy associated with the transfer of carriers across grain boundaries. Therefore, it does not depend much on the morphology of the grains and is almost invariant between different film. In the work of [Klemencic et al. \(2017\)](#), Γ was extracted from the 3D to quasi-0D crossover for all samples and they found a value of $\Gamma = 4.2 \pm 2.0 \mu\text{eV}$. On the other hand, the Thouless energy should be proportional to the inverse square of the mean grain size with the proportionality factor being the intragrain diffusion coefficient. Using this relation they found a value of $\mathcal{D}_g = 11.5 \pm 5.7 \text{ cm}^2/\text{s}$.

Overall, this experimental work is another example of fluctuation spectroscopy, which allows one to extract information about the granular structure in nanosolids from the

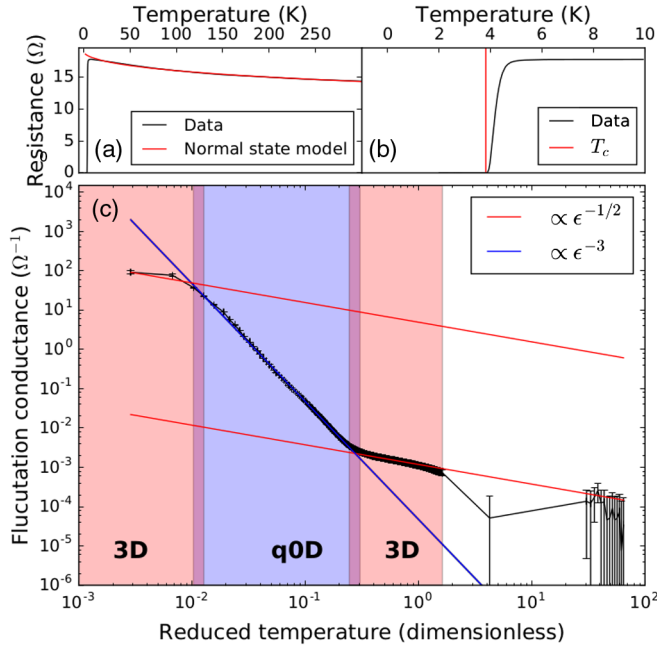


FIG. 44. Fluctuation spectroscopy of a 564-nm-thick BNCD film. (a) A fit to the high-temperature region reveals a $T^{0.5}$ dependence and allows extraction of the value of normal conductance. (b) T_{c0} is defined as the point at which the conductance diverges, depicted as a vertical line. (c) Fluctuation conductance as a function of reduced temperature ϵ . From Klemencic *et al.*, 2017.

observation of dimensional crossovers in the fluctuation regime. They concluded that this is a remarkably simple yet valuable tool for the characterization of microscopic properties of nanocrystalline superconductors.

E. Fluctuation spectroscopy of inhomogeneous films: Pseudogap and confinement

In this review, we considered fluctuations as deviations of the superconducting order parameter from its mean-field solution and their effect on various transport properties of SCs; i.e., we remained in the framework of the fermionic scenario of superconductivity relating the SC transition temperature to the appearance of a supercurrent as a response to an applied vector potential. Or, in other words, one identifies T_{c0} with the temperature at which a stable condensate of Cooper pairs with $\langle \Delta(\mathbf{r}, t) \rangle \neq 0$ appears.

The role of a weak disorder on the properties of SCs in the framework of the BCS theory was elucidated a long time ago in the seminal papers of Anderson (1959) and Abrikosov and Gor'kov (1958, 1959). It was demonstrated that in the case of SCs with isotropic spectrum and s -type pairing, which contain a not too high concentration of elastic impurities (the electronic mean free path is supposed to be much larger than the interatomic distance), the so-called Anderson theorem is valid. The latter states that to a first approximation the presence of impurities does not affect the thermodynamic properties of SCs.

Later, as the focus of attention shifted toward the study of properties of disordered and low-dimensional

superconductors, this traditional understanding of the role of impurities became the subject of revisions. Remaining in the fermionic paradigm of superconductivity, Finkel'shtein (1987) demonstrated that the delay in screening of the Coulomb interaction in a disordered two-dimensional SC leads to a decrease of the effective electron attraction and, as a result, a suppression of Cooper pair formation when the electronic mean free path becomes of the order of the interatomic distance.

Nowadays, the so-called bosonic scenario is discussed in which strong disorder may destroy the phenomenon of superconductivity by means of localization of unbroken Cooper pairs, giving rise to a specific normal pseudogap state. The way in which superconductivity is destroyed in such systems is still debated. A numerical approach to study the properties of uniformly disordered superconductors (Bouadim *et al.*, 2011) suggested that there is a continuous crossover (Trivedi *et al.*, 2012) from the weak disorder limit, where the system has a rather homogeneous fermionic character, to the strong disorder limit, where characteristic inhomogeneities appear in the superconducting order parameter. The latter has an emergent bosonic nature and is characterized by a single-particle gap, which persists on the insulating side of the transition.

Recent experiments on ultrathin NbN films seem to find indications of an intermediate regime between such fermionic and bosonic scenarios, where Cooper pairs start to localize, while still keeping their character of pairs of fermions. By combining transport and nanoscale studies of superconducting ultrathin NbN films, Carbillet *et al.* (2016) found that nanoscopic inhomogeneities emerge when the film thickness is reduced. For the thinnest films, scanning tunneling spectroscopy at low temperature unveils inhomogeneities in the superconducting properties of typical size L_i that are not directly correlated to any structural inhomogeneity and that are found to persist above the critical temperature in the form of a pseudogap [Fig. 45(c)]. Remarkably enough, while the thickest films display a purely two-dimensional behavior of SFs above the critical temperature [Fig. 45(a)], the paraconductivity in the pseudogap regime of the thinnest samples demonstrates SFs of the order parameter which formally corresponds to a 0D regime [Fig. 45(b)]. This 0D behavior eventually crosses over to 2D paraconductivity when T_{c0} is approached. Such behavior was ascribed to an anomalous slowing down of the diffusion process at long or intermediate wave vectors.

When $\Delta\sigma$ is converted into the measured paraconductance per square by means of the length scale l_{sg} , which represents the size of the 0D *supergrain* (sg) fluctuating domains, one obtains (analogously to Sec. X.D)

$$\sigma_{0D}^{(AL)} = \left(\frac{\xi}{l_{sg}}\right)^2 \frac{\pi e^2}{4\hbar\epsilon^2}.$$

Deducing $\xi \sim 5.5 \pm 0.5$ nm from the critical field H_{c2} , it is possible to extract the value of l_{sg} from the paraconductivity data. One finds $l_{sg} = 28$ nm for samples A_2 ($T_{c0} = 4.5$ K) and X_0 ($T_{c0} = 3.8$ K), $l_{sg} = 35$ nm for sample Y_0 ($T_{c0} = 4.3$ K), and $l_{sg} = 40$ nm for sample A_4 ($T_{c0} = 2.4$ K). These values of l_{sg} are in quantitative agreement with the typical domain

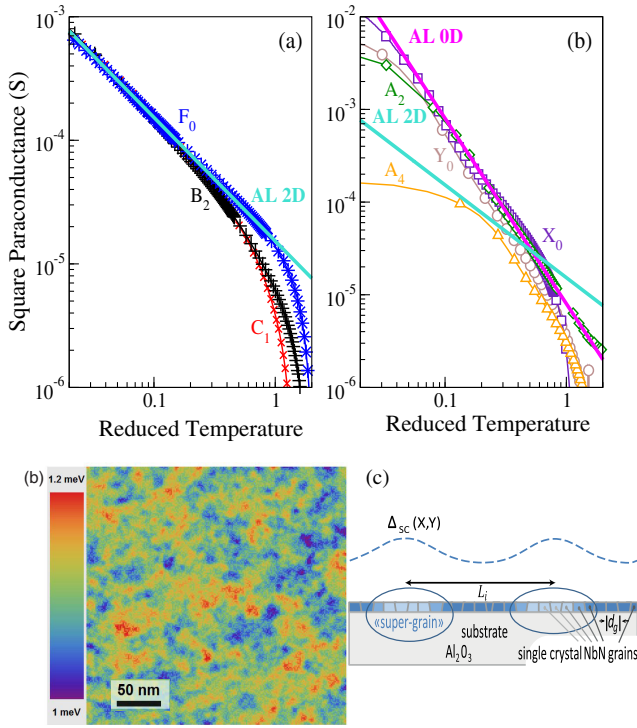


FIG. 45. (a) Extracted square paraconductance for three different, relatively thick samples B_2 ($T_{c0} = 7.1$ K, pluses), C_1 ($T_{c0} = 9.4$ K, crosses), and F_0 ($T_{c0} = 9.0$ K, asterisks) as a function of the reduced temperature $\epsilon = \ln(T/T_{c0})$. The agreement with the Aslamasov-Larkin prediction for a 2D system (cyan solid line) is excellent, without any adjustable parameter. (b) Extracted square paraconductance for the thinner samples Y_0 ($T_{c0} = 4.3$ K, open circles), X_0 ($T_{c0} = 3.8$ K, open squares), A_2 ($T_{c0} = 4.5$ K, open diamonds), and A_4 ($T_{c0} = 2.4$ K, open triangles). The pink solid line corresponds to $\sigma = 0.03e^2/(\epsilon^2)$. The expected AL 2D square paraconductance is also shown [thick cyan (light gray) solid line]. (c) Map displaying the superconducting gap inhomogeneities at 300 mK. Adapted from Carbillet *et al.*, 2016.

size $L_i/2 \sim 50$ nm extracted from STS data at 300 mK and at 4.2 K for sample X_0 ($T_{c0} = 3.8$ K). This means that it is the length $L_i/2 \sim l_{sg}$ instead of the real grain size $d_g \ll l_{sg}$ that sets the scale for the 0D fluctuating domains. Such situation remains until the temperature approaches T_{c0} so close that the coherence length $\xi_{GL}(\epsilon)$ becomes larger than L_i and the 2D behavior is recovered.

This scenario leads to a “temporary confinement” of SFs, which allows one to explain the paradoxical simultaneous presence of a pseudogap and 0D *amplitude* fluctuations of the order parameter (if the pseudogap indicates a simple localization of bosonic pairs, only phase fluctuations would be expected).

XI. NUMERICAL FLUCTUATION SPECTROSCOPY

In order to utilize the complete expressions for fluctuation corrections of conductivity $\sigma_{xx}^{(n)}(t, h)$ [Eq. (55)], NMR relaxation rate $W^{(n)}$ [Eq. (103)], Nernst coefficient $\nu^{(n)}$ [Eq. (80)], or tunneling current $I^{(n)}$ [Eq. (91)] to analyze experimental data, an efficient and accurate method to evaluate those

expressions numerically is needed. Here we review the numerical methods used for their evaluation with examples; we avoid discussing the actual implementation or technical programming issues, such as parallelization (which is straightforward for the problem discussed here). As supplementary information we provide a C++ implementation for the evaluation of all the fluctuation corrections mentioned [242].

The first important ingredient for all expressions is an efficient and accurate algorithm for the evaluation of the real and complex polygamma functions $\psi^{(n)}(z)$. The former is readily available in standard numerical toolkits such as the GNU Scientific Library (Galassi, 2009), but a complex version is a bit more difficult to find and we refer the interested reader to Jin and Zhang (1996). Another complication of most evaluations is that the summation cutoff parameter M_l can reach extremely large values at low temperatures [experimental values $(T_{c0}\tau)_{exp}^{-1}$ for materials near the superconductor-insulator transition can be on the order of 10^6], which slows the numerical procedure down significantly. The latter difficulty can be partially overcome by evaluation of the slowly divergent tails of the m sums, in Eq. (55), as integrals. Here we also note that for fitting purposes one does not need to choose actual, often extremely small, experimental values $(T_{c0}\tau)_{exp}$. To save CPU time, one can assume the value $(T_{c0}\tau)_{num}$ of this parameter to be much larger than $(T_{c0}\tau)_{exp}$ (but still much less than $T_{c0}\tau_\phi$). After the evaluation of the complete expression, the result can then be shifted by $\ln \ln (T_{c0}\tau)_{num}/(T_{c0}\tau)_{exp}$, which approximates the summands not explicitly evaluated. Nevertheless, the numerical task remains challenging: e.g., for the surface plot in Fig. 15 we evaluated 10^6 values for $\delta\sigma$ with the modest assumption $(T_{c0}\tau)_{num} = 0.01$, yet it still took three months of single core CPU time (in 2011) for its calculation.

The (convergent) integral contributions (typically z integrations) are least difficult to calculate and can be straightforwardly evaluated using a suitable quadrature scheme. It was found that the Gauss-Legendre five-point method was efficient and accurate, allowing also the integration of integrable poles or principle values. In practice, due to the presence of the $\sinh^{-2}(\pi z)$ term in the integrand, we can restrict the integration support to $z \in [-5, 5]$. Outside this interval the integrand is smaller than the numerical accuracy of double precision floating point numbers. Sums over Landau levels are calculated up to the cutoff $M_l = (tT_{c0}\tau)^{-1}$ explicitly.

In contrast, summations over k are more involved and only slowly converging or not converging at all as in the case for the susceptibility $\chi^{(n)}$ [Eq. (38), where the cutoff for Matsubara frequencies has to be taken into account]. For the numerical summation of the k sum we separate the $k = 0$ term and sum from $k = 1$ to k_{max} (with coefficient 2, due to symmetry) which is determined by the arguments of the $\psi^{(n)}$ functions being equal to $\Omega = 1000$. For $k \geq k_{max}$ we transform the sum into an integral and use only the asymptotic expressions for the polygamma functions as the difference to the exact expression is again below the floating point accuracy. Then the integration variable is inverted and we have a finite integral for the remaining part of the sum. In the case when the k sum is not converging, this integral was two nonzero finite limits.

As an example, we show the transformation of the k sum appearing in the NMR contribution, Eq. (103), to a suitable form for numerical evaluation (Glatz, Galda, and Varlamov, 2015):

$$S_m^{(\text{MT})} \equiv \sum_{k=-\infty}^{\infty} \frac{\mathcal{E}_m''(t, h, |k|)}{\mathcal{E}_m(t, h, |k|)}$$

and write

$$\begin{aligned} S_m^{(\text{MT})} &\doteq \left[\sum_{k=0}^{k_{\max}-1} (2 - \delta_{0,k}) + 2 \int_{k_{\max}}^{\infty} dk \right] \frac{\mathcal{E}_m''(t, h, |k|)}{\mathcal{E}_m(t, h, |k|)} \\ &\equiv S_m^{(\text{MT})(s)} + S_m^{(\text{MT})(i)} \end{aligned}$$

with

$$k_{\max} = \max \left\{ 2\Omega - \left\lfloor \frac{4h}{\pi^2 t} (2m+1) \right\rfloor, 1 \right\}.$$

Here we use \doteq to indicate “equal” in floating point precision.

The sum part $S_m^{(\text{MT})(s)}$ is calculated straightforwardly, which leaves the calculation of the “rest integral” $S_m^{(\text{MT})(i)}$:

$$\begin{aligned} S_m^{(\text{MT})(i)} &= \frac{1}{2} \int_{k_{\max}}^{\infty} dk \frac{\psi''[(1+k)/2 + x_m]}{\ln t - \psi(1/2) + \psi[(1+k)/2 + x_m]} \\ &\doteq -\frac{1}{2} \int_{k_{\max}}^{\infty} dk \frac{[(1+k)/2 + x_m]^{-2}}{\ln t - \psi(1/2) - \ln(2) + \ln(1+k + 2x_m)}, \end{aligned}$$

where we used the asymptotic behavior of the polygamma functions with

$$x_m \equiv \frac{2h(2m+1)}{t\pi^2}.$$

A convenient substitution is

$$\begin{aligned} \frac{1}{z} &= \frac{8}{\pi^2} + \frac{(1+k)t}{h(m+1/2)} = \frac{8}{\pi^2 x_m} \left[x_m + \frac{1+k}{2} \right], \\ \frac{dz}{z^2} &= -\frac{t}{h(m+1/2)} dk = -\frac{4}{\pi^2} \frac{dk}{x_m}, \\ z_{\max} &= \frac{\pi^2}{4} \left(2 + \frac{1+k_{\max}}{x_m} \right)^{-1}. \end{aligned}$$

Therefore,

$$\begin{aligned} S_m^{(\text{MT})(i)} &= \frac{\pi^2}{8} \int_{z_{\max}}^0 \frac{dz}{z^2} \frac{x_m(8z/\pi^2 x_m)^2}{\ln(t\pi^2 x_m/4) - \psi(1/2) - \ln(2) - \ln(z)} \\ &= -\frac{8}{\pi^2 x_m} \int_0^{z_{\max}} dz \frac{1}{A_m - \ln z} \\ &= -\frac{2t}{h(m+1/2)} \int_0^{z_{\max}} dz \frac{1}{A_m - \ln z} \end{aligned}$$

with $A_m \equiv \ln[h(m+1/2)] - \psi(1/2) - \ln(2)$. This integral is integrable and calculated by the Gauss-Legendre five-point method (which avoids the singular point at $z = 0$) with only a

few support points in the small interval 0 to z_{\max} (125 support points are sufficient to reach floating point precision).

Overall this yields a highly accurate numerical value of the k sums.

In the quasi-two-dimensional case the additional finite q integral is calculated by the Gauss-Legendre five-point method using 25 support points, which is sufficient to obtain high accuracy.

The k summations for all other fluctuation corrections can be treated in a similar fashion.

LIST OF SYMBOLS AND ABBREVIATIONS

c	speed of light (mostly set to 1)
$C^{(\text{fl})}$	fluctuation heat capacity
$C_n(\varepsilon_1, \varepsilon_2)$	four-leg Cooperon, Eq. (31)
d	effective dimension of the FCP motion
d_e	effective dimension of the electron motion
D	electron diffusion coefficient
D_g	intragrain diffusion coefficient
D_T	intergrain diffusion coefficient
e	electron unit charge
E_F	Fermi energy
E_{Th}	Thouless energy
$\mathcal{E}_m(x, t, h)$	auxiliary function inversely proportional to the fluctuation propagator, Eq. (33)
$F^{(\text{fl})}$	fluctuation correction to free energy, Eq. (37)
$G(\mathbf{p}, \varepsilon)$	one-electron Green’s function
g_{eff}	effective BCS interaction
$\text{Gi}_{(d)}$	Ginzburg-Levanyuk number, Eq. (28)
h	dimensionless magnetic field $H/\tilde{H}_{c2}(0)$
\hbar	Planck constant (mostly set to 1)
\tilde{h}	reduced magnetic field $[H - H_{c2}(0)]/H_{c2}(0)$
$H_{c2}(0)$	second critical field at zero temperature
$\tilde{H}_{c2}(0)$	second critical field extrapolated to zero temperature from the GL region
$I^{(\text{fl})}$	fluctuation correction to quasiparticle tunneling current
j_α	electric current density
\mathbf{j}^{mag}	density of persistent electric current induced by magnetization gradient
k_B	Boltzmann constant (mostly set to 1)
l	electron mean free path
ℓ_H	electron magnetic length $\sqrt{\hbar c/(eH)}$
ℓ_ϕ	phase relaxation length $v_F \tau_\phi$
l_T	thermal length $\sqrt{D/k_B T}$
$L(\mathbf{q}, \Omega_k)$	fluctuation propagator, Eq. (24)
$\mathcal{L}(p, p')$	two-particle Green’s function, Eq. (23)
m^*	effective mass of FCPs
m_e	electron mass
$m^{(\text{qp})}$	mass of quasiparticles

$M(h, t)$	magnetization, Eq. (50)	δ	phase-breaking parameter, Eq. (60)
$n(\mathbf{q})$	Bose-Einstein distribution, Eq. (5)	ϵ	reduced temperature $[T - T_{c0}]/T_{c0}$, Eq. (2)
$N_{(d)}$	FCP concentration in d dimensions, Eq. (7)	$\epsilon^{\alpha\beta\zeta}$	Levi-Civita symbol
\mathfrak{N}	Nernst signal, Eq. (74)	$\epsilon(\mathbf{q})$	kinetic energy of FCP, Eq. (6)
$n_F(E)$	Fermi distribution	ϵ_n	fermionic Matsubara frequency $(2n + 1)\pi k_B T$
$\hat{N}_{L,R}$	particle number operator in left or right electrode	$\theta(x)$	Heaviside step function
p_F	Fermi momentum	$\kappa^{\alpha\beta}$	heat conductivity tensor
$Q_{\alpha\gamma}$	“electric current–electric current” response operator	λ_F	electron Fermi length
$\tilde{Q}_{\alpha\gamma}$	“electric current–heat current” response operator	$\lambda_n(\epsilon_1, \epsilon_1)$	Cooperon, Eq. (30)
R_N	tunnel-junction resistance	μ	chemical potential
R_{\square}	sheet resistance	$\mu^{(\text{fl})}$	chemical potential of FCP close to T_{c0}
r_L	Larmor radius	$\mu^{(\text{QF})}$	chemical potential of FCP close to $H_{c2}(0)$
s	film thickness	$\mu^{(\text{QP})}$	chemical potential of quasiparticle
S	wire cross section	$\nu^{(d)}$	Nernst coefficient, Eq. (11)
T	temperature	$\nu^{(\text{fl})}$	fluctuation contribution to Nernst coefficient close to T_{c0}
t	dimensionless temperature T/T_{c0}	$\nu^{(\text{QF})}$	fluctuation contribution to Nernst coefficient close to $H_{c2}(0)$
$T_c(H)$	superconducting critical temperature	ν_e	electron contribution to Nernst coefficient
T_c^{BCS}	mean-field value of superconducting critical temperature followed from BCS theory	ρ_e	one-electron density of states
T_{c0}	superconducting critical temperature in zero field renormalized by fluctuations, Eq. (1)	$\rho_{L,R}$	density of states of the left (right) electrode
$T_{\mathbf{pk}}$	tunnel matrix element between states \mathbf{p} and \mathbf{k}	ξ	superconducting coherence length, Eq. (4)
v_F	electron Fermi velocity	$\xi_{\text{cl},D}$	coherence length for clean or dirty systems
v	dimensionless voltage $2(eV/\Delta_{\text{BCS}})$	ξ_{GL}	GL coherence length, Eq. (3)
V	voltage	ξ_{BCS}	BCS coherence length at zero temperature
V_{max}	voltage determining the pseudogap eV_{max} , Eq. (95)	ξ_{QF}	characteristic size of QF, Eq. (18)
W	NMR relaxation rate	$\Pi(\mathbf{q}, \Omega_k)$	polarization operator, Eq. (25)
α	GL parameter	$\sigma_{xx}^{(\text{AL}),(\text{MT})\dots}$	different fluctuation corrections to longitudinal conductivity
$\beta^{\alpha\beta}$	thermoelectric tensor relating electric current with temperature gradient	$\sigma_{xy}^{(\text{AL}),(\text{MT})\dots}$	different fluctuation corrections to Hall conductivity
$\beta_M^{\alpha\beta}$	part of the thermoelectric tensor related to magnetization currents	$\sigma_{xx}^{(\text{fl})}$	total fluctuation correction to conductivity, Eq. (55)
$\gamma^{\alpha\beta}$	thermoelectric tensor relating heat current with electric field	$\sigma_{xx}^{(e)}$	Drude conductivity
γ_E	exponential Euler-Mascheroni constant, Eq. (40)	$\delta\sigma_{\text{tun}}^{(\text{fl})}$	fluctuation correction to tunneling conductivity
γ_ϕ	phase-breaking parameter, Eq. (55)	ζ	particle-hole asymmetry parameter
Γ	tunneling rate	τ	elastic scattering time
$\Delta(\mathbf{r})$	superconducting order parameter	τ_{cp}	Cooper pair rotation period, Eq. (17)
Δ_{BCS}	order parameter at zero temperature	τ_{GL}	GL lifetime of FCP, Eq. (1)
$\Delta^{(\text{fl})}(\mathbf{r}, t)$	fluctuation order parameter	τ_{tr}	transport scattering time
Δ_q, Δ_q^*	Fourier components of the fluctuating order parameter	τ_ϕ	phase-breaking time
ΔE_s	binding energy of FCP close to T_{c0}	τ_{QF}	lifetime of FCP in QF regime, Eq. (17)
ΔE_{QF}	binding energy of FCP close to $H_{c2}(0)$	τ_{so}	spin-orbit scattering time
		χ_{\pm}	dynamic spin susceptibility

$\chi^{(fl)}$	fluctuation correction to magnetic susceptibility, Eq. (38)
χ_L	Landau diamagnetic susceptibility
$\psi(x), \psi^{(n)}(x)$	digamma, polygamma functions
ω	frequency
ω_c	electron cyclotron frequency $ eH/m_e c $
$\omega_c^{(qp)}$	cyclotron frequency of quasiparticles $ eH/m^{(qp)}c $
Ω_H	cyclotron frequency of FCP $4DeH/c$
ω_D	Debye frequency
Ω_k	bosonic Matsubara frequency of fluctuation Cooper pair $2\pi k_B T k$ ($k = 0, \pm 1, \pm 2, \dots$)
ω_n	bosonic Matsubara frequency corresponding to the external field $2\pi k_B T n$ ($n = 0, 1, 2, \dots$)
AL	Aslamasov-Larkin
BCS	Bardeen-Cooper-Schrieffer
BEC	Bose-Einstein condensation
BKT	Berezinskii-Kosterlitz-Thouless
DCR	diffusion coefficient renormalization
DOS	density of states
FCP	fluctuation Cooper pairs
fl	fluctuations
GL	Ginzburg-Landau
GM	Giaever and Megerle
HTS	high- T_c superconductors
ID	(corrections due to) interaction in diffusion channel
LBA	low-bias anomaly
LD	Lawrence-Doniach
LLL	lowest Landau level
MT	Maki-Thompson
(N + SF)	normal state with SF
NE	Nernst-Ettingshausen
NMR	nuclear magnetic resonance
NQR	nuclear quadrupole resonance
pg	pseudogap
QF	quantum fluctuations
qp	quasiparticles
QPT	quantum phase transition
SC	superconductor or superconducting
SF	superconducting fluctuations
STM/STS	scanning tunneling microscopy or scanning tunneling spectroscopy
WL	weak localization (corrections)

ACKNOWLEDGMENTS

We express our deep gratitude to A. Chubukov, Yu. Galperin, M. Grilli, A. Kavokin, A. Koshelev, V. Krasnov, V. Kravtsov, W. Kwok, K. Levin, A. Rigamonti, and

M. P. Smylie for reading the manuscript and valuable comments. We want to thank our coauthors T. Baturina, V. Galitsky, M. Serbyn, M. Skvortsov, and V. M. Vinokur for collaboration on several works on fluctuation spectroscopy, which are partially reviewed here. A. V. acknowledges financial support from the project CoExAn (HORIZON 2020, grant agreement 644076), from Italian MIUR through the PRIN 2015 program (Contract No. 2015C5SEJJ001). This work was supported by the U.S. Department of Energy, Office of Science, Office of Advanced Scientific Computing Research and Materials Sciences and Engineering Division, Scientific Discovery through Advanced Computing (SciDAC) program.

REFERENCES

- Abeles, B., R. Cohen, and C. Fuselier 1971, *Physica (Utrecht)* **55**, 275.
- Abrahams, E., R. Prange, and M. Stephen 1971, *Physica (Utrecht)* **55**, 230.
- Abrahams, E., M. Redi, and J. W. F. Woo 1970, *Phys. Rev. B* **1**, 208.
- Abrikosov, A. A., and L. P. Gor'kov, 1958, *Zh. Eksp. Teor. Fiz.* **35**, 1558 [*Sov. Phys. JETP* **8**, 1090 (1959)] [<http://www.jetp.ac.ru/cgi-bin/e/index/e/8/6/p1090?a=list>].
- Abrikosov, A. A., and L. P. Gor'kov, 1959, *Zh. Eksp. Teor. Fiz.* **36**, 319 [*Sov. Phys. JETP* **9**, 220 (1959)] [<http://www.jetp.ac.ru/cgi-bin/e/index/e/9/1/p220?a=list>].
- Abrikosov, A. A., 1988, *Fundamentals of Metal Theory* (Elsevier, New York).
- Abrikosov, A. A., L. P. Gor'kov, I. Y. Dzyaloshinskii, and D. Brown, 1965, *Quantum field theoretical methods in statistical physics* (Pergamon Press, Oxford), Vol. 2.
- Altshuler, B. L., M. Yu Reizer, and A. A. Varlamov, 1983, *Zh. Eksp. Teor. Fiz.* **84**, 2280 [*Sov. Phys. JETP* **57**, 1329 (1983)] [<http://www.jetp.ac.ru/cgi-bin/e/index/e/57/6/p1329?a=list>].
- Anderson, P. W., 1959, *J. Phys. Chem. Solids* **11**, 26.
- Angilella, G. G. N., R. Pucci, A. A. Varlamov, and F. Onufrieva, 2003, *Phys. Rev. B* **67**, 134525.
- Aronov, A., S. Hikami, and A. Larkin, 1995, *Phys. Rev. B* **51**, 3880.
- Aronov, A., and A. Rapoport, 1992, *Mod. Phys. Lett. B* **06**, 1083.
- Artemenko, S., I. Gorlova, and Y. Latyshev, 1989, *Phys. Lett. A* **138**, 428.
- Aslamasov, L., and A. Larkin, 1968, *Phys. Lett. A* **26**, 238.
- Aslamasov, L., and A. Varlamov, 1980, *J. Low Temp. Phys.* **38**, 223.
- Aslamazov, L. G., and A. I. Larkin, 1975, *Sov. Phys. JETP* **40**, 321 [<http://www.jetp.ac.ru/cgi-bin/e/index/e/40/2/p321?a=list>].
- Bardeen, J., L. N. Cooper, and J. R. Schrieffer, 1957a, *Phys. Rev.* **106**, 162.
- Bardeen, J., L. N. Cooper, and J. R. Schrieffer, 1957b, *Phys. Rev.* **108**, 1175.
- Baturina, T. I., S. V. Postolova, A. Y. Mironov, A. Glatz, M. R. Baklanov, and V. M. Vinokur, 2012, *Europhys. Lett.* **97**, 17012.
- Beasley, M. R., J. E. Mooij, and T. P. Orlando, 1979, *Phys. Rev. Lett.* **42**, 1165.
- Behnia, K., and H. Aubin, 2016, *Rep. Prog. Phys.* **79**, 046502.
- Beloborodov, I. S., and K. B. Efetov, 1999, *Phys. Rev. Lett.* **82**, 3332.
- Beloborodov, I. S., K. B. Efetov, and A. I. Larkin, 2000, *Phys. Rev. B* **61**, 9145.
- Beloborodov, I. S., A. V. Lopatin, V. M. Vinokur, and K. B. Efetov, 2007, *Rev. Mod. Phys.* **79**, 469.
- Belogolovskii, M. A., A. I. Khachaturov, and O. I. Chernyak, 1986, *Fiz. Nizk. Temp.* **12**, 1115 [*Sov. J. Low Temp. Phys.* **12**, 630 (1986)].

- Bennemann, K.-H., and J. B. Ketterson, 2008, Eds., *The Physics of Superconductors* (Springer, Berlin/Heidelberg).
- Bergmann, G., 1984, *Phys. Rev. B* **29**, 6114.
- Bernardi, E., A. Lascialfari, A. Rigamonti, L. Romanò, V. Iannotti, G. Ausanio, and C. Luponio, 2006, *Phys. Rev. B* **74**, 134509.
- Blonder, G. E., M. Tinkham, and T. M. Klapwijk, 1982, *Phys. Rev. B* **25**, 4515.
- Bouadim, K., Y. L. Loh, M. Randeria, and N. Trivedi, 2011, *Nat. Phys.* **7**, 884.
- Boyack, R., Q. Chen, A. A. Varlamov, and K. Levin, 2018, *Phys. Rev. B* **97**, 064503.
- Brenig, W., M. Paalanen, A. Hebard, and P. Wölfle, 1986, *Phys. Rev. B* **33**, 1691.
- Breznay, N. P., and A. Kapitulnik, 2013, *Phys. Rev. B* **88**, 104510.
- Breznay, N. P., K. Michaeli, K. S. Tikhonov, A. M. Finkel'stein, M. Tendulkar, and A. Kapitulnik, 2012, *Phys. Rev. B* **86**, 014514.
- Brinkmann, D., 1995, *Appl. Magn. Reson.* **8**, 67.
- Bruynseraede, Y., M. Gijs, C. Van Haesendonck, and G. Deutscher, 1983, *Phys. Rev. Lett.* **50**, 277.
- Bulaevskii, L. N., 1974, *Zh. Eksp. Teor. Fiz.* **66**, 2212 [*Sov. Phys. JETP* **39**, 1090 (1974)] [<http://www.jetp.ac.ru/cgi-bin/e/index/e/39/6/p1090?a=list>].
- Capan, C., K. Behnia, J. Hinderer, A. G. M. Jansen, W. Lang, C. Marcat, C. Marin, and J. Flouquet, 2002, *Phys. Rev. Lett.* **88**, 056601.
- Caprara, S., J. Biscaras, N. Bergeal, D. Bucheli, S. Hurand, C. Feuillet-Palma, A. Rastogi, R. C. Budhani, J. Lesueur, and M. Grilli, 2013, *Phys. Rev. B* **88**, 020504.
- Caprara, S., M. Grilli, L. Benfatto, and C. Castellani, 2011, *Phys. Rev. B* **84**, 014514.
- Caprara, S., M. Grilli, B. Leridon, and J. Lesueur, 2005, *Phys. Rev. B* **72**, 104509.
- Caprara, S., M. Grilli, B. Leridon, and J. Vanacken, 2009, *Phys. Rev. B* **79**, 024506.
- Carbillet, C., *et al.*, 2016, *Phys. Rev. B* **93**, 144509.
- Carlson, R. V., and A. M. Goldman, 1973, *Phys. Rev. Lett.* **31**, 880.
- Carretta, P., A. Lascialfari, A. Rigamonti, A. Rosso, and A. Varlamov, 2000, *Phys. Rev. B* **61**, 12420.
- Carretta, P., D. V. Livanov, A. Rigamonti, and A. A. Varlamov, 1996, *Phys. Rev. B* **54**, R9682.
- Chang, J., *et al.*, 2012, *Nat. Phys.* **8**, 751.
- Chen, Q., J. Stajic, S. Tan, and K. Levin, 2005, *Phys. Rep.* **412**, 1.
- Chubukov, A., 2012, *Annu. Rev. Condens. Matter Phys.* **3**, 57.
- Chubukov, A. V., D. Pines, and J. Schmalian, 2008, *The Physics of Superconductors* (Springer, Berlin), Chap. A, pp. 1349–1413.
- Cimberle, M. R., C. Ferdeghini, E. Giannini, D. Marré, M. Putti, A. Siri, F. Federici, and A. Varlamov, 1997, *Phys. Rev. B* **55**, R14745.
- Cohen, R. W., B. Abeles, and C. R. Fuselier, 1969, *Phys. Rev. Lett.* **23**, 377.
- Corti, M., B. J. Suh, F. Tabak, A. Rigamonti, F. Borsa, M. Xu, and B. Dabrowski, 1996, *Phys. Rev. B* **54**, 9469.
- Cucolo, A. M., M. Cuoco, and A. A. Varlamov, 1999, *Phys. Rev. B* **59**, R11675.
- Di Castro, C., R. Raimondi, C. Castellani, and A. A. Varlamov, 1990, *Phys. Rev. B* **42**, 10211.
- Dinter, M., 1977, *J. Low Temp. Phys.* **26**, 39.
- Dorin, V. V., R. A. Klemm, A. A. Varlamov, A. I. Buzdin, and D. V. Livanov, 1993, *Phys. Rev. B* **48**, 12951.
- Emery, V. J., and S. A. Kivelson, 1995, *Nature (London)* **374**, 434.
- Eschrig, M., D. Rainer, and J. A. Sauls, 1999, *Phys. Rev. B* **59**, 12095.
- Fay, D., J. Appel, C. Timm, and A. Zabel, 2001, *Phys. Rev. B* **63**, 064509.
- Feigel'man, M. V., L. B. Ioffe, and M. Mézard, 2010, *Phys. Rev. B* **82**, 184534.
- Ferrando, V., I. Pallecchi, A. Malagoli, M. Putti, X. Xi, A. Varlamov, A. Koshelev, and C. Ferdeghini, 2007, *Physica C (Amsterdam)* **460–462**, 608.
- Finkel'shtein, A. M., 1987, *Pis'ma Zh. Eksp. Teor. Fiz.* **45**, 37 [*JETP Lett.* **45**, 46 (1987)] [http://www.jetpletters.ac.ru/ps/1235/article_18665.shtml].
- Finkel'shtein, A. M., 1983, *Zh. Eksp. Teor. Fiz.* **84**, 168 [*Sov. Phys. JETP* **57**, 97 (1983)] [<http://www.jetp.ac.ru/cgi-bin/e/index/e/57/1/p97?a=list>].
- Fiory, A., A. Hebard, and W. Glaberson, 1983, *Phys. Rev. B* **28**, 5075.
- Forro, L., and A. Hamzić, 1989, *Solid State Commun.* **71**, 1099.
- Fukuyama, H., H. Ebisawa, and T. Tsuzuki, 1971, *Prog. Theor. Phys.* **46**, 1028.
- Galassi, M., *et al.*, 2009, *GNU Scientific Library Reference Manual* (Network Theory Ltd., Bristol), 3rd ed.
- Galfy, M., and E. Zirngiebl, 1988, *Solid State Commun.* **68**, 929.
- Galitski, V. M., and A. I. Larkin, 2001a, *Phys. Rev. Lett.* **87**, 087001.
- Galitski, V. M., and A. I. Larkin, 2001b, *Phys. Rev. B* **63**, 174506.
- Gantmakher, V. F., S. N. Ermolov, G. E. Tsydynzhapov, A. A. Zhukov, and T. I. Baturina, 2003, *JETP Lett.* **77**, 424.
- Geballe, T. H., A. Menth, F. J. Di Salvo, and F. R. Gamble, 1971, *Phys. Rev. Lett.* **27**, 314.
- Gershenson, M. E., V. N. Gubankov, and Yu E. Zhuravlev, 1983, *Zh. Eksp. Teor. Fiz.* **85**, 287 [*Sov. Phys. JETP* **58**, 167 (1983)] [<http://www.jetp.ac.ru/cgi-bin/e/index/e/58/1/p167?a=list>].
- Geshkenbein, V. B., L. B. Ioffe, and A. I. Larkin, 1997, *Phys. Rev. B* **55**, 3173.
- Giaever, I., and K. Megerle, 1961, *IRE Trans. Electron Devices* **ED-9**, 459.
- Ginzburg, V. L., 1960, *Sov. Phys. Solid State* **2**, 1824.
- Glatz, A., A. Galda, and A. A. Varlamov, 2015, *Phys. Rev. B* **92**, 054513.
- Glatz, A., A. A. Varlamov, and V. M. Vinokur, 2011a, *Phys. Rev. B* **84**, 104510.
- Glatz, A., A. A. Varlamov, and V. M. Vinokur, 2011b, *Europhys. Lett.* **94**, 47005.
- Glatz, A., A. A. Varlamov, and V. M. Vinokur, 2014, *Europhys. Lett.* **107**, 47004.
- Glover, R., 1967, *Phys. Lett. A* **25**, 542.
- Goldman, A. M., and N. Marković, 1998, *Phys. Today* **51**, No. 11, 39.
- Gollub, J. P., M. R. Beasley, R. Callarotti, and M. Tinkham, 1973, *Phys. Rev. B* **7**, 3039.
- Gordon, J. M., and A. Goldman, 1986, *Phys. Rev. B* **34**, 1500.
- Gordon, J. M., C. Lobb, and M. Tinkham, 1984, *Phys. Rev. B* **29**, 5232.
- Gor'kov, L. P., 1960, *Zh. Eksp. Teor. Fiz.* **37**, 1407 [*Sov. Phys. JETP* **10**, 998 (1960)] [<http://www.jetp.ac.ru/cgi-bin/e/index/e/10/5/p998?a=list>].
- Gorny, K., *et al.*, 1999, *Phys. Rev. Lett.* **82**, 177.
- Graybeal, J. M., J. Luo, and W. R. White, 1994, *Phys. Rev. B* **49**, 12923.
- Gusynin, V. P., V. P. Loktev, and I. A. Shovkovyi, 1995, *Zh. Eksp. Teor. Fiz.* **107**, 2007 [*Sov. Phys. JETP* **80**, 1111 (1995)] [<http://www.jetp.ac.ru/cgi-bin/e/index/e/80/6/p1111?a=list>].
- Hagen, S., C. Lobb, R. Greene, M. Forrester, and J. Kang, 1990, *Phys. Rev. B* **41**, 11630.
- Hagen, S. J., *et al.*, 1993, *Phys. Rev. B* **47**, 1064.
- Halperin, B. I., and D. R. Nelson, 1978, *Phys. Rev. Lett.* **41**, 121.
- Halperin, B. I., and D. R. Nelson, 1979, *J. Low Temp. Phys.* **36**, 599.
- Hartnoll, S. A., P. K. Kovtun, M. Müller, and S. Sachdev, 2007, *Phys. Rev. B* **76**, 144502.

- Haviland, D. B., Y. Liu, and A. M. Goldman, 1989, *Phys. Rev. Lett.* **62**, 2180.
- Helfand, E., and N. R. Werthamer, 1966, *Phys. Rev.* **147**, 288.
- Heym, J., 1992, *J. Low Temp. Phys.* **89**, 869.
- Hirschfeld, P. J., M. M. Korshunov, and I. I. Mazin, 2011, *Rep. Prog. Phys.* **74**, 124508.
- Howson, M. A., M. B. Salamon, T. A. Friedmann, J. P. Rice, and D. Ginsberg, 1990, *Phys. Rev. B* **41**, 300.
- Inoue, T., S. Miwa, K. Okamoto, and M. Awano, 1979, *J. Phys. Soc. Jpn.* **46**, 418.
- Ioffe, L. B., and A. I. Larkin, 1981, *Zh. Eksp. Teor. Fiz.* **81**, 707 [*Sov. Phys. JETP* **54**, 378 (1981)] [<http://www.jetp.ac.ru/cgi-bin/e/index/e/54/2/p378?a=list>].
- Ioffe, L. B., A. I. Larkin, A. A. Varlamov, and L. Yu, 1993, *Phys. Rev. B* **47**, 8936.
- Iye, Y., S. Nakamura, and T. Tamegai, 1989, *Physica C (Amsterdam)* **159**, 616.
- Jacobs, T., S. O. Katterwe, and V. M. Krasnov, 2016, *Phys. Rev. B* **94**, 220501.
- Jin, J. M., and S. J. Zhang, 1996, *Computation of Special Functions* (Wiley, New York).
- Jin, K., B. Y. Zhu, B. X. Wu, J. Vanacken, V. V. Moshchalkov, B. Xu, L. X. Cao, X. G. Qiu, and B. R. Zhao, 2008, *Phys. Rev. B* **77**, 172503.
- Johnston, D. C., 2010, *Adv. Phys.* **59**, 803.
- Kapitulnik, A., A. Palevski, and G. Deutscher, 1985, *J. Phys. C* **18**, 1305.
- Kartsovnik, M., G. Logvenov, K. Maki, and N. Kushch, 1999, *Synth. Met.* **103**, 1827.
- Kavokin, A. V., and A. A. Varlamov, 2015, *Phys. Rev. B* **92**, 020514.
- Kittel, C., 2012, *Introduction to Solid State Physics* (Wiley, New York), 8th ed.
- Klein, T., *et al.*, 2010, *Phys. Rev. B* **82**, 184506.
- Klemencic, G. M., J. M. Fellows, J. M. Werrell, S. Mandal, S. R. Giblin, R. A. Smith, and O. A. Williams, 2017, *Phys. Rev. Mater.* **1**, 044801.
- Kokubo, N., J. Aarts, and P. H. Kes, 2001, *Phys. Rev. B* **64**, 014507.
- Komendová, L., M. V. Milošević, A. A. Shanenko, and F. M. Peeters, 2011, *Phys. Rev. B* **84**, 064522.
- Koshelev, A., and A. Varlamov, 2014, *Supercond. Sci. Technol.* **27**, 124001.
- Koshelev, A. E., and A. A. Golubov, 2004, *Phys. Rev. Lett.* **92**, 107008.
- Koshelev, A. E., A. A. Varlamov, and V. M. Vinokur, 2005, *Phys. Rev. B* **72**, 064523.
- Krasnov, V. M., H. Motzkau, T. Golod, A. Rydh, S. O. Katterwe, and A. B. Kulakov, 2011, *Phys. Rev. B* **84**, 054516.
- Kuboki, K., and H. Fukuyama, 1989, *J. Phys. Soc. Jpn.* **58**, 376.
- Kulik, I., O. Entin-Wohlman, and R. Orbach, 1981, *J. Low Temp. Phys.* **43**, 591.
- Kurkijärvi, J., V. Ambegaokar, and G. Eilenberger, 1972, *Phys. Rev. B* **5**, 868.
- Landau, L., 1930, *Z. Phys.* **64**, 629.
- Lang, W., G. Heine, W. Kula, and R. Sobolewski, 1995, *Phys. Rev. B* **51**, 9180.
- Larkin, A., 1980, *JETP Lett.* **31**, 219 [http://www.jetpletters.ac.ru/ps/1343/article_20284.shtml].
- Larkin, A., and A. Varlamov, 2009, *Theory of Fluctuations in Superconductors*, International Series of Monographs on Physics (OUP, Oxford).
- Lascialfari, A., and A. Rigamonti, 2017, *Il Nuovo Saggiatore* **33**, 5 [http://www.ilnuovosaggiatore.sif.it/download.php?id=VTJGc2-RHVmtYMSiRRXpXWfPH_OEFTWmZXODg1Z25oR3ltV253-MUZmZHI5UT0=].
- Lascialfari, A., A. Rigamonti, and I. Zucca, 2005, *Phys. Rev. B* **71**, 214510.
- Lawrence, W. E., and S. Doniach, 1971, in *Proceedings of the 12th International Conference on Low Temperature Physics*, edited by E. Kanda (Keikagu, Tokyo), p. 361.
- Leridon, B., J. Vanacken, T. Wambecq, and V. V. Moshchalkov, 2007, *Phys. Rev. B* **76**, 012503.
- Lerner, I. V., A. A. Varlamov, and V. M. Vinokur, 2008, *Phys. Rev. Lett.* **100**, 117003.
- Levanyuk, A. P., 1959, *Zh. Eksp. Teor. Fiz.* **36**, 810 [*Sov. Phys. JETP* **9**, 571 (1959)] [<http://www.jetp.ac.ru/cgi-bin/e/index/e/9/3/p571?a=list>].
- Levchenko, A., M. R. Norman, and A. A. Varlamov, 2011, *Phys. Rev. B* **83**, 020506.
- Li, P., and R. L. Greene, 2007, *Phys. Rev. B* **76**, 174512.
- Liu, W., T. W. Clinton, A. W. Smith, and C. J. Lobb, 1997, *Phys. Rev. B* **55**, 11802.
- Livanov, D. V., G. Savona, and A. A. Varlamov, 2000, *Phys. Rev. B* **62**, 8675.
- Loktev, V. M., and Yu. P. Pogorelov, 2015, *Dopants and Impurities in High-Tc Superconductors* (Academperiodica, Kiev).
- Lopes dos Santos, J. M. B., and E. Abrahams, 1985, *Phys. Rev. B* **31**, 172.
- Lowe, A. J., S. Regan, and M. A. Howson, 1993, *Phys. Rev. B* **47**, 15321.
- Mahan, G. D., 2000, *Many-Particle Physics* (Springer, Boston).
- Maki, K., 1968, *Prog. Theor. Phys.* **39**, 897.
- Maki, K., 1973, *Phys. Rev. Lett.* **30**, 648.
- Maki, K., and H. Takayama, 1971, *J. Low Temp. Phys.* **5**, 313.
- Maniv, T., and S. Alexander, 1977, *J. Phys. C* **10**, 2419.
- Matsuda, A., S. Sugita, and T. Watanabe, 1999, *Phys. Rev. B* **60**, 1377.
- Michaeli, K., and A. M. Finkel'stein, 2009a, *Europhys. Lett.* **86**, 27007.
- Michaeli, K., and A. M. Finkel'stein, 2009b, *Phys. Rev. B* **80**, 214516.
- Michaeli, K., K. S. Tikhonov, and A. M. Finkel'stein, 2012, *Phys. Rev. B* **86**, 014515.
- Micklitz, T., and M. R. Norman, 2009, *Phys. Rev. B* **80**, 220513.
- Mineev, V. P., and M. Sigrist, 2001, *Phys. Rev. B* **63**, 172504.
- Mitrović, V. F., H. N. Bachman, W. P. Halperin, M. Eschrig, J. A. Sauls, A. P. Reyes, P. Kuhns, and W. G. Moulton, 1999, *Phys. Rev. Lett.* **82**, 2784.
- Mitrović, V. F., H. N. Bachman, W. P. Halperin, A. P. Reyes, P. Kuhns, and W. G. Moulton, 2002, *Phys. Rev. B* **66**, 014511.
- Morris, R. C., and R. V. Coleman, 1973, *Phys. Rev. B* **7**, 991.
- Mosconi, P., A. Rigamonti, and A. Varlamov, 2000, *Appl. Magn. Reson.* **19**, 345.
- Moskalenko, V., 1959, *Fiz. Met. Metalloved.* **8**, 503.
- Nagaoka, T., Y. Matsuda, H. Obara, A. Sawa, T. Terashima, I. Chong, M. Takano, and M. Suzuki, 1998, *Phys. Rev. Lett.* **80**, 3594.
- Nelson, D. R., and B. I. Halperin, 1979, *Phys. Rev. B* **19**, 2457.
- Nelson, D. R., and J. M. Kosterlitz, 1977, *Phys. Rev. Lett.* **39**, 1201.
- Obraztsov, Yu. N., 1964, *Sov. Phys. Solid State* **6**, 331.
- Paalanen, M. A., A. F. Hebard, and R. R. Ruel, 1992, *Phys. Rev. Lett.* **69**, 1604.
- Paglione, J., and R. L. Greene, 2010, *Nat. Phys.* **6**, 645.
- Palestini, F., A. Perali, P. Pieri, and G. C. Strinati, 2012, *Phys. Rev. B* **85**, 024517.
- Park, M., M. S. Isaacson, and J. M. Parpia, 1995, *Phys. Rev. Lett.* **75**, 3740.
- Patton, B. R., V. Ambegaokar, and J. W. Wilkins, 1969, *Solid State Commun.* **7**, 1287.

- Perali, A., C. Castellani, C. Di Castro, M. Grilli, E. Piegari, and A. A. Varlamov, 2000, *Phys. Rev. B* **62**, R9295.
- Perali, A., P. Pieri, G. C. Strinati, and C. Castellani, 2002, *Phys. Rev. B* **66**, 024510.
- Podolsky, D., S. Raghu, and A. Vishwanath, 2007, *Phys. Rev. Lett.* **99**, 117004.
- Pourret, A., H. Aubin, J. Lesueur, C. Marrache-Kikuchi, L. Berge, L. Dumoulin, and K. Behnia, 2006, *Nat. Phys.* **2**, 683.
- Pourret, A., H. Aubin, J. Lesueur, C. A. Marrache-Kikuchi, L. Bergé, L. Dumoulin, and K. Behnia, 2007, *Phys. Rev. B* **76**, 214504.
- Pourret, A., K. Behnia, D. Kikuchi, Y. Aoki, H. Sugawara, and H. Sato, 2006, *Phys. Rev. Lett.* **96**, 176402.
- Prando, G., P. Carretta, A. Lascialfari, A. Rigamonti, S. Sanna, L. Romanò, A. Palenzona, M. Putti, and M. Tropeano, 2010, *Adv. Sci. Technol.* **75**, 141.
- Prange, R. E., 1970, *Phys. Rev. B* **1**, 2349.
- Pratt, F., J. Caulfield, L. Cowey, J. Singleton, M. Doport, W. Hayes, J. Perenboom, M. Kurmoo, and P. Day, 1993, *Synth. Met.* **56**, 2289.
- Raffy, H., R. Laibowitz, P. Chaudhari, and S. Maekawa, 1983, *Phys. Rev. B* **28**, 6607.
- Raghu, S., D. Podolsky, A. Vishwanath, and D. A. Huse, 2008, *Phys. Rev. B* **78**, 184520.
- Randeria, M., and A. A. Varlamov, 1994, *Phys. Rev. B* **50**, 10401.
- Ranninger, J., J. M. Robin, and M. Eschrig, 1995, *Phys. Rev. Lett.* **74**, 4027.
- Reggiani, L., R. Vaglio, and A. A. Varlamov, 1991, *Phys. Rev. B* **44**, 9541.
- Reizer, M. Y., 1993, *Phys. Rev. B* **48**, 13703.
- Reizer, M. Y., and A. V. Sergeev, 1994, *Phys. Rev. B* **50**, 9344.
- Renner, C., B. Revaz, J.-Y. Genoud, K. Kadowaki, and O. Fischer, 1998, *Phys. Rev. Lett.* **80**, 149.
- Ri, H.-C., R. Gross, F. Gollnik, A. Beck, R. P. Huebener, P. Wagner, and H. Adrian, 1994, *Phys. Rev. B* **50**, 3312.
- Richardson, W., 1997, *Phys. Lett. A* **235**, 186.
- Rigamonti, A., F. Borsa, and P. Carretta, 1998, *Rep. Prog. Phys.* **61**, 1367.
- Sacépé, B., C. Chapelier, T. I. Baturina, V. M. Vinokur, M. R. Baklanov, and M. Sanquer, 2008, *Phys. Rev. Lett.* **101**, 157006.
- Sacépé, B., C. Chapelier, T. I. Baturina, V. M. Vinokur, M. R. Baklanov, and M. Sanquer, 2010, *Nat. Commun.* **1**, 140.
- Sacépé, B., T. Dubouchet, C. Chapelier, M. Sanquer, M. Ovadia, D. Shahar, M. Feigel'man, and L. Ioffe, 2011, *Nat. Phys.* **7**, 239.
- Samoilov, A. V., 1994, *Phys. Rev. B* **49**, 1246.
- Santhanam, P., and D. Prober, 1984, *Phys. Rev. B* **29**, 3733.
- Scalapino, D. J., 1970, *Phys. Rev. Lett.* **24**, 1052.
- Scalapino, D. J., 2012, *Rev. Mod. Phys.* **84**, 1383.
- Scherpelz, P., D. Wulin, K. Levin, and A. K. Rajagopal, 2013, *Phys. Rev. A* **87**, 063602.
- Schmid, A., 1969, *Phys. Rev.* **180**, 527.
- Schmidt, H., 1968, *Z. Phys.* **216**, 336.
- Schmidt, V. V., 1966, *Pis'ma Zh. Eksp. Teor. Fiz.* **3**, 141 [*Schmidt, V. V. JETP Lett.* **3**, 89 (1966)] [http://www.jetpletters.ac.ru/ps/1612/article_24708.shtml].
- Serafin, A., A. I. Coldea, A. Y. Ganin, M. J. Rosseinsky, K. Prassides, D. Vignolles, and A. Carrington, 2010, *Phys. Rev. B* **82**, 104514.
- Serbyn, M. N., M. A. Skvortsov, A. A. Varlamov, and V. Galitski, 2009, *Phys. Rev. Lett.* **102**, 067001.
- Skocpol, W., and M. Tinkham, 1975, *Rep. Prog. Phys.* **38**, 1049.
- Slichter, C. P., 1990, *Principles of magnetic resonance*, Vol. 1 (Springer-Verlag, Berlin).
- Smith, A. W., T. W. Clinton, C. C. Tsuei, and C. J. Lobb, 1994, *Phys. Rev. B* **49**, 12927.
- Sondheimer, E., 1948, *Proc. R. Soc. A* **193**, 484.
- Steiner, M., and A. Kapitulnik, 2005, *Physica C (Amsterdam)* **422**, 16.
- Stewart, G. R., 2011, *Rev. Mod. Phys.* **83**, 1589.
- Suhl, H., B. T. Matthias, and L. R. Walker, 1959, *Phys. Rev. Lett.* **3**, 552.
- Suzuki, M., S.-i. Karimoto, and K. Namekawa, 1998, *J. Phys. Soc. Jpn.* **67**, 732.
- Suzuki, T., and T. Tsuboi, 1977, *J. Phys. Soc. Jpn.* **43**, 444.
- Tafti, F. F., F. Laliberté, M. Dion, J. Gaudet, P. Fournier, and L. Taillefer, 2014, *Phys. Rev. B* **90**, 024519.
- Tan, S., and K. Levin, 2004, *Phys. Rev. B* **69**, 064510.
- Tao, H., F. Lu, and E. Wolf, 1997, *Physica C (Amsterdam)* **282–287**, 1507.
- Teller, E., 1931, *Z. Phys.* **67**, 311.
- Thompson, R. S., 1970, *Phys. Rev. B* **1**, 327.
- Tikhonov, K. S., G. Schwiete, and A. M. Finkel'stein, 2012, *Phys. Rev. B* **85**, 174527.
- Trivedi, N., Y. L. Loh, K. Bouadim, and M. Randeria, 2012, *J. Phys. Conf. Ser.* **376**, 012001.
- Tsuboi, T., and T. Suzuki, 1977, *J. Phys. Soc. Jpn.* **42**, 437.
- Tsuei, C. C., and J. R. Kirtley, 2000, *Rev. Mod. Phys.* **72**, 969.
- Ullah, S., and A. T. Dorsey, 1990, *Phys. Rev. Lett.* **65**, 2066.
- Ullah, S., and A. T. Dorsey, 1991, *Phys. Rev. B* **44**, 262.
- Ussishkin, I., 2003, *Phys. Rev. B* **68**, 024517.
- Ussishkin, I., and S. L. Sondhi, 2004, *Int. J. Mod. Phys. B* **18**, 3315.
- Ussishkin, I., S. L. Sondhi, and D. A. Huse, 2002, *Phys. Rev. Lett.* **89**, 287001.
- Varlamov, A., and V. Dorin, 1983, *Sov. Phys. JETP* **57**, 1089.
- Varlamov, A. A., and D. V. Livanov, 1990, *Zh. Eksp. Teor. Fiz.* **98**, 584 [*Sov. Phys. JETP* **71**, 325 (1990)] [<http://www.jetp.ac.ru/cgi-bin/e/index/e/71/2/p325?a=list>].
- Varlamov, A. A., and V. V. Dorin, 1986, *Sov. Phys. JETP* **64**, 1159.
- Varlamov, A. A., and A. V. Kavokin, 2009, *Europhys. Lett.* **86**, 47007.
- Varlamov, A. A., and L. Yu, 1991, *Phys. Rev. B* **44**, 7078.
- Wang, Y., L. Li, and N. P. Ong, 2006, *Phys. Rev. B* **73**, 024510.
- Wang, Y., N. P. Ong, Z. A. Xu, T. Kakeshita, S. Uchida, D. A. Bonn, R. Liang, and W. N. Hardy, 2002, *Phys. Rev. Lett.* **88**, 257003.
- Wang, Y., Z. Xu, T. Kakeshita, S. Uchida, S. Ono, Y. Ando, and N. Ong, 2001, *Phys. Rev. B* **64**, 224519.
- Watanabe, T., T. Fujii, and A. Matsuda, 1997, *Phys. Rev. Lett.* **79**, 2113.
- Watanabe, T., T. Fujii, and A. Matsuda, 2000, *Phys. Rev. Lett.* **84**, 5848.
- Wen, H. H., Z. Y. Liu, Z. A. Xu, Z. Y. Weng, F. Zhou, and Z. X. Zhao, 2003, *Europhys. Lett.* **63**, 583.
- Wu, C., and J. Lin, 1994, *Phys. Rev. B* **50**, 385.
- Xi, X. X., 2008, *Rep. Prog. Phys.* **71**, 116501.
- Xu, Z. A., N. P. Ong, Y. Wang, T. Kakeshita, and S. Uchida, 2000, *Nature (London)* **406**, 486.
- Xu, Z. A., J. Q. Shen, S. R. Zhao, Y. J. Zhang, and C. K. Ong, 2005, *Phys. Rev. B* **72**, 144527.
- Yamashita, T., *et al.*, 2015, *Nat. Phys.* **11**, 17.
- Zheng, G.-q., W. G. Clark, Y. Kitaoka, K. Asayama, Y. Kodama, P. Kuhns, and W. G. Moulton, 1999, *Phys. Rev. B* **60**, R9947.
- Zheng, G.-q., H. Ozaki, W. G. Clark, Y. Kitaoka, P. Kuhns, A. P. Reyes, W. G. Moulton, T. Kondo, Y. Shimakawa, and Y. Kubo, 2000, *Phys. Rev. Lett.* **85**, 405.
- Zimmermann, H., M. Mali, M. Bankay, and D. Brinkmann, 1991, *Physica C (Amsterdam)* **185–189**, 1145.
- Zuo, F., J. A. Schlueter, and J. M. Williams, 1999, *Phys. Rev. B* **60**, 574.
- See Supplemental Material at <http://link.aps.org/supplemental/10.1103/RevModPhys.90.015009> for numerical codes needed to fit experimental data and to extract the fundamental microscopic parameters of the superconducting systems.